A DATA-DRIVEN MULTI-SCALE STATISTICAL INVESTIGATION OF REGIONAL SOURCES AND SINKS TO IMPROVE KNOWLEDGE OF TERRESTRIAL CARBON CYCLING

by

Kimberly L. Mueller

A dissertation submitted in partial fulfillment
of the requirements for the degree of
Doctor of Philosophy
(Environmental Engineering)
in the University of Michigan
2011

Doctoral Committee:

Associate Professor Anna Marta Michalak, Chair
Professor Peter Adriaens
Professor Mary Anne Carroll
Assistant Professor Valeriy Y. Ivanov

ACKNOWLEDGEMENTS

I would like to thank my Advisor Anna Michalak for the support she has provided me over the last six years. Due to Anna's efforts, I've been able to meet and collaborate with other researchers throughout the field which has substantially improved the quality of my work. Thank you Anna. I also appreciate the advice from my dissertation committee, Peter Adrieans, Mary Anne Carroll, and Valeriy Ivanov each of whom has provided me input that has helped me in various ways.

I would especially like to thank Mary Anne Carroll along with Steve Bertman and Dave Karowe as founders of the NSF Biospheric-Atmospheric Research and Training Program (BART) based out of the University of Michigan Biological Station (UMBS). The BART program allowed me to gain valuable insights into the biospheric component of my work that would have otherwise would have been difficult to obtain. The program also provided me financial support that allowed me to fully concentrate on my work. I also enjoyed working with many of the researchers associated with this program especially Steve Garriety. I was fortunate to be a part of a field experiment at UMBS in the summer of 2008 with Steve where he taught me a lot about forest ecology.

Throughout the summer I began to understand the challenges of collecting measurements and thus, I have greater respect and appreciation for those individuals that are committed to compiling long term observations. Thank you also Chris Vogel, Peter Curtis, and my BART cohort all of whom contributed to my research at UMBS. Finally, I would like to thank the director of the biostation Knute Nadelhoffer whose leadership is an inspiration to many.

My research is almost entirely dependent upon the data that collected by others and therefore, I am very grateful to all the Principal Investigators associated with collecting and quality controlling CO_2 observations, eddy-covariance flux measurements, and environmental datasets. I specifically would like to acknowledge Arlyn Andrews from the National Oceanic and Atmospheric Administration (NOAA) who has devoted

many years to expand and improve the network of towers that continuously sample CO_2. I also appreciate her interest in my research and her advice significantly improved the quality of my work. I would also like to thank Mike Trudeau from NOAA who spent countless hours improving transport model code and running jobs and all the folks at the NASA help desk (especially Johnny Chang). Unfortunately, the larger community does not appreciate this work as much as it should but without Mike's efforts and help from NASA, my PhD would not have been completed.

I would also like to thank everyone in the PUORG research group. In particular, I would like to thank the members of C-PUORG, Sharon Gourdji and Vineet Yadav. Sharon is an excellent researcher with whom I have been fortunate enough to work closely with over the past six years. Thank you Sharon for your diligence, patience, and insights and also for being a good friend. I also would like to thank Vineet who spent many hours writing and improving code at his own personal expense. Without his work, I would not have been able to finish my PhD. I will always be grateful to him.
Finally, I would like to thank my family. I am not sure how I would have survived the past six years without their support, patience and encouragement. I would also like to thank my friends, especially Sandra, Deepak, Amanda, Monica, and all the folks associated with Plymouth Crossfit who all helped me keep some balance in my life. In addition, I would like to thank Marla Booth for helping me bring my final dissertation together; she is a lifesaver. Last, but not least, I would like to thank my husband Alex Martin. He sacrificed so much over the past several years so that I could achieve my goals. He is my best friend, my constant and without his support (especially over the last six months), I would have lost all sanity. I love you Alex.

Portions of this work were adapted from the following manuscripts:

- Mueller, K. L., S. M. Gourdji, and A. M. Michalak (2008), Global monthly averaged CO_2 fluxes recovered using a geostatistical inverse modeling approach: 1. Results using atmospheric measurements, *Journal of Geophysical Research-Atmospheres*, 113, D21114, doi:10.1029/2007JD009734.

- Mueller, K. L., V. Yadav, P. S. Curtis, C. Vogel, and A. M. Michalak (2010), Attributing the variability of eddy-covariance CO_2 flux measurements across

temporal scales using a geostatistical regression for a mixed northern hardwood forest, *Global Biogeochem. Cycles*, 24, GB3023, doi:10.1029/2009GB003642.

The co-authors of these manuscripts are gratefully acknowledged.

TABLE OF CONTENTS

LIST OF FIGURES

LIST OF TABLES

LIST OF EQUATIONS

3.16 $BIC_j = -n\ln\frac{RSS}{n} + k\ln(n)$ 34

3.17 35

$$L_{\theta_{\mathbf{Q,R}}} =$$

$$(1/2)ln|\mathbf{\Omega}| + (1/2)ln|\mathbf{F}^T\mathbf{\Omega}^{-1}\mathbf{F}| + (1/2)\boldsymbol{z}^T(\mathbf{\Omega}^{-1} - \mathbf{\Omega}^{-1}\mathbf{F}(\mathbf{F}^T\mathbf{\Omega}^{-1}\mathbf{F})^{-1}\mathbf{F}^T\mathbf{\Omega}^{-1})\boldsymbol{z}$$

3.18 $\chi^2 = (1/n)(\boldsymbol{z} - \mathbf{H}\boldsymbol{s}_{sci})^T(\mathbf{R})^{-1}(\boldsymbol{z} - \mathbf{H}\boldsymbol{s}_{sci})$ 36

4.1 $L_{s,\beta} = \frac{1}{2}(\mathbf{z} + \mathbf{Hs})^T\mathbf{R}^{-1}(\mathbf{z} + \mathbf{Hs}) + \frac{1}{2}(\mathbf{s} + \mathbf{X\beta})^T\mathbf{Q}^{-1}(\mathbf{s} + \mathbf{X\beta})$ 41

4.2 $\mathrm{E}(\mathbf{s}) = \mathbf{X\beta}$ 44

4.3 $$\mathbf{Q} = \begin{bmatrix} \mathbf{Q}_{1,1} & \mathbf{0} & \cdots & \mathbf{0} \\ \mathbf{0} & \mathbf{Q}_{2,2} & \mathbf{0} & \vdots \\ \vdots & \vdots & \ddots & \vdots \\ \mathbf{0} & \mathbf{0} & \cdots & \mathbf{Q}_{60,60} \end{bmatrix}$$ 45

4.4 $\mathrm{Q_{i,j}}\left(h_{i,j}|\sigma^2, l\right) = \sigma_Q^2 exp\left(-\frac{h_{i,j}}{l_Q}\right)$ 45

4.5 $$\mathbf{R} = c \times \begin{bmatrix} \sigma^2_{\mathbf{R}_{i,1}} & \mathbf{0} & \cdots & \mathbf{0} \\ \mathbf{0} & \sigma^2_{\mathbf{R}_{i,2}} & \mathbf{0} & \vdots \\ \vdots & \vdots & \ddots & \vdots \\ \mathbf{0} & \mathbf{0} & \cdots & \sigma^2_{\mathbf{R}_{i,n}} \end{bmatrix}$$ 46

5.1 $L_{s,\beta} = \frac{1}{2}(\mathbf{z} + \mathbf{Hs})^T\mathbf{R}^{-1}(\mathbf{z} + \mathbf{Hs}) + \frac{1}{2}(\mathbf{s} + \mathbf{X\beta})^T\mathbf{Q}^{-1}(\mathbf{s} + \mathbf{X\beta})$ 72

5.2 $\mathbf{Q}\left(h_x, h_t|\sigma_Q^2, l_Q, \tau_Q\right) = \sigma_Q^2 exp\left(-\frac{h_x}{l_Q}\right) exp\left(-\frac{h_t}{\tau_Q}\right)$ 75

5.3 $\mathbf{Q}\left(h_x|\sigma_Q^2, l_Q\right) = \sigma_Q^2 exp\left(-\frac{h_x}{l_Q}\right)$ 75

6.1 $\boldsymbol{z} = \mu + \boldsymbol{\varepsilon}$ 118

6.2 $Q\left(h_{i,j}\right) = E\left[\varepsilon(t_i)\varepsilon\left(t_j\right)\right]$ 118

6.3 $$\mathrm{Q}\left(h_{i,j}\right) = \begin{cases} \sigma^2_{n,Q} + \sigma^2_{s,Q} & h_{i,j} = 0 \\ \sigma^2_{s,Q} exp\left(-\frac{h_{i,j}}{\tau_Q}\right), & h_{i,j} > 0 \end{cases}$$ 119

CHAPTER 1

Introduction

Human activities and the natural carbon cycle are fundamentally linked. Carbon dioxide (CO_2) is considered the primary greenhouse gas of concern (Denman et al., 2007), because of its abundance in the atmosphere, its ability to trap heat close to the surface and thus change climate, as well as the strong influence human activities have on the overall concentration of atmospheric CO_2. Emissions from human activities annually introduce a significant amount of mass of carbon to the atmosphere from carbon pools that would otherwise be stored as fossil fuel deposits or detrital carbon. The ocean and terrestrial biosphere have responded unexpectedly, reabsorbing approximately 50% of human emissions even though the amount of carbon removed from the atmosphere by natural sinks varies from year to year. Since the amount of atmospheric CO_2 is growing exponentially, both human and earth systems, including the natural carbon sinks that are counteracting human emissions, are increasingly vulnerable to changes in climate and biogeochemical cycles. Locating natural sources and sinks, determining what processes are controlling these sinks, and predicting how they will be influenced by changes in atmospheric CO_2 and climate are all domestic and international policy priorities. In other words, this knowledge is essential for designing policies to stabilize atmospheric CO_2 concentrations.

Much of what we know about carbon cycling, or surface flux exchange, has been derived from the information contained in observations. Such observations include measurements of atmospheric CO_2 mass taken at remote locations such as Mona Loa, Hawaii which contain clear signals of surface fluxes from hemispheric regions or latitudinal bands. Thus, these observations provide valuable information regarding inter-annual trends of atmospheric CO_2. Additionally, scientists have a good mechanistic understanding of how a plant will assimilate CO_2 in response to light and water

availability from laboratory and plot-level measurements. As such, carbon cycling at small and very large scales is considered well-known.

Currently, CO_2 fluxes cannot be directly measured at any scale larger than the approximately $1km^2$ footprint of an eddy-covariance flux tower, described in more detail in Chapter 2. CO_2 fluxes at larger spatial scales (e.g. 1km to 1000km) instead are provided by suite of different models. Unfortunately, the estimates from various models disagree both in terms of the magnitudes of carbon fluxes, e.g. differences can be greater than 1 PgC/month for North America, and their seasonal behavior. This lack of consensus indicates that our knowledge of carbon cycle processes associated with large resolutions is limited.

A better understanding of CO2 flux at larger scales (e.g. at the scale of political entities like countries and individual states or provinces) is needed to develop climate change mitigation policies. Specifically we must be able to budget CO_2 fluxes and understand how they behave over time at resolutions that are useful for formulating and implementing carbon accounting programs. These programs could enable the use agricultural or forest offsets for carbon credit systems if reliable carbon budgets were available at regional scales. An understanding of the processes driving regional or continental fluxes is also essential for predicting future concentrations of atmospheric CO_2, in order to evaluate interactions between the carbon cycle and climate change. Currently, the uncertainty associated with our understanding of carbon cycling at larger scales is hindering our attempts to forecast climate change and manage the carbon cycle through the protection and/or enhancement of natural sinks.

This dissertation challenges the perception that the atmospheric observations of CO_2 and flux measurements are too limited to quantify surface fluxes (for carbon accounting) and improve process-based understanding at continental, regional, and local scales (for predicting future flux scenarios). As such, statistical techniques are first employed to ascertain the information content of atmospheric observations of CO_2 in regards to surface flux exchange. Second, statistical methods are applied to fully take advantage of the observational constraint to estimate regional and continental sources and sinks. Finally, statistical tools are developed to estimate the relationship of carbon flux to

the environmental drivers that appear the most dominant in controlling terrestrial carbon cycling at various spatial and temporal scales.

1.0 What do we know about natural carbon cycling?

As mentioned, our current knowledge about carbon cycling at the global scale has been derived from CO_2 observations from remote locations coupled with atmospheric transport models. Since the mid-1950s, measurements of atmospheric CO_2 concentrations have been precise enough (Keeling et al, 1985; Bacastow et al., 1985) to provide a reliable measure of the annual increase of CO_2 in the atmosphere (Le Quere et al., 2009), as well as an indication of the seasonality of natural sources and sinks. These measurements, along with information related to surface flux exchange, such as vegetative indices from remote-sensing datasets, have furthered the understanding of global trends in carbon cycling. Some of the major advances in our understanding of the carbon cycle are listed below:

(1) The oceans and terrestrial biosphere absorb roughly half of the annual of CO_2 emissions from human activities (Conway, et al., 1994), although the efficiency of these sinks may be declining (e.g. Canadell et al., 2007);

(2) The majority of the terrestrial uptake of atmospheric CO_2 occurs within the Northern mid-latitudes (Tans et al., 1990; Keeling et al, 1989; Fan et al., 1999). However, there is some debate as to the magnitude and location of this sink (e.g. Ciais et al., 2010);

(3) Net uptake of CO_2 by the terrestrial biosphere varies significantly from year to year (e.g. Le Quere 2010);

(4) Shifts in the timing and amplitude of the seasonal cycle of both direct measurements of CO_2 flux (e.g. Desai et al., 2010) and atmospheric CO_2 concentrations (Running et al., 1999; Randerson et al., 1997; Field et al., 1998) suggest that the seasonality of terrestrial carbon exchange is changing (Running et al., 1999; Schwartz and Hanes, 2010);

(5) The global climate system has impacts on the terrestrial carbon cycle, as seen by the strong correlations between variations in the globally annually averaged growth rate of atmospheric CO_2 to the El Niño–Southern Oscillation (Heimann and Reichstein, 2008); and finally,

(6) The amount of CO_2 in the atmosphere from human (a.k.a. anthropogenic) activities released into the atmosphere in 2008 was approximately 8.7+/-0.5 Pg/yr which is an increase of 2% from 2007, 29% from 2000, and 41% above anthropogenic emissions in 1990 (Le Quere et al, 2009).

We have also learned a great deal about the mechanics of terrestrial carbon exchange through small-scale laboratory experiments (e.g. Lloyd and Taylor, 1994; Farquhar et al., 1980; Montieth, 1966; Running et al., 2004), *in situ* biometric data collected at small field sites (e.g. Curtis et al., 2002), and plot-level studies such as the Free Air CO_2 Enrichment (FACE) experiments (Schlesinger et al., 2006), which examine the effects of elevated CO_2 on terrestrial ecosystems. We know physiologically that gross productivity (i.e. photosynthesis) is primarily controlled by the interaction of light, water, temperature, and nutrients (Farquhar et al., 1980, Monteith et al., 1966) and that one or more of these factors can play a limiting role in the amount of carbon fixed by plants. We also know that several factors control how much plants and soils respire or release CO_2 to the atmosphere (autotrophic and heterotrophic respiration, respectively), including the amount of photosynthate supplied to roots, substrate quality and availability, temperature, and soil moisture (e.g. Hibbard et al., 2005; Reichenstein et al., 2003). As a result, we have a thorough understanding of how photosynthesis and respiration instantaneously respond to climate variables. What is less certain, is how these instantaneous changes or responses affect overall photosynthetic capacity, biomass allocation within plants and ecosystems, nutrient availability and the longevity of vegetation (Field, 2001).

2.0 What information are we lacking in terms of natural carbon cycling?

Even though we have an understanding of the carbon-cycling globally and at the physiological (small) scale, there still remains much uncertainty about how biogeochemical processes, disturbances, and climate influence surface exchange at large regional scales (e.g. $1km^2$ to continental scales) over diurnal, seasonal, annual, and inter-annual timeframes (e.g. Denman et al., 2007; King et al., 2007, Dolman et al., 2006; Desai et al., 2010; Denning et al., 2005). For example, we do not understand where and why the biosphere is reabsorbing a substantial portion of human emissions. Figure 1.1 presents a conceptual representation of the level of understanding related to terrestrial

carbon cycling at different spatial and temporal scales while Figure 1.2 shows that the largest gaps in our understanding of carbon-cycling are at spatiotemporal resolutions where we rely more on models than on observations.

The models referred to in Figure 1.2 generally can be classified as either processed-based (aka biospheric) or atmospheric inversions. Biospheric models and atmospheric inversions are used to quantify and identify carbon sources and sinks, whereas biospheric models additionally are used to learn more about the interaction between the eco-climatic variables and land-atmosphere carbon exchange in order to predict climate-carbon feedbacks. Although models are important tools for furthering our understanding of the carbon cycle, they need to be validated against observational data. Hence, our greatest uncertainty of carbon cycling exists at regional and continental resolutions given the lack of validation data at these scales.

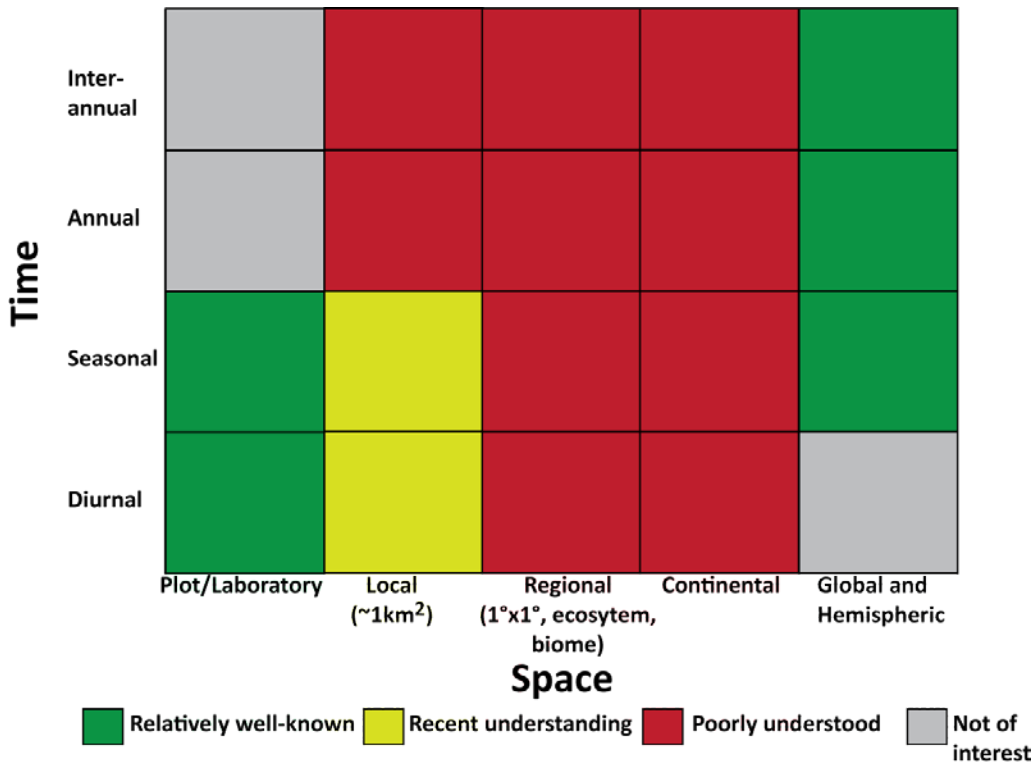

Figure 1.1: A general pictorial summary of the state of knowledge in regards to terrestrial carbon cycling at different spatial and temporal scales. Grey boxes indicate spatiotemporal scales that are currently not of interest to the scientific community.

Biospheric models estimate CO_2 fluxes directly for large areas (approximately 100km by 100km) by scaling up mechanistic understanding derived from experimental studies at smaller scales. However, scaling up process-based understanding of surface flux is complicated by the heterogeneity in land cover and emergent processes encountered at larger scales. Recently, terrestrial biospheric model results were compared (Huntzinger et al., in prep) as part of a synthesis initiative of the North American Carbon Program (NACP). The comparison clearly illustrates the spread of modeled estimates of net primary productivity (Figure 1.3) and thus the lack of understanding of the processes controlling large scale carbon cycling.

Differences between modeled estimates from biospheric models are due in part to the various purposes for which the models were generated (e.g., carbon management or prediction), as well as the variety of forcing factors (e.g., land-use history, meteorology) used to drive the models (Huntzinger et al., in prep). Differences can also be attributed to how physiological relationships are scaled within the models. For example, how leaf-level relationships derived at specific field sites are scaled-up and applied to larger areas and ecosystems.

In contrast to biospheric models, inverse models trace back variations in measured atmospheric CO_2 concentrations to the most likely configuration of surface sources and sinks with the aid of simulated atmospheric transport (Enting, 2002). However, atmospheric mixing tends to make CO_2 inverse problems ill-conditioned, so that it is impossible to identify a unique solution of surface flux estimates that can reproduce the available measurement data (e.g. Enting, 2002). In addition, the limited number of *in situ* surface measurements results in an under-determined problem if the number of estimated fluxes is greater than the available measurement data. To regularize the problem and to estimate a unique solution, most inversion methods use flux results from a biospheric model (henceforward referred to as explicit priors) (e.g. Enting, 2002). As with biospheric models, inter-comparison studies focused on contrasting carbon budgets from atmospheric inversions show a lack of convergence among model estimates (e.g., Desai et al., 2010).

Given that atmospheric measurements of CO_2 are linked in an inversion to surface exchange fluxes using simulated atmospheric transport, some of the observed variability

among inversion estimates cannot be resolved until there are improvements in atmospheric transport modeling. However, different setup choices, such as the use of observations, the regularization structure and choice of explicit prior flux estimates, as well as the resolution at which fluxes are estimated, also contribute to the spread of the estimates. Numerical approximations used to limit the computational cost of estimating fluxes at resolutions finer than continents at sub-monthly timescales (Knorr, 2000) can also impact estimates. Such approximations include reducing the number of estimates by solving sources and sink at continental scales and then down-scaling the estimates to smaller regions.

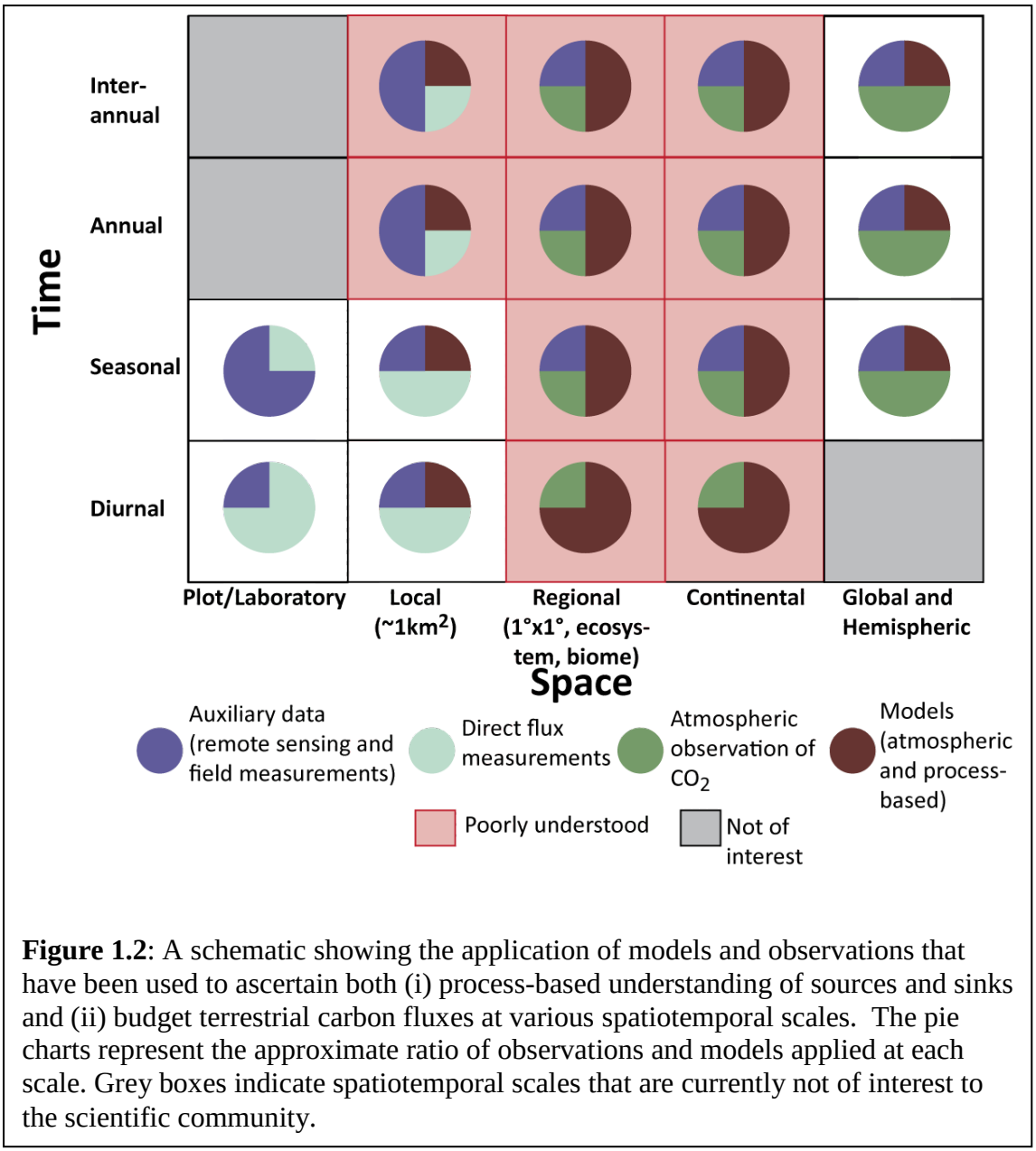

Figure 1.2: A schematic showing the application of models and observations that have been used to ascertain both (i) process-based understanding of sources and sinks and (ii) budget terrestrial carbon fluxes at various spatiotemporal scales. The pie charts represent the approximate ratio of observations and models applied at each scale. Grey boxes indicate spatiotemporal scales that are currently not of interest to the scientific community.

To assess the impact of assumptions and model choices in both biospheric models and atmospheric inversions, we need to compare biospheric results to flux estimates that are largely based on observations, such as inventory-based assessments, direct measurements, or atmospheric CO_2 observations. Direct measurements of flux are spatially limited (i.e., only represent a $1km^2$ area around a flux tower site) while inventory-based assessments are temporally limited (i.e. only provide annual assessments). There is also a common belief that atmospheric data, both atmospheric observations of CO_2 and surface flux exchange measurements, are too limited at

resolutions greater than the plot-scale to provide information about the diurnal, seasonal, and annual behavior (e.g. Gurney et al., 2002, Schuh et al., 2010, etc.) of surface exchange. As a result, most atmospheric inversions and process-based models use information or parameters derived from other models. This interdependence complicates comparison studies aimed at identifying which factors and assumptions have the greatest influence on the spread of models estimates.

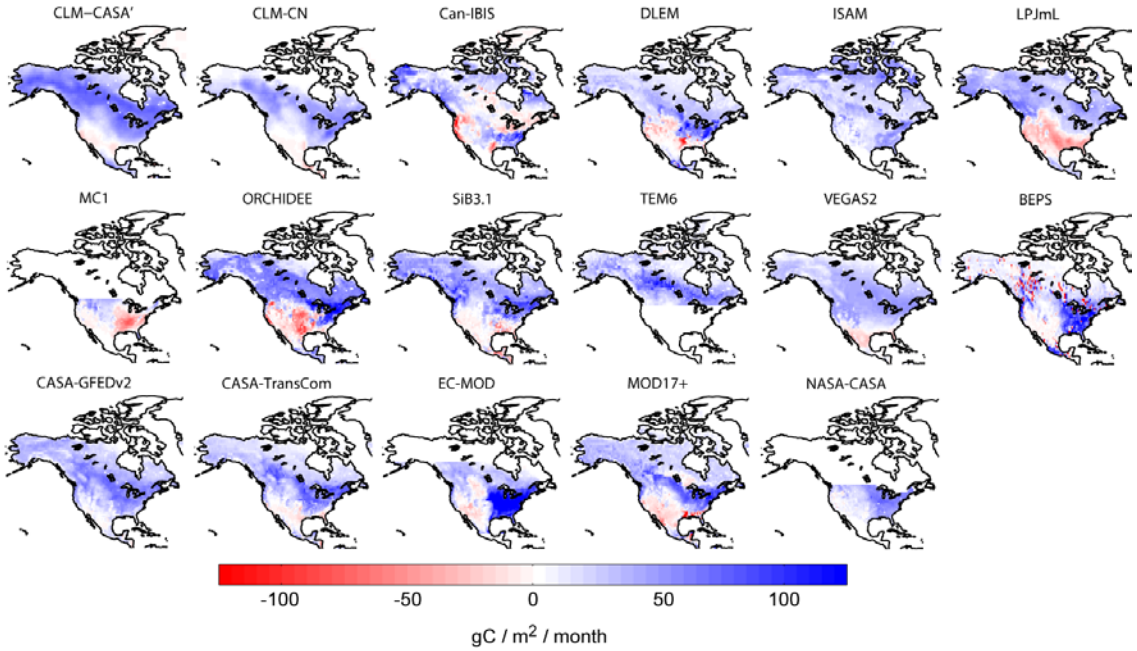

Figure 1.3: Long-term mean (2000-2005) summer (June, July, and August) net ecosystem productivity (NEP) estimated from different terrestrial biospheric models for North America. Positive values indicate net terrestrial carbon uptake and negative values a net C release with respect to the atmosphere. Grey areas indicate areas not covered by a given model's estimate of flux. Courtesy of D.N. Huntzinger (Huntzinger et al., in prep).

3.0 Goals of the dissertation

Reducing the uncertainty associated with regional and continental carbon budgets at various timeframes has become a policy priority (e.g. Canadell et al.; 2007, Rapauch et al., 2010; Le Quere 2010). As such, over the past decade there have been several coordinated research endeavors such as the NACP (http://www.nacarbon.org/nacp/) and the CarboEurope project (http://www.carboeurope.org/). The aim of these initiatives is to reduce the uncertainty associated with fluxes at resolutions greater than the plot-scale,

specifically for ecosystem-scale fluxes. From such activities and other initiatives, a variety of information is now available at multiple spatial and temporal scales. These initiatives include NASA's Earth Observing System (EOS) which has collected a variety of variables associated with carbon cycling (e.g. Leaf Area Index, Enhance Vegetative Index, etc.) over the past decade, the expansion of NOAA's CO_2 measurement network (http://www.esrl.noaa.gov/gmd/dv/site/site_table2.html), and the growth of FluxNET (Baldocchi et al., 2003). The availability of data presents new opportunities to quantify and understand the dynamics of carbon cycling at a variety of spatiotemporal scales.

Thus, the overarching goal of this research is to take advantage of the available measurements by applying geostatistical methods, which rely on relatively fewer assumptions compared to other widely used approaches and to infer surface fluxes that are independent of process-based models. Specifically, this dissertation consists of three main objectives. The first two objectives test whether or not atmospheric observations of CO_2 contain enough information to help inform the types of carbon budgets of most interest to policy-makers. In order to answer this question, statistical methods are applied to generate land-atmosphere carbon flux estimates. The methods employed are specifically designed to be independent of other approaches. Thus inferred estimates can be compared to results from other methods to help reconcile differences among models and build consensus on our carbon cycle knowledge at regional and continental scales. The results can also be used to help identify the simplifying assumptions that have the largest impact on carbon budgets at different spatiotemporal scales.

Objective three tests whether statistical methods can be used with flux measurements to assess how the relationships between carbon exchange and environmental factors, such as leaf phenology, change with temporal scale. For example, the study explores whether the seasonal driver(s) of photosynthesis differ from those variables that control the synoptic uptake of CO_2. This study is conducted using direct measurements of flux representative of a local scale (~1km^2). Even though field studies have improved our understanding of carbon cycling at local scales, the temporal dependence of mechanistic relationships is less well-understood, particularly in terms of modeling these relationships at much larger spatiotemporal resolutions. Being able to

ascertain which relationships can be “scaled-up” or “scaled-down” from one resolution to another may result in a better convergence of estimates from various models.

These three objectives are summarized below. In addition, Figure 1.4 shows how the objectives fit into the community-wide effort to reduce the uncertainty associated with large scale carbon cycling:

(1) Objective 1: Estimate global monthly CO_2 surface flux at a 3.75° latitude × 5° longitude resolution for 1997-2001. This research quantifies the degree to which the global observational network can inform the distribution of CO_2 fluxes at various spatial and temporal scales. Another purpose of the work is to demonstrate the capability of the statistical approach used for this work (as presented in detail in Chapter 3), which limits the use of simplifying assumptions, relative to other inversion and biospheric methods, that are known to have a large impact on flux estimates;

(2) Objective 2: Assess the impact of additional (in space and time) CO_2 measurements in helping to constrain (i.e., diagnose) monthly fluxes for North America. This component focuses on estimating 1°x1° surface fluxes for North America and their corresponding uncertainties at various temporal resolutions for 2008 using (i) 10 measurement sites of continental tower locations employed in various 2004 regional inversion studies, and (ii) 35 measurement sites available in 2008. This sensitivity analysis highlights the impact the measurement information has on budgeting both regional and continental CO_2 in light of other inversion setup choices; and,

(3) Objective 3: Assess drivers of CO_2 variability at a landscape scale, as inferred by a statistical regression model. This component develops a statistical framework using direct estimates of flux along with other micrometeorological and environmental datasets to infer the dominant controls on carbon flux at multiple temporal scales. Flux measurements from the University of Michigan Biological Station (UMBS) tower site are used as a test case (described in detail in Chapter 3), thus the method is also used to test current understanding of carbon cycling at this site (representing a mixed-hardwood forest ecosystem) at the daily, weekly, and monthly timescales.

The dissertation is organized in the following manner: Chapter 2 consists of a literature review providing the conceptual motivation for the statistical approaches used throughout the dissertation. Chapter 3 presents the methods used in this study and Chapters 4 through 6 outline the specific contributions of the dissertation through the three objectives outlined above. Finally, Chapter 7 summarizes the contributions from the individual chapters towards improving our understanding of carbon cycling at local, regional, and continental scales. Chapter 7 also suggests future directions for the work presented in the
dissertation.

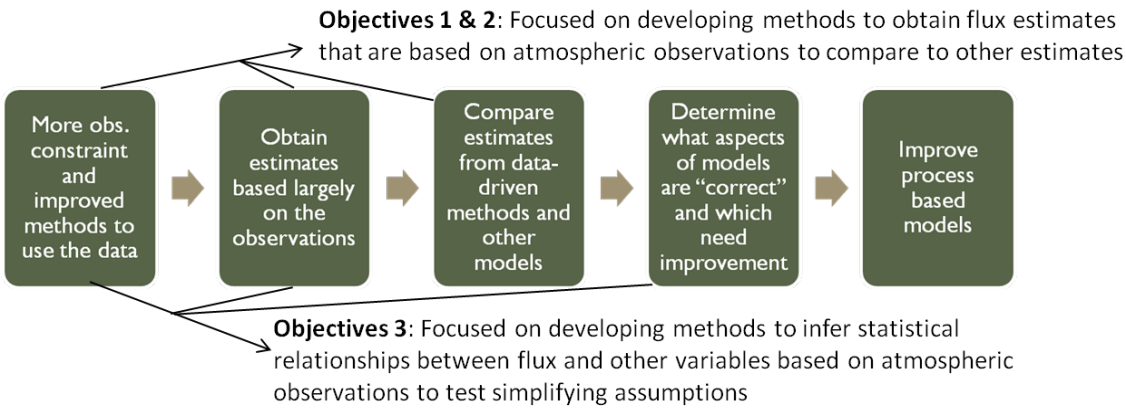

Figure 1.4: A schematic showing how the specific objectives of the dissertation fall within the overall community-wide process of reducing the uncertainty associated with regional and continental fluxes.

CHAPTER 2

Literature Review

1.0 Scientific need for improved understanding of the carbon cycle

Carbon dioxide (CO_2) is the primary greenhouse gas contributing to global climate change, and numerous studies have focused on developing a thorough understanding of the regional, continental, and global budgets of CO_2. As mentioned in Chapter 1, although significant progress has been made in understanding the processes controlling the sources and sinks of CO_2, important questions still remain regarding their magnitude, timing and geographic distribution.

In terms of natural carbon cycling, the science community has focused on answering the following questions at regional and continental resolutions over the past decade (King et al., 2007; Denning et al., 2005):

(1) Where are sources and sinks and how are they changing with time?
(2) What are the main drivers of natural fluxes at seasonal, annual, and inter-annual scales?
(3) What are the feedbacks between climate, vegetation, substrate availability, and atmospheric carbon exchange and do these feedbacks have spatiotemporal dependencies?
(4) How much of human emissions do natural sinks absorb and does this vary throughout time?

The ability to identify sources and sinks of carbon at regional and continental scales are important because a strong understanding of the carbon cycle is required to develop effective carbon management strategies. While CO_2 emissions from human activity are relatively small compared to those from the natural carbon cycle, their net contribution toward the amount of CO_2 mass in the atmosphere is large given that the natural carbon fluxes should on average balance. Given the large magnitudes of the

individual natural flux components of the land and oceans, relatively small changes in their behavior of CO_2, due to climate-carbon feedbacks, can lead to disproportionate increases in atmospheric CO_2 (Friedlingstein and Prentice, 2010). Therefore, a better understanding of carbon cycle is required to enable policy makers to focus on policy driven questions such as:

(1) What sort of policy options could be implemented to enhance natural sinks and reduce sources?
(2) How do we monitor and assess carbon management schemes that aim to sequester atmospheric CO_2?

2.0 Approaches to understanding carbon cycling

By definition, a terrestrial carbon budget of any area (local, regional, or global) at any timeframe (daily, monthly, annually, inter-annually) is the difference between its carbon gains and losses. In general, terrestrial ecosystems gain carbon through photosynthesis, which assimilates carbon into vegetative biomass, and lose it primarily as CO_2 through respiration which releases CO_2 into the atmosphere. Respiration can be further subdivided into its heterotrophic component from free-living soil microbes, animals, and fungi along with its autotrophic component from roots, mycorrhizae, leafs, stems and photosynthetic bacteria. These natural cycling processes are controlled not only by vegetation type and soils, but also by a number of environmental variables. These variables include the amount of available sunlight, water availability, nutrient cycling, and temperature. In addition, other processes such as disturbance (e.g. forest fires, windstorms, large-scale herbivory events), also have unique set(s) of drivers and associated scale of impact, constituting significant sources of atmospheric CO_2. Although photosynthesis and respiration are the two main components of terrestrial carbon cycling, disturbance (fire, herbivory losses) (Gough et al., 2007a) and the release of volatile organic compounds (VOCs) by vegetation (Brilli et al., 2007), can also contribute to losses of carbon to the atmosphere from an ecosystem.

While small scale studies have enabled scientists to develop some theories with respect to the mechanics of photosynthesis and respiration, attempts to extrapolate this understanding to spatial scales larger than those of plot experiments have proven difficult

(e.g. West et al., 2009). Quantifying and predicting terrestrial budges is difficult because we (i) do not have the means to directly measure CO_2 surface exchange for areas larger than $1km^2$ and (ii) have limited understanding of how carbon and associated nutrients are used within photosynthesis and respiration as well as exchanged with the atmosphere at multiple spatial and temporal resolutions (e.g. Heimann and Reichstein, 2008). Regional scales also often contain multiple landuse types, heterogeneous terrain, as well as urban areas which further complicate scaling plot-level understanding to these larger spatial scales.

Attempts to study carbon cycling at these larger resolutions ($1km^2$ to continental scales) are generally classified into three approaches. The first of these approaches, i.e. "top-down" methods or inverse models, trace back variations in the measured atmospheric CO_2 signals to either (i) estimate the most probable net surface source and sink distribution or (ii) optimize biospheric model parameters with the aid of an atmospheric transport model (e.g. TM3, Heimann et al. (2003), STILT, Lin et al. (2003); Schuh et al. (2010)). The second can be characterized as "bottom-up" (e.g. biospheric models and inventory datasets), where each flux component is accounted for separately, i.e. gross productivity, respiration, fossil fuel combustion, land use change, and disturbance. Biospheric or process-based models "scale-up" mechanistic relationships derived from controlled experiments (e.g. Simple Biosphere Model (SiB 3.0) Baker et al. (2008); the Carnegie Ames Stanford Approach (CASA) Potter et al. (1993)). The final approach involves estimating surface flux directly for an approximately $1km^2$ area using the eddy covariance (EC) method to study the diurnal, seasonal, and annual behavior of the local flux. These estimates can also be compared to other datasets, such as leaf area indices (LAI) or temperature, to elicit carbon-climate interactions (e.g. Law et al., 2002; Curtis et al., 2003, etc.). A few studies have combined more than one of these approaches (e.g. Pacala et al., 2001; Riley et al., 2009). However, each of these approaches has limitations, primarily revolving around simplifying assumptions known to have a large impact on flux, as outlined in the following sections, which in part, provide the motivation for the data-driven methods employed in this dissertation.

The following sections of this chapter provide a brief summary of main methods that have been used to inform our current knowledge of CO_2 flux at regional and

continental scales. The purpose of presenting these approaches is to outline their advantages and drawbacks in order to show why the statistical methods employed in this dissertation are needed to help fill in the gaps in our understanding of natural carbon cycling.

2.1 Top-Down Approaches

Observations of atmospheric concentrations contain information regarding sources and sinks at the Earth's surface (Ciais et al., 2010). Starting from a set of atmospheric CO_2 concentration observations, coupled to an atmospheric transport model, it is possible to infer information on the distribution of surface carbon exchange. This process is known as inverse modeling (also referred to as "top-down" approaches) and consists of finding a set of statistically optimal fluxes. These methods were developed in an effort to make more use of the atmospheric data in estimating carbon budgets more consistent with the atmospheric signal (Enting, 2002). For conservative tracers such as CO_2, atmospheric chemistry does not need to be considered since the influence of surface fluxes on observations is modified only by transport. The signal within the atmospheric observations is an integration of contributions from all flux components including natural sources and sinks and fossil fuel emissions at continental and regional scales (Ciais et al., 2010).

2.1.1 Budgeting of CO_2 surface exchange fluxes at continental scales

Traditionally, inverse modeling approaches have been employed to improve continental or large ocean estimates of carbon flux at monthly to annual timeframes using flask measurements from global observational networks (e.g http://www.esrl.noaa.gov/gmd/ccgg/globalview/). The flask observations are taken weekly at remote locations, and therefore measure background air that represent fluxes from large continental or ocean areas. Given the coarse temporal coverage of the observations and the fact that the measurement locations tends to be biased toward wealthier continents in the Northern Hemisphere, the network is considered limited in its ability to inform surface flux exchange.

The nature of atmospheric transport (e.g., mixing, diffusion, influence of weather patterns) and its associated uncertainties limit the information content of available

observations. As a result, atmospheric inversions are generally ill-posed, with substantially different flux distributions yielding similar modeled mixing ratios at observational network sites (Enting, 2002). As a result, uncertainties in observational data and transport models lead to high uncertainties on estimated fluxes (Enting and Newsam, 1990; Brown, 1993; Hein et al., 1997).

In order to circumvent this ill-posedness and to compensate for the assumed limited amount of information within atmospheric network in regards to surface flux exchange, additional information on CO_2 sources and sinks is typically introduced into inversions in the form of explicit prior estimates of surface flux. This approach, commonly referred to as synthesis Bayesian inversion, typically obtains these *a priori* flux estimates from process-based models and/or inventories (e.g., Kaminski et al., 1999; Rödenbeck et al., 2003; Gurney et al., 2004; Baker et al., 2006). Process-based, or biospheric, models apply knowledge of small-scale causal mechanisms to predict carbon exchange at larger scales (e.g. Carnegie-Ames-Stanford Approach (CASA) model, Randerson et al., 1997; Lund-Postdam Jena (LPJ) Dynamic Global Vegetation Model, Sitch et al., 2003). However, the introduction of explicit flux estimates has the ability to introduce biases in estimates of sources and sink because *a posteriori* estimates to revert to *a priori* assumptions in under-constrained regions. Therefore, an error or bias in the explicit prior will be present in fluxes yielded from a synthesis Bayesian inversion.

Because the current global CO_2 monitoring network is sparse, some regions of the world remain poorly constrained even after the introduction of *a priori* assumptions about flux distributions. Therefore, to avoid an under-determined problem, synthesis Bayesian inversions often estimate fluxes for a small number of pre-specified regions loosely based on continental boundaries (e.g. Gurney et al., 2003, 2004; Law et al., 2003; Baker et al., 2006), or, more recently, based on biomes or land cover types (e.g. Peters et al., 2007), while keeping the flux patterns within regions fixed. This approach can lead to aggregation errors (Kaminski et al., 2001), where the inferred net flux estimate from a region can be biased by any inaccuracies in the flux patterns assumed within that region. In a few cases, sources and sinks have been estimated at finer scales to reduce such errors, by including a covariance matrix that describes the assumed spatial autocorrelation between fluxes (e.g. Rödenbeck et al., 2003; Rödenbeck, 2005).

As with all models, flux estimates and uncertainties derived from atmospheric inversions are sensitive to setup choices, such as the selection of observations, the transport model, prior information, prescribed flux patterns, and error covariance parameters. Although errors associated with simulated transport have a large contribution to the observed inconsistencies between reported flux estimates from various inversion studies due to varying rates of inter-hemispheric transport and vertical mixing (Gurney et al., 2003), different simplifying assumptions and setup choices also can have a large impact. For example, there is a growing awareness of the strong influence of these assumptions, especially in regards to the use of explicit prior flux estimates from bottom-up models to define the magnitude and spatial distribution of fluxes (e.g. Michalak et al., 2004; Rödenbeck, 2005). As mentioned earlier, this influence not only contributes to aggregation errors, but can also cause *a posteriori* flux estimates to revert to *a priori* assumptions in under-constrained regions. More importantly, estimates from synthesis Bayesian inversions are not independent from their explicit prior estimates, and therefore cannot be used directly to reconcile process-based understanding of flux behavior with the information content of atmospheric observations. The sensitivity of estimates to other assumptions and setup choices has also been recognized, with researchers attempting to systematically quantify the magnitude and impact of model-data mismatch and *a priori* flux uncertainties (e.g. Engelen et al., 2002, 2006; Krakauer et al., 2004; Michalak et al., 2005).

Due to the strong influence of inverse modeling assumptions on estimated sources and sinks, there is a need for an inverse modeling approach for CO_2 flux estimation that can more directly reflect the information content of available atmospheric measurements. Such an approach, based on a geostatistical inverse modeling framework (as described in Chapter 3), was proposed by Michalak et al. (2004). This method aims to reduce the influence of modeling assumptions that are known to have a strong influence on flux estimates by (1) avoiding the use of bottom-up flux estimates for defining the magnitude and spatial patterns of fluxes, (2) estimating sources and sinks at resolutions that minimize the risk of aggregation errors, and (3) using a rigorous statistical framework for quantifying model-data mismatch and the degree of spatial autocorrelation in the flux distribution. In this manner, the approach yields CO_2 flux estimates that are more

strongly representative of the spatial and temporal variability of CO_2 fluxes as seen through the atmospheric measurement network. The research presented in Chapter 4 represents the first application of the geostatistical inverse modeling approach for estimating CO_2 fluxes using atmospheric observations.

2.1.2 Budgeting of CO_2 surface exchange fluxes at regional scales

Until recently, inversions could not be used to budget CO_2 at regional resolutions due to the spatiotemporal limitations of the global network atmospheric CO_2 flask network and the coarseness of global atmospheric transport models. However, within the past decade, regional scale "top-down" estimates (e.g. Gerbig et al., 2003a) have become possible due in part to recent improvements in meso-scale transport models (e.g. Lin et al., 2003; Nicholls et al., 2004; Nehrkorn et al., 2010), which are able to utilize meteorological information at fine spatiotemporal resolutions, far beyond those applied at global scales. In addition, continuous concentrations from a number of land-based towers have been made available (e.g. NOAA, www.noaa.gov/esrl; Environment Canada, http://gaw.kishou.go.jp/cgi-bin/wdcgg/catalogue.cgi). These measurements have much finer temporal resolution (e.g. hourly) and better spatial coverage than the observations from the flask network. As such, several studies (e.g. Carouge et al., 2010a, Carouge et al., 2010b, Schuh et al., 2010, Gourdji et al., 2010, Butler et al., 2010) have estimated regional-scale fluxes for either the North American or European continents.

However, regional atmospheric inversions are much more complicated than global inversions, thereby requiring additional assumptions to constrain estimates. For example, the use of continuous measurements in regional inversions puts more demands on atmospheric transport models (Geels et al., 2007; Gerbig et al., 2003a), requiring higher spatial resolutions, as well as the ability to reproduce diurnal planetary boundary layer (PBL) dynamics and synoptic shifts in transport (Carouge et al. 2010a). As such, errors associated with transport are assumed to be larger in regional inversions compared to global inversions, and, therefore, the choice of observations to use within the inversion can significantly alter final flux estimates (Gourdji et al. in prep). Additional complications relative to global inversions include the need to specify atmospheric CO_2 boundary conditions for the region of interest to account for the influence of fluxes that occurred outside of the domain of interest. Regional flux estimates have been shown to

be very sensitive to the choice of boundary conditions (Peylin et al., 2005; Schuh et al., 2010). Finally high frequency continuous CO_2 measurements tend to be located both in highly productive areas but also near major urban centers. As such, the observations tend to be much noisier than flask measurements and contain multiple scales of variability. Ascertaining long term temporal trends from small-scale frequency or fossil fuel spikes pose unique challenges to regional inversions that use these concentrations.

Aggregation error is likely to be more serious with the use of continuous data since continuous data have such strong diurnal and synoptic flux variability (Law et al., 2002). To reduce aggregation errors, most regional inversion studies estimate fluxes at finer spatial and temporal resolutions than global inversions in order to account for the potential responses of various vegetation types, resolve fine-scale variability in regional transport, and isolate anthropogenic emissions (e.g. Gerbig et al., 2003a; Peylin et al., 2005; Lauvaux et al., 2008; Schuh et al., 2010; Gourdji et al., 2010; Carouge et al., 2010a). Gourdji et al. (2010) showed that the choice of temporal estimation scale has a large impact on the aggregation errors in a 2004 North American regional inversion studied using measurements from 9 different towers. From this study, it was concluded that a temporal scale of estimation that accounted for the diurnal cycle was best for avoiding temporal aggregation errors for North America. Hence, Gourdji et al. (2010) estimated an average four day diurnal cycle (discretized into 3 hourly bins) to account for flux variability throughout the day.

It is widely assumed that more continental measurements, along with improvements in modeling of atmospheric transport, will help overcome some of the complications of regional inversions, especially in areas with dense measurement coverage (Peylin et al., 2005; Gerbig et al., 2009; Matross et al., 2006; Lauvaux et al., 2008). However, this hypothesis has not yet been tested due to sparseness of regional networks. At present, regional inversion that have focused on the North American continent have only been able to use concentrations from at most 10 tower locations to constrain estimates (e.g. Schuh et al., 2010, Butler et al., 2010). These different North American inversions have yielded a wide spread of both monthly and annual sources and sinks presumably from different choices (e.g. boundary condition, scale of estimation, etc.) employed in each study as well as the choice of atmospheric transport. As such,

regional budgets from atmospheric inversions remain highly uncertain and the information content of continuous measurement to constrain regional carbon budgets is unknown.

Since the number of locations that continuously sample atmospheric CO_2 in North America increased by almost fourfold from 2004 to 2008, there is now the opportunity to assess whether the expanded network can constrain regional budgets at monthly and annual timescales. It remains to be seen if additional measurements will help limit the sensitivity of flux estimates to inversion choices. Without understanding the influence of these measurements on estimates of sources and sinks of CO_2, especially in the context of the other modeling choices associated with regional inversions, it is impossible to assess the incremental net benefit of adding more observations as opposed to focusing other inversion refinements, such as improving boundary conditions and regional transport or minimizing temporal aggregation error. It is also crucial that we understand what knowledge these measurements are able to provide in terms of both anthropogenic and natural carbon cycling, and to develop tools on how to best extract both the small and large scale variability from continuous observations from regional networks.

The research presented in Chapter 5 explores the impact of the expanding continuous atmospheric CO_2 measurement network on the estimates of surface flux at various spatial (1°x1° to continental) and temporal (monthly and annual) scales within the North American Continent for 2008.

2.2 Bottom-up Approaches

As noted in Chapter 1, bottom approaches include both biospheric models and inventory data. Biospheric models generally "scale-up" biophysical and ecological processes (such as gross photosynthesis and respiration) using relationships derived from mechanistic studies performed at a leaf or plant scale and at shorter or sporadic timeframes (Chen et al., 2003). For regional carbon budgeting, these estimates are then combined with inventory emission data such as Vulcan (Gurney et al., 2009) or the Global Fire Emissions Database (GFED v2 Giglio et al. (2006)) which account for fossil fuel emissions, disturbance, land use change, and biomass burning. Using the knowledge of small-scale causal mechanisms, biospheric models estimate carbon exchange for areas ranging in size from a specific location to continental regions at short (3 hour or daily)

(e.g., Simple Biosphere Model (SIB3) available at 3-hour resolution, Baker et al. (2008)) to longer (monthly, annual) time scales (e.g. Carnegie-Ames-Stanford Approach coupled with GFEDv2 (CASA-GFED), (http://www.ess.uci.edu/~jranders/); Lund-Postdam Jena (LPJ) Dynamic Global Vegetation Model, Sitch et al. (2003)). The ultimate goals of such modeling endeavors is to both diagnose current and past regional and local carbon budgets as well predict future carbon cycling scenarios (Huntzinger et al., 2010).

However, as shown in Figure 1.2, there are large discrepancies between flux estimates from different biospheric models (Huntzinger et al., in prep.). In addition, bottom-up flux estimates coupled with atmospheric transport models have difficulty reproducing measured atmospheric CO_2 concentrations (Heimann et al., 1998; Nevison et al., 2008; Dargaville et al., 2002; Denning et al., 2003). Although there may be several reasons for these inconsistencies, the spread of estimates require testing certain simplifying assumptions, e.g. that relationships between flux and their mechanistic controls linearly scale to larger regions or to large temporal resolutions. As such, there is a need to study the relationships between critical biophysical and ecological processes and carbon exchange at resolutions larger than the plot scale at different timeframes.

2.3 Empirical methods employed in flux tower studies

The eddy covariance (EC) method provides the opportunity to study relationships between environmental datasets and surface flux exchange at an approximately $1km^2$ scale at various timeframes, because it provides a direct measurement of the flux density between vegetation and the atmosphere (Baldocchi at al., 2008). These measurements are also referred to as the net ecosystem exchange (NEE). NEE estimates are derived from the covariance of the deviations in atmospheric CO_2 concentrations and vertical wind speed from their mean concentrations at a given flux tower site (e.g. Canadell et al., 2000; Baldocchi et al., 2001). Eddy-covariance measurements are generally continuous in time providing ample temporal coverage (e.g. 30 minute averages) for long durations (e.g. greater than 5 yrs). In addition, the observations are made in situ so they are generally non-intrusive compared to other field equipment such as flux chambers. Today, numerous research groups collect EC measurements forming regional networks such as CarboEuroflux, AmeriFlux, Fluxnet-Canada, China-Flux, AsiaNet, Ozflux and LBA (Brazil) which further combined into a global network (FLUXNET). Towers are

located on temperate conifer and broadleaf forest, tropical and boreal forests, crops, grasslands, chaparral, wetlands, and tundra as well as in urban areas (Baldocchi et al., 2000).

These long term measurements provide an integrated perspective of the environment they represent and reflect the response of total surface flux (i.e. photosynthesis and respiration) to climatic changes (e.g. increased temperature), maturation of the environment (e.g. age of trees) and disturbances (e.g. insect outbreaks or fire) (Barr et al., 2007, Bradford et al., 2006, Gilmanov et al., 2006, Houghton et al., 2000). Although there can be large uncertainties associated with these half-hourly measurements (Richardson et al., 2006), NEE estimates have been used to improve understanding of the temporal variability of CO_2 surface flux of particular ecosystems through statistically inferred relationships at daily or longer temporal scales (Law et al., 2002).

One of the benefits of using high frequency eddy-covariance data to investigate the relationship between fluxes and environmental factors is that both long and short term trends can be inferred from the measurements (e.g. Stoy et al., 2009). Statistical approaches such as neural networks (e.g. Stoy et al., 2009) and linear regression (e.g. Law et al., 2002; Hui et al., 2003) have been used to understand the climatic controls of both the inter-annual and seasonal variability of carbon cycling at flux tower sites. Regression methods have the advantage of providing statistical relationships between given variables and flux. However, traditional regression approaches are limited by (1) the approach used to select the variables to include in the regression, (2) the assumption of independent and identically distributed residuals, and (3) assumptions regarding the dependent variable (i.e., how to best decompose NEE into photosynthetic uptake and respiration). Each of these limitations is further described within the proceeding paragraphs.

The first of these limitations centers on the methods used to select the variables to include in the regression model, referred to henceforth as the model of the trend. Frequently, only a subset of available variables is included in the analysis (e.g. PAR, soil temperature, air temperature, LAI, etc.) (e.g. Urbanski et al., 2007) while other potentially important data are not used (e.g. friction velocity, Normalized Difference

Vegetative Index (NDVI), etc.). From this subset, every variable is typically regressed individually against flux measurements to infer relationships (Law et al., 2002; Hui et al., 2003). Such an approach could lead to environmental variables obscuring each other's effects (Faraway, 2005). For example, Gross Ecosystem Exchange (GEE, which represents the photosynthetic component of NEE) is a function of both air temperature and light (Blackman, 1905). If each variable is regressed separately, the effect of air temperature could mask the effect of light, making this second variable appear not to be significant (Faraway, 2005). This problem can be avoided if joint contributions between auxiliary variables were allowed. Although some studies have included more than one variable in regression analyses (e.g. Hibbard et al., 2005), sequential methods based on F-tests for selecting the variables used in the regression do not account for the joint contributions of all possible combinations of variables.

Second, it is likely that the CO_2 flux regression residuals will be temporally correlated, especially at sub-monthly scales. Ignoring this correlation can lead to a misrepresentation of the relationship between an environmental variable and flux (e.g. Hoeting et al., 2006). As such, temporal correlation must be assessed and included in both the model selection scheme and the statistical regression. Although noted as a limitation (Law et al., 2002), previous studies have not accounted for correlation in regression residuals.

The final limitation is related to the eddy-covariance measurements themselves. Conceptually, NEE is the small difference between two large fluxes, namely photosynthetic carbon uptake via gross ecosystem exchange (GEE) and release of CO_2 into the atmosphere through a combination of heterotrophic and autotrophic respiration (R_{h+a}). Each of these fluxes is affected differently by environmental controls. In addition, variables such as light, nutrient availability, and water stress have complex interactions with each other and with each flux component, making it difficult to ascertain the influence of a particular variable on either GEE or R_{h+a}. In past studies, statistical regression methods (such as simple and multiple linear regression) have been used to infer relationships between flux components (GEE or R_{h+a}) and either a single environmental variable or some predetermined combination of variables (e.g. Law et al., 2002; Urbanski et al., 2007). This requires the measured NEE signal to be separated into

GEE and R_{h+a} prior to the analysis. This is generally achieved using one of three methods: (1) by subtracting the night-time NEE from the day-time NEE signal (Urbanski et al., 2007), (2) by deriving R_{h+a} from a regression using night-time fluxes at high friction velocity and an exponential transformation of soil temperatures (e.g. Law et al., 1999a; Hibbard et al., 2005), or (3) by modeling GEE using photosynthetically active radiation (PAR). Some studies have shown that these methods for dividing NEE into separate parts lead to large uncertainties in the inferred R_{h+a} (e.g. Janssens et al., 2001), possibly biasing inferred relationships.

The research in Chapter 6 involves a new application of a geostatistical regression (GR) (described in Chapter 3) algorithm designed to elucidate processes controlling carbon exchange at various temporal scales at eddy covariance towers at the University of Michigan Biological Station (UMBS). UMBS is one of the few sites where concurrent biometric and NEE measurements have been conducted along with annual assessments of carbon storage based on accounting methods (e.g. Curtis et al., 2002; Gough et al., 2008). GR addresses the first two limitations described above by employing a method to select the variables to include within the regression while also accounting for temporal correlation. In regards to the third limitation, the ability of the GR method to separate the auxiliary variables associated individually with carbon uptake and release is also investigated. The extensive research that has been conducted at UMBS provides a unique context for interpreting the results of the GR analysis.

CHAPTER 3

Methods

1.0 Background of geostatistical methods

Geostatistical techniques, as extensions of traditional statistical models, are powerful, "data-driven" methods used for inference and estimation. However, unlike traditional statistical models that assume that observations are independently and identically distributed (i.i.d.), geostatistics can account for the underlying spatial or temporal correlation in the measurements. In some cases, traditional statistical models use a linear combination of one or more variables (referred henceforward as a model of a trend) to account for correlation in observations. A trend can also be used to estimate statistical relationships between the observation variable (i.e., dependent variable) and those variables in the trend (i.e., auxiliary variables). However, a model of trend still may not be able to capture the full extent variability in the observations due to the lack of explanatory variables or the presence of nonlinear relationships, etc. When this occurs, the residuals, or the portion of the observations that is not explained by the model of the trend, are not random. Non-random residuals can result in biased estimates and Type II errors (e.g. inferring a significant inferred relationship between the dependent and auxiliary variable when it actually it is not significant) (Ravishanker and Dey, 2002). Geostatistical methods have the ability to account for the underlying autocorrelation of the data better than traditional statistics (Chilès and Delfiner 1999).

Geostatistical methods are used in this research to improve the general understanding of natural carbon cycling between the atmosphere and the terrestrial biosphere from currently available data (e.g. NEE measurements, observations of atmospheric CO_2 concentrations, auxiliary variables such as air temperature). Specifically, geostatistical methods allow for (i) the investigation of relationships between surface flux and auxiliary variables (e.g. temperature, net solar radiation), (ii) the assessment of surface flux variability that is not explained by a model of the trend, and

hence (iii) the estimation of CO_2 surface fluxes and associated uncertainties. Importantly, each of these items can be assessed at various spatial and temporal scales using geostatistics so that simplifying assumptions that are known to have a large influence on flux estimates, such as the scaling up of a relationship from one resolution to another, can be avoided. This section provides the background of the geostatistical approaches that form the framework for the specific research components outlined in later chapters.

2.0 The geostatistical model

The geostatistical model views an observed dataset as a regionalized variable representative of a realization from a random, i.e. stochastic, process (Wackernagel, 2003). In this dissertation, the random process refers to the distribution of CO_2 flux in space and/or in time. In this case, a model of the trend (also referred to as a deterministic component) cannot explain the regional variable to the extent to which the residuals exhibit completely random behavior. The geostatistical model assumes that the correlation in the residuals, and therefore the underlying random process, is dependent upon location in both space and time, x (Olea, 1994) of the observations. In other words, measurements that are closer to each other tend to be more similar than the ones taken further apart.

Theoretically, the model of the random process, $\mathbf{S}(x)$ can be expressed as the sum of a deterministic component ($\boldsymbol{\mu}(x)$), or expected value, and a stochastic term (ε_x) representing zero-mean residuals. The first component represents the large scale mean structure and can possibly depend on some variables related to the random process, i.e. auxiliary variables (Huang et al., 2007) while the second seeks to describe the variation in $\boldsymbol{S}(x)$ that cannot be explained by the deterministic component.

$$\mathbf{S}(x) = \boldsymbol{\mu}(x) + \boldsymbol{\varepsilon}_x \tag{3.1}$$

As with multi-linear regression, the deterministic component captures the structure of the random process using a model of the trend. This model can range in complexity from a single average to a linear combination of many variables that are related to $\boldsymbol{S}(x)$. The trend itself is represented as a matrix $\mathbf{X}$ $(m \times k)$ of k auxiliary variables that are scaled by a $(k \times 1)$ vector of unknown drift coefficients ($\boldsymbol{\beta}$). The individual columns in $\mathbf{X}$ also are sometimes referred to as basis functions. Even though

the individual basis functions are linearly related to $\mathbf{S}(x)$ the basis functions themselves can be either linear or nonlinear functions of auxiliary variables, e.g. exp(temperature), sin(latitude), etc. (e.g. Erickson et al., 2005).

Geostatistical methods can be used to estimate the unknown drift coefficients, $\boldsymbol{\beta}$, and their corresponding uncertainties, $\sigma_{\boldsymbol{\beta}}^2$ for inference studies. However, in most cases, geostatistical models infer these relationships to help with estimation of the random variable, (e.g. CO_2 flux) at specific unsampled locations and/or times. The estimates, $\hat{\mathbf{s}}$, are representative of a spatial or temporal resolution (e.g. monthly estimate of CO_2 for a 1°x1° area) henceforward referred to as the scale of estimation.

As mentioned, the second part of equation (3.1) ε_x, models the residuals or portion of the random process that cannot be explained by the model of the trend. In traditional statistics, it is assumed that residuals are identically and independently distributed (i.i.d.) as well as Gaussian. However, in most environmental processes, including the distribution of CO_2 flux, the residuals are generally spatially and/or temporally correlated, especially as the scale of estimation becomes smaller. If the residuals are second-order stationary, i.e. they have a constant mean and the covariance of a pair of residuals is only dependent upon the distance between their two locations (pictorially shown in Figure 3.1), the correlation in the residuals can be modeled using a stationary variogram (e.g. Cressie, 1993). The variogram of the residuals is given by:

$$\gamma(h_{i,j}) = (1/2)\mathrm{E}[(\varepsilon(x_i) - \varepsilon(x_j))^2] \tag{3.2}$$

where $h_{i,j}$ is the scalar separation distance between locations x_i and x_j, $\gamma(h_{i,j})$ is the semivariance for points separated by a distance $h_{i,j}$, and E[ ] denotes the expected value operator.

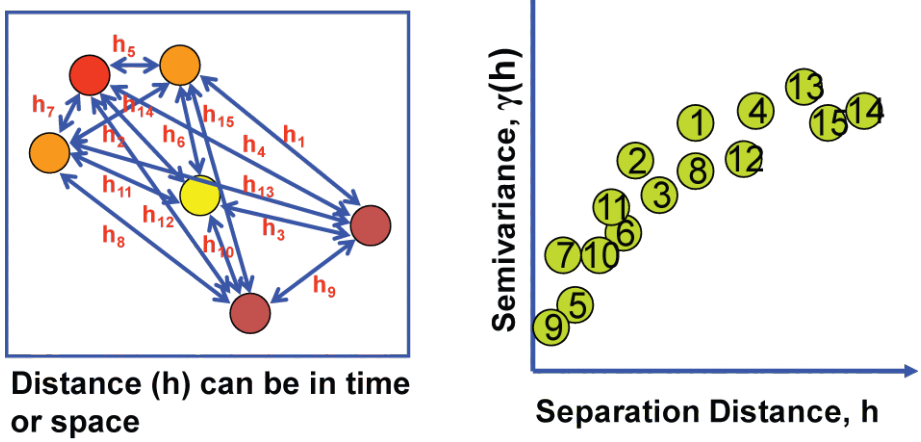

Figure 3.1: Illustration of correlation of residuals is a function of their location. The colors of the circles in the left plot indicate different residual values. The plot on the right represents the squared difference of the residual values as a function of their separation distance (equation 3.2). The plot is adapted from a version by Tyler Erickson.

There are many types of variogram functions that are available to model the expected behavior of the residuals in equation (3.2) (e.g. Chilès and Delfiner, 1999). However, the exponential variogram function has been shown to aptly model the spatial semivariance of surface CO_2 flux and their residuals (Michalak et al., 2004; Mueller et al., 2008; Gourdji et al., 2008) and is defined as:

$$\gamma(h_{i,j}|\sigma_{\mathbf{Q}}^2, l_{\mathbf{Q}}) = \sigma_{\mathbf{Q}}^2\left[1 - exp\left(-\left(\frac{h_{i,j}}{l_{\mathbf{Q}}}\right)\right)\right] \quad (3.3)$$

The practical range of correlation is approximately $3l_{\mathbf{Q}}$, beyond which $\sigma_{\mathbf{Q}}^2$ represents the expected variance of independent flux residuals. An exponential model assumes spatial correlation while also allowing for continuous but not differentiable small-scale variability. The corresponding covariance function is:

$$Q_{i,j}(h_{i,j}|\sigma_{\mathbf{Q}}^2, l_{\mathbf{Q}}) = \sigma_{\mathbf{Q}}^2 exp\left[-\left(\frac{h_{i,j}}{l_{\mathbf{Q}}}\right)\right] \quad (3.4)$$

The exponential variogram can be modified to model the temporal semivariance of CO_2 measurements and their residuals (Mueller et al., 2010) so that the corresponding covariance function becomes:

$$Q\left(h_{i,j}|\sigma_{n,Q}^2,\sigma_{\mathbf{Q}}^2,l_{\mathbf{Q}}\right)=\begin{cases}\sigma_{n,Q}^2+\sigma_Q^2, & h_{i,j}=0\\ \sigma_Q^2 exp\left(-\frac{h_{i,j}}{\tau_Q}\right), & h_{i,j}>0\end{cases} \quad (3.5)$$

where the practical temporal range of correlation is approximately 3τ, beyond which $\sigma_{n,Q}^2, +\sigma_Q^2$ represents the variance of independent flux residuals. The nugget, $\sigma_{n,Q}^2$, represents variability at time scales below the averaging time used for the observation and measurement error. The nugget, $\sigma_{n,Q}^2$, is not unique to temporal analysis, but is not included in Equation 3.4 as the variability at spatial distances that are less than the smallest separation distance between flux estimates is assumed to be zero and uncorrelated.

3.0 Geostatistical approaches

The specific applications used in this research are (i) geostatistical regression (GR) and (ii) geostatistical inversion modeling (GIM). The principle difference between these two methods is whether the random process that is being modeled is sampled directly (GR) (as with eddy-covariance measurements) or indirectly (GIM) (as with atmospheric observations of CO_2). This difference affects how each model is able to deal with the resolution of data and estimates. For example, for GR, as with multilinear regression, all auxiliary and dependent variables have the same spatial and temporal scale and are collected at coincident locations and times. Conversely, GIM (as is the case with all inversions) translates information across temporal and spatial scales because the observations are made at an earlier time and at a different location than either auxiliary variables or estimations. In GIM, the observations are linked to the auxiliary variables and estimates using an atmospheric transport model.

Both methods are considered best linear unbiased estimation (BLUE) methods where the estimates yield the lowest mean square error (e.g. Kitanidis, 1997). Assuming that the residuals are normally distributed, both geostatistical regression (GR) and the geostatistical inverse approach (GIM) can be generally expressed mathematically (presented in a similar manner in Zhou et al. (2009)) as:

$$\begin{bmatrix}\mathbf{\Omega} & \mathbf{F}\\ (\mathbf{F})^T & \mathbf{0}\end{bmatrix}\begin{bmatrix}\mathbf{\Lambda}^T\\ \mathbf{M}\end{bmatrix}=\begin{bmatrix}\mathbf{\Omega_o}\\ \mathbf{F_o}^T\end{bmatrix} \quad (3.6)$$

Table 3.1 defines $\mathbf{\Omega}$, $\mathbf{\Omega}_0$, $\mathbf{F}$, and $\mathbf{F}_0$ for each application:

Table 3.1: Components for Geostatistical Regression (GR) and Geostatistical Inverse Modeling (GIM)

	$\boldsymbol{\Omega}$	$\boldsymbol{\Omega}_0$	$\mathbf{F}$	$\mathbf{F}_0^T$
GR	$\mathbf{Q}_{(nxn)}$	$\mathbf{Q}_{(nxn)}$	$\mathbf{X}_{(nxk)}$	$\mathbf{X}_{(kxn)}^T$
GIM	$\mathbf{H}_{(nxm)}\mathbf{Q}_{(mxm)}\mathbf{H}_{(mxn)}^T + \mathbf{R}_{(nxn)}$	$\mathbf{H}_{(nxm)}\mathbf{Q}_{(mxm)}$	$\mathbf{HX}_{(nxk)}$	$\mathbf{X}_{(kxm)}^T$

In this table, m denotes the number of flux estimates for the GIM approach while the number of observations is n for both methods. As such, **Q** represents the covariance matrix characterizing the spatiotemporal covariance of the residuals for GIM and GR using equation (3.4 or 3.5). As mentioned in Section 2.0, **X** defines the k components, or covariates, of the spatiotemporal model of the trend and is $(m \times k)$ for GIM and $(n \times k)$ for GR. $\boldsymbol{\beta}$ is a $k \times 1$ vector of unknown drift coefficients that scale the components in **X**. As such, $\mathbf{X}\boldsymbol{\beta}$ is the resulting trend, where $\boldsymbol{\beta}$ is estimated as part of the inversion process or regression. For GIM, **H** is a $n \times m$ matrix defining the sensitivity of each CO_2 concentration measurement to an estimated surface flux location as derived from an atmospheric transport model. The **H** matrix is used in the inversion to translate observational information across temporal and spatial scales into flux space.

The model data mismatch covariance matrix **R** (which is only employed in GIM in this work) is usually modeled as a diagonal matrix which assumes the variances along the diagonal are independent from one another. The diagonal entries σ_R^2 represent errors associated with measurement, transport, aggregation, and representation errors for each observation. As described in Chapter 2, Section 2.1, aggregation errors occur when fluxes are estimated at spatial and temporal resolutions that are too coarse to account for the sensitivity of observations only to a small portion of the underlying flux variability (Kaminski et al., 2001). Representation errors refer specifically to the mismatch in scale between a point-based measurement of CO_2 and the coarser resolution of the transport model and driving meteorology (e.g. Tolk et al., 2008). Further descriptions of each of these components as applied to the specific research of the dissertation are presented in relevant Chapters.

The set of covariance parameters ($\theta_{\mathbf{Q}}$) can include $\sigma_{n,Q}^2, \sigma_Q^2, \tau_Q, l_{\mathrm{Q}}$ but the specific set depends on the specific geostatistical application. For GIM, the set of covariance parameters (θ_R) is the number of different σ_R^2 in the diagonal. Parameters ($\theta_{\mathbf{Q,R}}$) for both the spatiotemporal covariance matrix (**Q**) and model data mismatch covariance matrix (**R**) are optimized using the Restricted Maximum Likelihood method presented in Section 5.0.

For GIM, solving the linear system in equation 3.6 yields the weights $\mathbf{\Lambda}$ $(m \times n)$ and Lagrange multipliers, **M** $(k \times m)$. $\mathbf{\Lambda}$ and **M** and are used to define the flux estimates ($\hat{\mathbf{s}}$) using the measurements, **z** (e.g. Kitanidis 1995; Michalak et al., 2004), as:

$$\hat{\boldsymbol{s}} = \mathbf{\Lambda z}, \tag{3.7}$$

Alternatively, the flux estimates (*a posteriori*) can be expressed in the same manner as equation 3.1. That is, the fluxes can be considered as the sum of the deterministic model of the trend ($\mathbf{X}\widehat{\boldsymbol{\beta}}$) and a spatiotemporally correlated stochastic component:

$$\hat{\mathbf{s}} = \mathbf{X}\widehat{\boldsymbol{\beta}} + \mathbf{Q}\mathbf{H}^T(\mathbf{H}\mathbf{Q}\mathbf{H}^T + \mathbf{R})^{-1}\left(\mathbf{z} - \mathbf{H}\mathbf{X}\widehat{\boldsymbol{\beta}}\right) \tag{3.8}$$

The uncertainties associated with the flux estimates along with the covariances between flux uncertainties are provided the following covariance matrix (*a posteriori*):

$$\mathbf{V}_{\hat{s}} = -\mathbf{F}_0\mathbf{M} + \mathbf{\Omega} - \mathbf{\Omega}_{\mathrm{o}}^T\mathbf{\Lambda}^T \tag{3.9}$$

The estimates of the drift coefficients, $\widehat{\boldsymbol{\beta}}$, and their uncertainty covariance ($\mathbf{V}_{\widehat{\boldsymbol{\beta}}}$) are calculated as in Chilès and Delfiner (1999), as:

$$\widehat{\boldsymbol{\beta}} = (\mathbf{F}^T\mathbf{\Omega}^{-1}\mathbf{F})^{-1}\mathbf{F}^T\mathbf{\Omega}^{-1}\mathbf{y} \tag{3.10}$$

$$\mathbf{V}_{\widehat{\boldsymbol{\beta}}} = (\mathbf{F}^T\mathbf{\Omega}^{-1}\mathbf{F})^{-1} \tag{3.11}$$

where $\boldsymbol{y}$ is either the best estimates in the case of GIM (i.e. $\mathbf{\Lambda z}$) or the measurements **z**, for GR. The diagonal elements of $\mathbf{V}_{\widehat{\boldsymbol{\beta}}}$ represent the uncertainties associated with the drift coefficients and the off-diagonal terms in $\mathbf{V}_{\widehat{\boldsymbol{\beta}}}$ represent their error covariances between $\widehat{\boldsymbol{\beta}}$**'s**.

GIM will be used in Chapters 4 and 5 to assess the information content of both global and regional observational networks to estimate monthly flux at continental and regional scales, respectively. Chapter 6 presents the first application of GR to investigate

the temporal scale dependency of the statistical relationships between auxiliary variables and eddy covariance flux estimates.

4.0 Variable selection techniques

As mentioned, the model of the trend is one of two portions of the geostatistical model. As such, it is important to correctly identify the variables to include within **X**. As noted by Burnham and Anderson (1998), identifying the structure of the deterministic component is conceptually more difficult than estimating drift coefficients and associated uncertainties. Traditionally, candidate models that include different sets of auxiliary explanatory variables are chosen based on mechanistic studies, or general knowledge of the problem. The challenge is to choose the appropriate dimensionality of a model that will fit a given set of observations (Schwarz, 1978). On one hand, as more variables are added to the model of the trend, the deterministic component is better able to capture the variability in the observations. On the other hand, although the fit of the model to the data will invariably improve with additional parameters, some of these may serve only to reproduce spurious correlations (Forster, 2000), thereby confounding the analysis. Therefore, the overall aim is to balance the amount of variability explained by adding variables to the trend along with the loss of the degrees of freedom inherent to a more complex model.

One of the most widely used model selection techniques is the Bayes Information Criterion (BIC) (Schwarz, 1978) because it is able to evaluate non-nested competing models and their joint probabilities (Ward, 2008). This method does not use the traditional hypothesis testing paradigm and, therefore, cannot be used to make conclusions regarding the statistical significance of a parameter or reject a particular model. Instead, BIC ranks how well the data supports each model, taking into account both the goodness of fit, i.e. sum of the squared residuals, and the number of variables in each candidate model. BIC is generally favored over other information criteria methods when explanation and inference (not solely prediction) are of principle interest (Wasserman, 2000) because it penalizes the loss of degrees of freedom more than other methods, resulting in a smaller model.

BIC is loosely based on the idea that candidate models should be compared by their posterior probabilities, which, when the prior odds of each model are equal is

equivalent to Bayes factors (Wasserman, 2000). The BIC or Schwarz criterion (Schwarz, 1978) of a particular model, $\mathbf{X}_j$, of k_j auxiliary variables and n NEE measurements is given by:

$$BIC_j = -2ln(\hat{L}_j) + kln(n) \tag{3.12}$$

Assuming that the residuals follow a Gaussian distribution, the likelihood of a particular model is given by:

$$\hat{L}_j(\mathbf{X}_j\widehat{\boldsymbol{\beta}}_j|\mathbf{y}) = \frac{1}{2\pi^{\frac{1}{n}}|\boldsymbol{\Omega}|^{\frac{1}{2}}} exp\left[-\tfrac{1}{2}(\mathbf{y}-\mathbf{X}_j\boldsymbol{\beta})^T\boldsymbol{\Omega}^{-1}(\mathbf{y}-\mathbf{X}_j\boldsymbol{\beta})\right], \tag{3.13}$$

where n is the number of observations, $\mathbf{y}$ is either the best estimates in the case of geostatistical inversion modeling (i.e. $\boldsymbol{\Lambda}\mathbf{z}$) or the measurements $\mathbf{z}$ for geostatistical regression, and $\boldsymbol{\beta}$ are the unknown drift coefficients. $\boldsymbol{\Omega}$ is the spatio-temporal covariance matrix given by equation (3.5) whose parameters ($\theta_{\mathbf{Q,R}}$), are estimated using Restricted Maximum Likelihood method presented in Section 5.0. The negative log-likelihood of equation (3.13) is:

$$-ln\hat{L}_j(\mathbf{X}_j\widehat{\boldsymbol{\beta}}_j|\mathbf{y}) = \tfrac{n}{2}\ln(2\pi) + \tfrac{1}{2}\ln|\boldsymbol{\Omega}| + \tfrac{1}{2}(\mathbf{y}-\mathbf{X}\boldsymbol{\beta})^T\boldsymbol{\Omega}^{-1}(\mathbf{y}-\mathbf{X}\boldsymbol{\beta}). \tag{3.14}$$

As seen in Kitanidis (1997) and Hoeting et al. (2006), the third term can be modified to remove any bias associated with the unknown drift coefficients, $\boldsymbol{\beta}$, by setting $\boldsymbol{\beta} = (\mathbf{X}^T\boldsymbol{\Omega}^{-1}\mathbf{X})^{-1}\mathbf{X}^T\boldsymbol{\Omega}^{-1}\mathbf{y}$. After removing the constant term, replacing $\boldsymbol{\beta}$, rearranging terms, and combining with equation (3.13), the newly adapted BIC equation that can account for correlated residuals becomes:

$$BIC_j = \ln|\boldsymbol{\Omega}| + [\mathbf{y}^T(\boldsymbol{\Omega}^{-1} - \boldsymbol{\Omega}^{-1}\mathbf{X}(\mathbf{X}^T\boldsymbol{\Omega}^{-1}\mathbf{X})^{-1}\mathbf{X}^T\boldsymbol{\Omega}^{-1})\mathbf{y}] + k\ln(n). \tag{3.15}$$

For GR, in the special case of independent residuals, $\boldsymbol{\Omega} = \mathbf{Q} = \sigma^2\mathbf{I}$, where $\mathbf{I}$ is an identity matrix, and equation (3.14) reduces to the more conventional form where RSS is the residual sum of squares:

$$BIC_j = -n\ln\tfrac{RSS}{n} + k\ln(n) \tag{3.16}$$

For conventional BIC applications, it is assumed that the set of true explanatory variables and the observations, conditioned on these variables, are independent and identically distributed, i.e. in the geostatistical regression case, $\mathbf{\Omega} = \mathbf{Q} = \sigma^2\mathbf{I}$. However, as of yet, a BIC has not been applied for spatially nor for temporally correlated residuals (Huang, 2007). This dissertation presents the first study of this modified BIC approach.

Equation (3.14) and the BIC approach for identifying the model of the trend is used in Chapter 6 to identify the set of variables that best explain the variability in eddy covariance fluxes at daily, seasonal, and inter-annual timescales. The method was designed and developed for this dissertation and therefore, is an overall contribution of the research. Note that the approach was further extended and applied to a geostatistical inversion approach mentioned in Chapter 5 but is not a part of this dissertation research.

5.0 Restricted Maximum Likelihood (RML)

Along with the deterministic component (**Xβ**) in equation (3.8) and equation (3.10), the model-data mismatch, **R**, (for GIM) and spatiotemporal covariance, **Q** (for GIM and GR) matrices, and thereby their respective covariance parameters, play a critical role in the geostatistical model. The Restricted Maximum Likelihood (RML) approach (e.g. Kitanidis, 1995) provides an objective means for identifying covariance parameters that maximize the likelihood of available observations, **z**. In practice, RML minimizes the negative logarithm of the likelihood of the available data with respect to a set of parameters $\theta_{\mathbf{Q,R}}$ (e.g. in equation 3.4, optimizing for τ, $\sigma_{n,Q}^2, \sigma_Q^2$) yielding the following objective function:

$$L_{\theta_{\mathbf{Q,R}}} = (1/2)ln|\mathbf{\Omega}| + (1/2)ln|\mathbf{F}^T\mathbf{\Omega}^{-1}\mathbf{F}| + (1/2)\mathbf{z}^T(\mathbf{\Omega}^{-1} - \mathbf{\Omega}^{-1}\mathbf{F}(\mathbf{F}^T\mathbf{\Omega}^{-1}\mathbf{F})^{-1}\mathbf{F}^T\mathbf{\Omega}^{-1})\mathbf{z} \quad (3.17)$$

All terms are as described in Table 3.1. RML accounts for the loss in degrees of freedom associated with the estimation of the deterministic component, i.e. **Xβ** and therefore, provides unbiased estimates of the covariance parameters (Swallow and Monahan, 1984). RML is used in Chapters 4, 5, and 6 to optimize for the covariance parameters used in both GR and GIM.

6.0 Goodness of fit (χ^2) test for GIM

A goodness of fit test, i.e. χ^2 test, can be used with GIM to assess whether the optimized covariance parameters from RML, $\theta_{\mathbf{Q,R}}$, are consistent with the amount of variability in the flux estimates. The χ^2 is calculated using the covariance parameters, $\theta_{\mathbf{R}}$, (used to characterize the portion of the flux not explained observations) with the following equation:

$$\chi^2 = (1/n)(\mathbf{z} - \mathbf{H}\mathbf{s}_{ci})^T \mathbf{R}^{-1}(\mathbf{z} - \mathbf{H}\mathbf{s}_{ci}) \quad (3.18)$$

since the $(\mathbf{z} - \mathbf{H}\mathbf{s}_{ci})$ from GIM should follow a χ^2 distribution Michalak et al (2004). $\mathbf{s}_{ci}$ are conditional realizations, $\mathbf{z}$ are observations of atmospheric CO_2 and n is the total number of observations used in the inversion. A conditional realization is an equally likely flux distribution that follows the correlation structure, **Q**, and reproduces the observations **z** within the measurement error as provided in **R** (Michalak et al. 2004). Tarantola (2005) describes that the χ^2 values are expected to be close to 1. If the values of χ^2 are much larger than 1, the covariance parameters $\theta_{\mathbf{R}}$ underestimate the ability of the inversion to reproduce the variability in the observations whereas if they are much lower than 1, the inversion is able to reproduce the measurements more accurately than the covariance parameters suggest. As such, χ^2 values can provide a means to verify that the covariance parameters (as optimized by RML) are consistent with the inversion setup.

7.0 Advantages and limitations of the geostatistical approach

As shown throughout the Chapter, one of the distinct advantages the geostatistical approaches has over other Bayesian inversion and regression methods is that the approach maximizes the extent to which the observations can inform each component of the geostatistical model. For example, covariance parameters that have been specified in previous studies using "expert knowledge" are optimized using the atmospheric observations using RML. In addition, the geostatistical approach uses more statistical approach for selecting variables to include within the model of the trend compared to other regression studies. As such, estimates (both fluxes and drift coefficients) as well as their associated uncertainties reflect the information content of the atmospheric observation to infer carbon cycling dynamics.

Because the estimates and uncertainties are data-driven they reflect the information regarding source and sink distribution contained within the observations including the limitations of the measurements. For example, with GIM we expect that flux estimates in poorly-constrained regions to revert to the model of the trend while having wide associated uncertainty bounds. In addition, any uncertainty associated with the relationship between flux and a variable in the trend in GR will be included in the uncertainty estimates. That is, any error that is associated with an auxiliary variable will ultimately reduce the significance within the trend. Therefore, the geostatistical approach is not the best choice for every study that aims to investigate carbon cycling. Nevertheless, the geostatistical methods are very useful for research, as with this dissertation, that involves assessing the degree to which atmospheric data themselves can constrain fluxes or statistical relationships. The methods are also useful for obtaining more independent estimates from inversions, which is not possible using a synthesis Bayesian setup. As mentioned in Chapter 1, independent estimates are necessary for inter-comparison studies with process-based models.

The geostatistical approach, like any model, has assumptions in both the deterministic and stochastic components that have the ability to impact estimates. First, the model of the trend in GR assumes a linear relationship between the variables and flux. As noted in Section 2.0, the model of the trend can contain nonlinear functions of auxiliary variables (e.g. exp(temperature)) but if the nonlinear relationship is unknown, it may be difficult to detect using the geostatistical approach or any statistical method for that matter. In addition, in GR, there is uncertainty associated with selecting a single "best" model of the trend when multiple sets of auxiliary variables provide comparable fits to the available observations. Finally, for estimation, the model relies heavily on the statistical model of the trend, estimated by the observations in well constrained areas, to regions that are not well covered by the network. If the relationship between an auxiliary variable and flux is significantly different in the under-constrained area, then fluxes will be biased in areas with few measurement locations.

The other major assumptions of the geostatistical model involve the stochastic component. For example, in GIM as in most inversions, the structure of the covariance matrices assumes that the errors associated with transport and measurement are random

and independent from one another. At finer spatial and temporal scales (as will be used in Chapter 5), this assumption may be violated as we know that the simulated regional transport has systematic errors due to representing more complex atmospheric behavior such as development of the planetary boundary layer (PBL) height throughout the course of the day. In addition, some observation, especially those made at a high frequency, may have calibration drifts. Any systematic errors associated with measurements and transport could bias both flux and uncertainty results from GIM or from most inversion models for that matter.

In addition, the spatiotemporal covariance matrix assume that the difference in the magnitudes of the fluxes decays exponentially in all directions (in either space as in GIM or in time as in GR) and becomes constant beyond a correlation range defined by the correlation length covariance parameter. However, it is likely that fluxes have multiple scales of variability. In this case, the optimized spatiotemporal covariance parameters would be overestimated or underestimated, negatively impacting both flux and uncertainty estimates. Again, a violation of this assumption is more likely at finer spatiotemporal scales.

Many sensitivity tests were conducted for each study presented in this dissertation to try to assess the impact of many of the assumptions of the geostatistical applications. Although not shown for the sake of brevity within each Chapter, most of the major limitations were assessed and addressed for each objective. Chapter 7 will outline future work required to address the major limitations that remain in terms of applying the geostatistical approach to infer carbon cycling dynamics.

CHAPTER 4

Global monthly averaged CO_2 fluxes recovered using a geostatistical inverse modeling approach

This Chapter addresses objective 1 of the dissertation and involves the use of atmospheric CO_2 observations to estimate global monthly CO_2 surface flux at a 3.75° latitude × 5° longitude resolution for 1997-2001. Overall, this research quantifies the degree to which the global observational network can inform the distribution of CO_2 fluxes at various spatial and temporal scales.

1.0 Introduction

As discussed in Section 2.1.1 in Chapter 2, flux estimates and uncertainties derived from atmospheric inversions are sensitive to *a priori* assumptions, such as the selection of observations, the transport model, prior information, prescribed flux patterns, and error covariance parameters. These differences lead to the observed inconsistencies between reported flux estimates from various inversion studies. There is a growing awareness of the strong influence of these assumptions, especially in regards to the use of explicit prior flux estimates from bottom-up models to define the magnitude and spatial distribution of fluxes (e.g., Michalak et al., 2004; Rödenbeck, 2005). This influence not only contributes to aggregation errors, but can also cause *a posteriori* estimates to revert to prior assumptions in underconstrained regions. As such, estimates from synthesis Bayesian inversions cannot be used directly to reconcile process-based understanding of flux behavior with the information content of atmospheric observations. The sensitivity of estimates to other assumptions has also been recognized, with researchers attempting to systematically quantify the magnitude and impact of model-data mismatch and *a priori* flux uncertainties (e.g., Engelen et al., 2002; Engelen, 2006; Krakauer et al., 2004; Michalak e al., 2005).

Owing to the strong influence of inverse modeling assumptions on estimated sources and sinks, there is a need for an inverse modeling approach for CO_2 flux

estimation that can more directly reflect the information content of available atmospheric measurements. Such an approach, based on a geostatistical inverse modeling framework, was proposed by Michalak et al. (2004). This method aims to reduce the influence of modeling assumptions by (1) avoiding the use of bottom-up flux estimates for defining the magnitude and spatial patterns of fluxes, (2) estimating sources and sinks at resolutions that minimize the risk of aggregation errors, and (3) using a rigorous statistical framework for quantifying model-data mismatch and the degree of spatial autocorrelation in the flux distribution. In this manner, the approach yields CO_2 flux estimates that are more strongly representative of the spatial and temporal variability of CO_2 fluxes as seen through the atmospheric measurement network.

This work presents the first application of the geostatistical inverse modeling approach for estimating CO_2 fluxes using atmospheric observations. The objectives of this work are to (1) explore the ability of the approach to constrain global fluxes with a level of uncertainty comparable to synthesis Bayesian inversions, (2) identify the information content of available observations with regard to the global CO_2 flux distribution and its variability at various spatial and temporal scales, and (3) elucidate the impact of prior assumptions used in synthesis Bayesian inversions on flux estimates from previous studies.

Monthly-averaged CO_2 fluxes are estimated at the resolution of the implemented atmospheric transport model, 3.75° latitude by 5° longitude, for 1997-2001, using observations from a subset of the NOAA-ESRL cooperative air sampling network. To further avoid the use of *a priori* assumptions, fossil fuel fluxes are not assumed known, contrary to past inverse modeling studies. Instead, this research estimates total flux, including biospheric, oceanic, and anthropogenic contributions, which avoids the possibility of aliasing the uncertainties and seasonality of fossil fuel emissions (Gurney et al., 2005) onto the estimated biospheric or oceanic flux signal. Estimated fluxes are compared at various spatial and temporal scales to bottom-up estimates of biospheric (Randerson et al. 1997), oceanic (Takahashi et al., 2002), and fossil fuel (Brenkert 1998) fluxes, as well as estimates from the synthesis Bayesian inversion estimates of the TransCom3 Level 3 intercomparison (Baker et al., 2006) and the Rödenbeck et al. (2003) study. A companion piece of work (Gourdji et al., 2008) explores the ability of auxiliary

environmental variables (e.g. air temperature, leaf area index, etc.) to further constrain flux distributions within the geostatistical inverse modeling framework, especially at fine spatial resolutions. This companion work will not be presented as part of this dissertation but a summary of the findings from Gourdji et al (2008) is presented in Chapter 7.

2.0 Methods

The surface flux estimates presented in this chapter are obtained using a geostatistical inverse modeling approach (GIM); a full description of this method and the overall algorithm are presented in Michalak et al. (2004).

The GIM approach involves minimizing the following objective function:

$$L_{s,\beta} = \frac{1}{2}(\mathbf{z}+\mathbf{Hs})^T\mathbf{R}^{-1}(\mathbf{z}+\mathbf{Hs}) + \frac{1}{2}(\mathbf{s}+\mathbf{X\beta})^T\mathbf{Q}^{-1}(\mathbf{s}+\mathbf{X\beta}) \quad (4.1)$$

where the vector $\mathbf{z}$ $(n \times 1)$ represents the atmospheric CO_2 measurements, and $\mathbf{s}$ $(m \times 1)$ is the vector of unknown best estimates of surface fluxes. $\mathbf{H}$ $(n \times m)$ contains the sensitivity of CO_2 measurements to surface fluxes as derived from an atmospheric transport model (further described in Section 4.2), with units of $\mathrm{ppm}/(\mu\mathrm{mol}/(\mathrm{m}^2\mathrm{s}))$. $\mathbf{X}$ is a known $(m \times k)$ matrix which is the model of the trend. $\boldsymbol{\beta}$ are $(k \times 1)$ unknown drift coefficients, so that $\mathbf{X}\widehat{\boldsymbol{\beta}}$ is the resulting trend. The two covariance matrices in the objective function, $\mathbf{R}$ $(n \times n)$ and $\mathbf{Q}$ $(m \times m)$, balance the relative weight of the atmospheric data and the trend in the estimate on of fluxes, $\hat{\mathbf{s}}$. The structure of $\mathbf{R}$ and $\mathbf{Q}$ covariance matrices are further described in Section2.4 and 2.5.

Chapter 3 presents a further summary of the method presenting the system of linear equations (3.6) used to estimate the best estimates ($\hat{\mathbf{s}}$, 3.7), drift coefficients ($\widehat{\boldsymbol{\beta}}$, 3.10), and their associated uncertainties ($\mathbf{V}_{\hat{s}}$, 3.9 and $\mathbf{V}_{\widehat{\boldsymbol{\beta}}}$, 3.11).

A schematic (Figure 4.1) is presented herein to help the reader understand the different model extensions. In this work, the geostatistical approach is used to estimate monthly CO_2 surface fluxes from January 1997 to December 2001 at a 3.75° latitude by 5° longitude resolution. Overall, the inversion estimates 3456 monthly fluxes for a total of 207,360 unknowns, using 2275 known observations from 44 measurement locations.

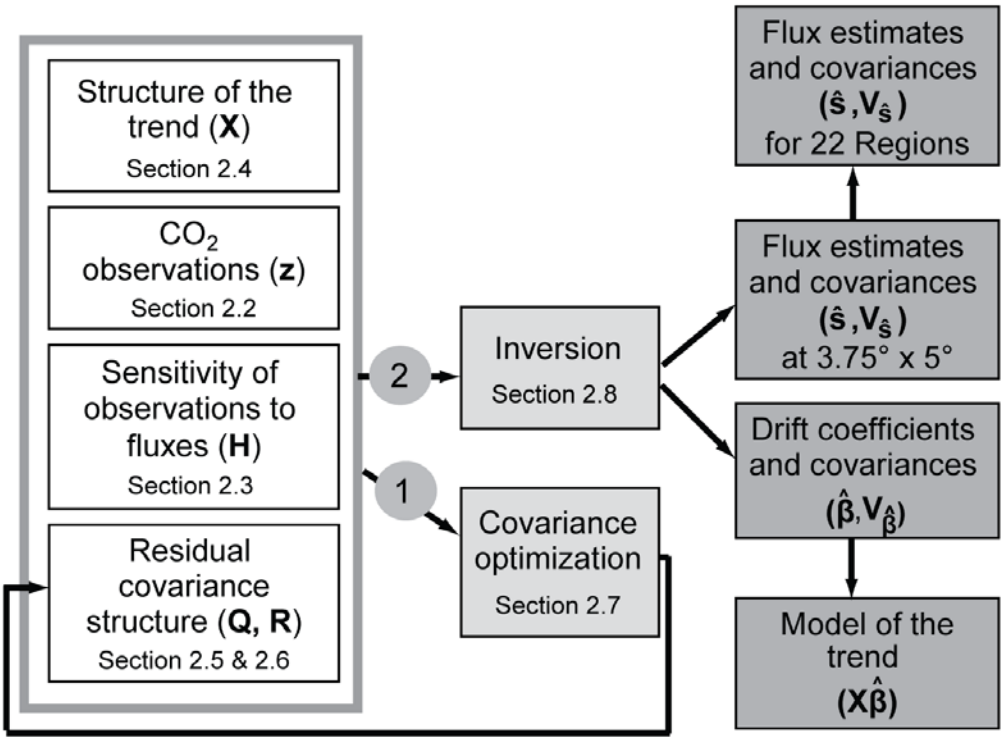

Figure 4.1: Schematic of geostatistical inversion components and algorithm. White boxes indicate inversion inputs, light gray boxes indicate inversion steps, and dark gray boxes represent inversion outputs. Gray circles indicate the sequence of steps in the algorithm.

2.1 Observational data (z)

Fluxes are estimated using monthly-averaged CO_2 concentration measurements from 44 of the measurement locations in the NOAA Earth System Research Laboratory (ESRL) Global Monitoring Division cooperative air sampling network (Tans and Conway, 2005) as shown in Figure 4.2. The number of measurements for any given month ranges from 35 to 42, as some locations have missing data during the examined time period.

The subset of the observational network used in this application is similar to that used in Rödenbeck et al. (2003), who used measurements from locations with observational data gaps of less than two months to ensure spatial and temporal consistency. Although this approach limits the number of measurement sites used in the

analysis, it reduces the risk of flux estimates being unduly affected by monthly changes in the monitoring network (Law et al., 2003; Rödenbeck et al., 2003). Two stations, SYO (Syowa Station, Antarctica, Japan) and GOZ (Dwejra Point, Gozo, Malta), are added to the measurement network used in Rödenbeck et al. (2003).

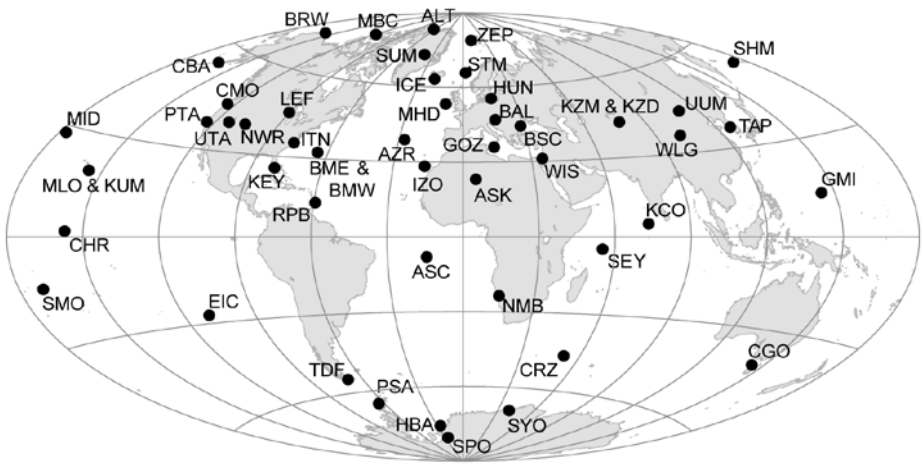

Figure 4.2: NOAA-ESRL cooperative air sampling network measurement locations (Tans and Conway, 2005) used in the current study. Note that some locations do not have measurements for all months.

2.2 Transport model (H)

Linear inverse modeling requires the formulation of a Jacobian matrix, H, representing the sensitivities of observations at each measurement location-month to a pulse of CO_2 emitted at each estimation location-month. This Jacobian matrix was derived from an adjoint implementation of the TM3 transport model (Heimann and Körner, 2003) which has a spatial resolution of 3.75° latitude by 5° longitude, 19 vertical levels and inter-annually varying winds derived from the National Centers for Environmental Prediction (NCEP) Reanalysis (Kalnay et al., 1996). Transport information relating monthly-averaged CO_2 observations to monthly grid-scale fluxes were calculated by Rödenbeck et al. (2003) for 1982-2001, and the subset for 1997 to 2001 is used here.

2.3 Model of the trend (Xβ)

The flux distribution (**s**) and the drift coefficients (**β**) are estimated concurrently as part of the inversion. The resulting estimated model of the trend (**Xβ**) represents the expected spatiotemporal pattern in the flux distribution:

$$\mathrm{E}(\mathbf{s}) = \mathbf{X}\boldsymbol{\beta} \tag{4.2}$$

The estimated *a posteriori* fluxes ($\hat{\mathbf{s}}$) are defined as the sum of this deterministic component (**Xβ**) and a stochastic component, which is a function of the *a priori* correlation structure in **Q** as described in Section 2.3. Hence **Xβ**, along with the *a posteriori* fluxes and uncertainties, largely reflects the information content of the atmospheric observations.

For this application, the structure of the trend (**X**) assumes a constant mean flux for all land and all ocean regions, as in the Michalak et al. (2004) study. However, in this study, the mean land and ocean flux is allowed to vary seasonally, with a different average for each calendar month. As such, the **X** matrix has dimensions $m \times 24$, where within each column, all elements are zero except for ones corresponding to land or ocean gridcells for a given calendar month. Thus, the expected value of surface fluxes for any gridcell and month is ultimately represented by a single unknown **β**, corresponding to a particular monthly mean of land or ocean flux. Note that the Gourdji et al., 2008 companion work incorporates auxiliary environmental variables into the model of the trend in order to better define grid-scale flux variability in the spatiotemporal trend.

2.4 Spatial covariance matrix (Q)

The covariance matrix **Q** $(m \times m)$ defines the *a priori* spatiotemporal autocorrelation of flux deviations from the unknown trend (**Xβ**) at the scale of the *a posteriori* flux estimates. In the current implementation, spatial but not temporal correlation is assumed *a priori*. Therefore, the **Q** matrix is block diagonal, with each block $\mathbf{Q}_{i,i}$ having dimensions $(m_i \times m_i)$, where $m_i = 3456$, i.e. the number of fluxes estimated every month at a 3.75° × 5° resolution. Each block represents the spatial covariance between flux residuals at all pairs of estimation locations within a given month. No *a priori* temporal correlation was assumed to avoid unrealistic smoothing of

relatively fast events such as leaf-out in spring. The same block is repeated for all months of the inversion, i.e. $\mathbf{Q}_{1,1} = \mathbf{Q}_{2,2} = \cdots = \mathbf{Q}_{60,60}$:

$$\mathbf{Q} = \begin{bmatrix} \mathbf{Q}_{1,1} & \mathbf{0} & \cdots & \mathbf{0} \\ \mathbf{0} & \mathbf{Q}_{2,2} & \mathbf{0} & \vdots \\ \vdots & \vdots & \ddots & \vdots \\ \mathbf{0} & \mathbf{0} & \cdots & \mathbf{Q}_{60,60} \end{bmatrix} \tag{4.3}$$

The covariance is assumed to decay exponentially with separation distance:

$$\mathrm{Q_{i,j}}\left(h_{i,j}|\sigma^2, l\right) = \sigma_Q^2 exp\left(-\frac{h_{i,j}}{l_Q}\right) \tag{4.4}$$

where $h_{i,j}$ is the separation distance between two estimation locations, σ_Q^2 is the variance of flux residuals at large separation distances, and l is the correlation range parameter such that the covariance approaches zero for separation distances on the order of $3l$. The choice of the exponential covariance function is based both on the work of Michalak et al. (2004) and on a variogram analysis of the spatial variability of typical land and ocean bottom-up estimates. An exponential model assumes spatial correlation while also allowing for continuous but not differentiable small-scale variability. In this work, spatial correlation is assumed among land and ocean flux residuals but not between them, as different processes drive CO_2 fluxes in each domain.

The parameters σ_Q^2 and l are optimized using a Restricted Maximum Likelihood approach, as described in Chapter 3, equation 3.17. Because the deterministic component of the flux distribution (**Xβ**) is constant for a given month for both land and ocean fluxes, the spatial covariance of the flux residuals simply represents the autocorrelation of the fluxes themselves for this particular application. Note that this is not the case for a more complex model of the trend, as presented in the companion work (Gourdji et al., 2008).

2.5 Model-data mismatch covariance matrix (R)

The model-data mismatch covariance matrix **R** is a diagonal matrix whose elements represent the variances associated with measurement, transport, and representation errors (Engelen et al., 2002; Engelen 2006) for each observation location-month. In this study, the variances in **R** are obtained by optimizing a single scaling factor (c) applied to a vector of squared residual standard deviations (RSD's) for each measurement location. The RSD's are monthly-averaged deviations from a smooth curve

fitted to all observations at every location (GLOBALVIEW-CO2, 2008). This setup is similar to that used in Gurney et al. (2004), and assumes that the model-data mismatch uncertainty associated with each of the 44 locations scales proportionately with their squared RSD's. This approach has been shown to yield results that are comparable in terms of residual statistics to more complex setups that separate measurement locations into multiple subgroups (Michalak et al., 2005). In this setup, **R** is defined as:

$$\mathbf{R} = c \times \begin{bmatrix} \sigma^2_{\mathbf{R}_{i,1}} & \mathbf{0} & \cdots & \mathbf{0} \\ \mathbf{0} & \sigma^2_{\mathbf{R}_{i,2}} & \mathbf{0} & \vdots \\ \vdots & \vdots & \ddots & \vdots \\ \mathbf{0} & \mathbf{0} & \cdots & \sigma^2_{\mathbf{R}_{i,n}} \end{bmatrix} \tag{4.5}$$

where $\sigma^2_{R_i}$ is the squared RSD for measurement location i.

3.0 Results and Discussion

3.1 Optimized covariance parameters

The optimized covariance parameters used to construct the *a priori* (**Q**) and model-data mismatch (**R**) covariance matrices are presented in Table 4.1. Results show that the inferred flux variability at a 3.75°× 5° resolution is higher for terrestrial fluxes relative to oceanic fluxes, with a land variance ($\sigma^2_{\mathbf{Q}_{land}}$) two orders of magnitude higher than that for the oceans ($\sigma^2_{\mathbf{Q}_{ocean}}$) and a terrestrial flux correlation length (l_{land}) approximately half that of oceanic fluxes (l_{ocean}). This inferred regional variability is consistent with previous assessments of ocean and land fluxes that have shown that terrestrial fluxes are much more variable than their oceanic counterparts (e.g., Bousquet et al. (2000)). Note that the variability at a 3.75°× 5° resolution may be different than that observed at finer spatial scales, because processes that drive small-scale fluxes, such as regional droughts or biomass burning, are averaged out over larger regions.

Table 4.1: Optimized Model-Data Mismatch (**R**) and Spatial Covariance Parameters (**Q**) with ±1 Standard Deviation.

Covariance Matrix	Sill Variance σ^2, $[\mu mol_{CO2}/(m^2 s)]^2$	Correlation Length *l*, km	Scaling Factor *c*
Q_{land}	0.40 +/- 0.03	2700 +/- 200	-
Q_{ocean}	0.0030 +/- 0.0003	5700 +/- 500	-
R	-	-	0.63 +/- 0.04

The estimated correlation lengths presented here are longer than those used in Rödenbeck et al. (2003) (henceforth referred to as CR03), which were 1275 km for land and 1912 km for oceans. These dissimilarities may be due to the differences in covariance parameter optimization schemes, bottom-up fluxes used to assess flux variability, and/ or other constraints. For example, CR03 constrained the total amount of global *a priori* uncertainty to that reported for global land and ocean flux estimates by the IPCC (2001), and then downscaled this amount to the grid-scale. The difference in correlation lengths implies that the scale over which measurements are assumed to be representative of the underlying flux distribution was smaller in the CR03 study relative to this work. Because the spatial scales of flux variability may change from one geographic location to another, and different factors may drive this variability at smaller versus larger scales, it is difficult to directly validate the correlation length estimates presented in either of the two studies. However, the differing assumptions regarding *a priori* information on *a posteriori* results from these studies will be further examined in Section 3.4.2.

The optimized scaling factor (*c*), also presented in Table 4.1, produces model-data mismatch variances at individual measurement locations that range from 0.09 ppm to 5.3 ppm. The majority of these uncertainties are either similar to or somewhat higher than those employed by CR03 and Baker et al. (2006) (henceforth referred to as DFB06) for coincident locations (Figure 4.3). One reason for the higher model-data mismatch estimates in the current work is the fact that DFB06 used smoothed Globalview (GLOBALVIEW-CO2, 2008) measurements, which are generally easier to reproduce

than the flask measurements used here. In addition, the geostatistical inversion presented in this work uses an *a priori* constant spatial mean for land and oceans per month, which may not be able to represent small-scale flux variability relative to studies using explicit prior flux estimates, particularly in under-constrained regions.

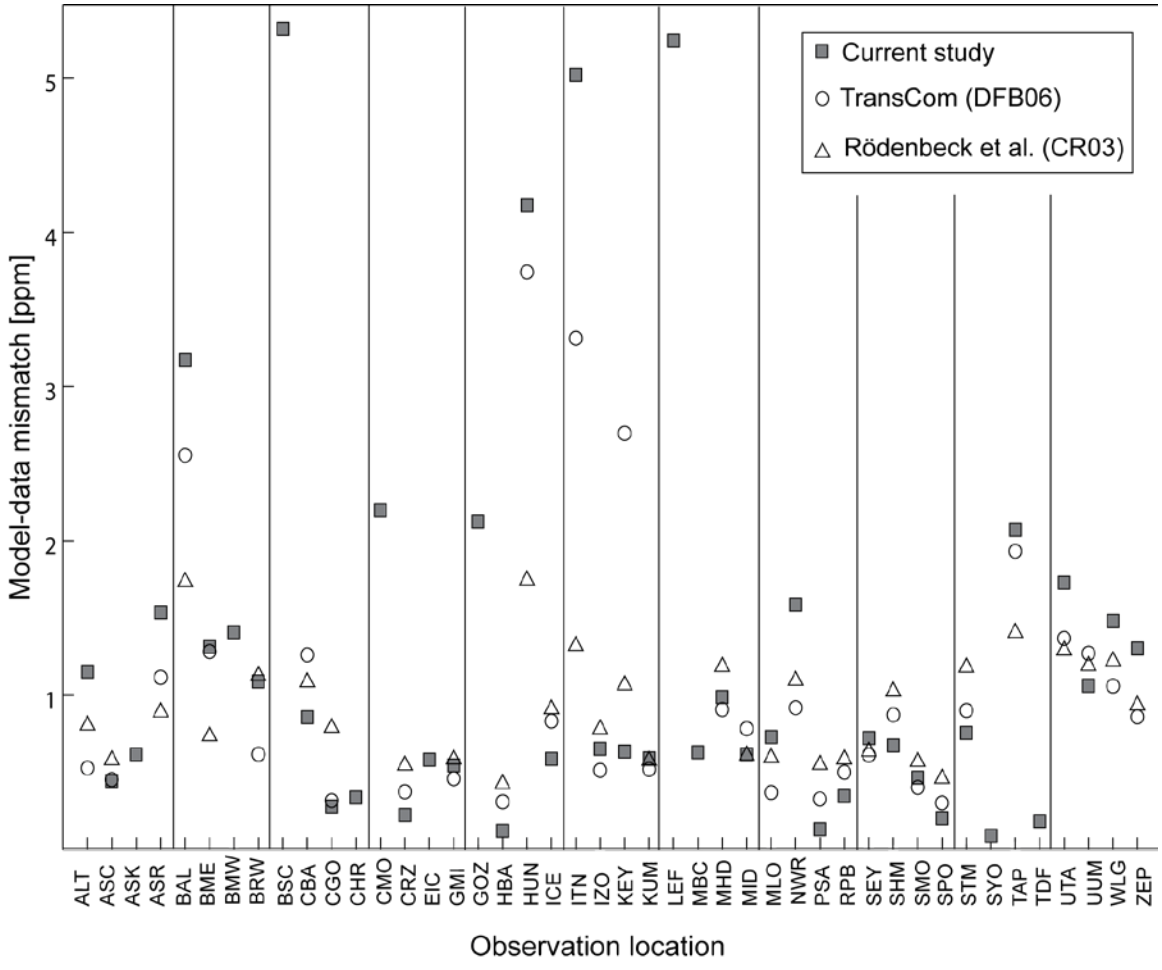

Figure 4.3: Model-data mismatch standard deviation for observation locations used in this study and coincident locations used in CR03 and the DFB06.

The optimized scaling factor (c) and the resulting model-data mismatch uncertainties were further evaluated using the $\chi^2_{\mathbf{R}}$ statistic for each measurement location using conditional realizations of the *a posteriori* flux distribution, as described in Chapter 3, equation 3.18 and Michalak et al. (2005). The $\chi^2_{\mathbf{R}}$ statistic averaged over all measurement locations is 1.0, indicating that measurements are reproduced to the degree assumed by the optimized model-data mismatch covariance matrix. Because the $\chi^2_{\mathbf{R}}$

statistic in this application is calculated using conditional realizations of flux, this statistic can also be evaluated for individual measurement locations (Michalak et al., 2005), as shown in Figure 4.4. This figure demonstrates that most locations have $\chi^2_{\mathbf{R}}$ values that cluster around 1.0 with most deviating by less than +/- 0.5. The $\chi^2_{\mathbf{R}}$ values for marine boundary layer sites have less scatter than for continental sites. Two locations (Easter Island, Chile (EIC) and Hegyhatsal, Hungary (HUN)) in particular have relatively large $\chi^2_{\mathbf{R}}$ values. As such, the amount of uncertainty specified in the R matrix overestimates the ability of the inversion to reproduce measurements at these specific locations as noted by previous studies (e.g. Law et al. (2003)). In future work, a more complex structure could be considered for the R matrix, similar to those examined in (Michalak et al., 2005), to account for the additional uncertainty at these locations.

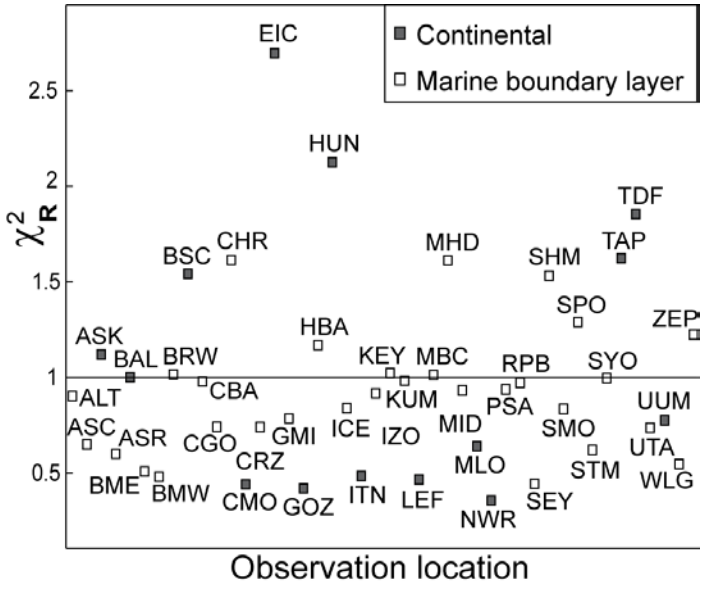

Figure 4.4: $\chi^2_{\mathbf{R}}$ for each observation location calculated from conditional realizations of the a posteriori fluxes resulting from inversion with optimized covariance parameters. The solid line represents $\chi^2_{\mathbf{R}}$ = 1.0, which is also the mean $\chi^2_{\mathbf{R}}$ across stations.

3.2 Drift coefficients ($\widehat{\boldsymbol{\beta}}$) and uncertainties ($\boldsymbol{\sigma}_{\widehat{\boldsymbol{\beta}}}$)

The drift coefficients and their associated uncertainties, representing monthly averages of terrestrial and oceanic fluxes, are presented in Figure 4.5. As emphasized in

Chapter 3, Section 2.0, the drift coefficients are estimated as part of the geostatistical inversion and therefore reflect the information content of the atmospheric measurements.

The terrestrial drift coefficients representing monthly land averages, including both fossil fuel emissions and biospheric sources and sinks, show a seasonal cycle which is noticeably more representative of the behavior of the Northern Hemisphere fluxes. This is an expected result given that the Northern Hemisphere is better constrained by atmospheric measurements, and that a larger fraction of land mass is north of the equator. Conversely, the average ocean monthly fluxes lack a strong seasonality. These drift coefficients indicate that the oceans act as significant net sinks of CO_2 in March, July, August and September. As will be discussed in Section 4.4.1, the magnitude of this sink may be partially due to aliasing of the Northern hemisphere photosynthetic signal onto the oceans during these months. Nevertheless, the ocean coefficients generally agree with other estimates of average ocean source/sink behavior (e.g. Takahashi et al., 2002). The uncertainty bounds for the ocean coefficients are narrower relative to their terrestrial counterparts, primarily because the inferred oceanic flux variability is smaller than that of land fluxes as indicated by the longer correlation length, l_{ocean}, and smaller sill variance, σ^2_{ocean}parameters presented in Section 3.1. This low variability implies that limited knowledge about oceanic fluxes is sufficient to inform their overall mean behavior.

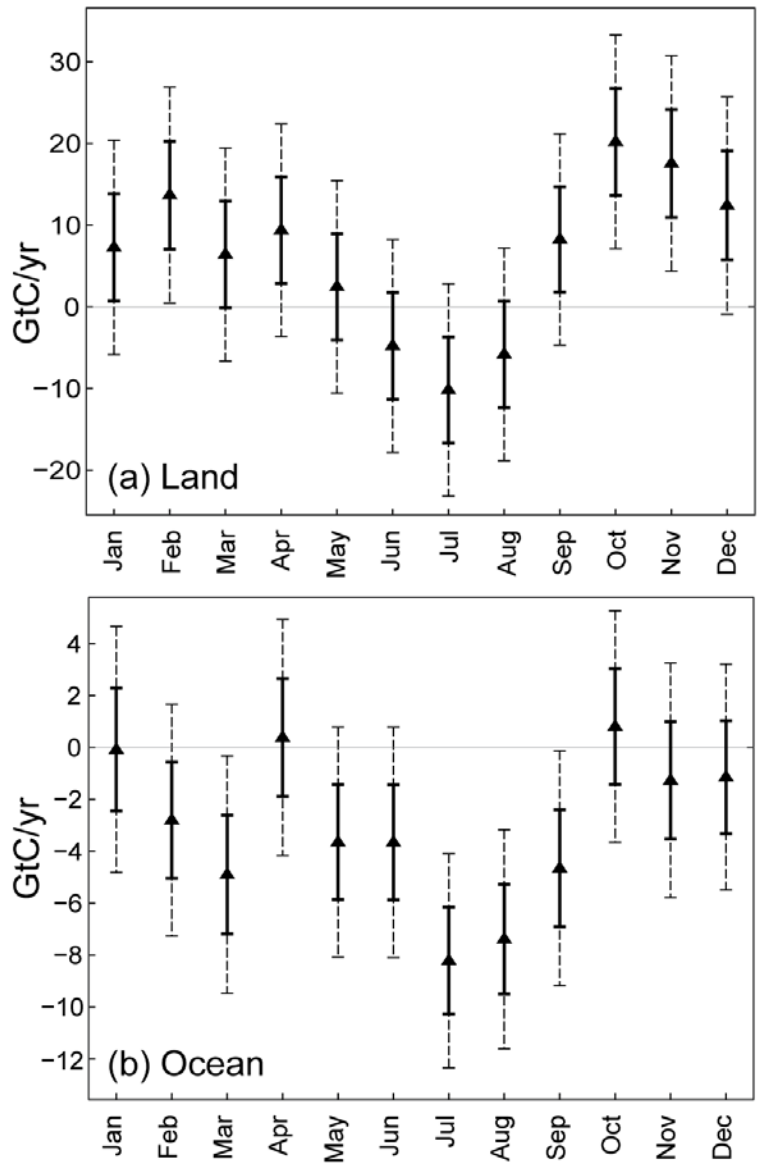

Figure 4.5: Estimated monthly land and ocean constants (**β**) (+/-$\sigma_{\boldsymbol{\beta}}$) in solid lines and +/-2$\sigma_{\boldsymbol{\beta}}$) in dashed lines). For the model of the trend used here, these coefficients represent the average monthly flux (**Xβ**) for land and ocean.

3.3 *A posteriori* grid-scale flux estimates ($\hat{\mathbf{s}}$) and uncertainties ($\sigma^2_{\hat{s}}$)

The *a posteriori* flux estimates, including anthropogenic sources and their associated uncertainties, are shown in Figure 4.6 at the recovered flux resolution of 3.75°× 5° for the sample months of January and July, 2000. In well-constrained areas, particularly in the Northern Hemisphere, the geostatistical inversion is able to estimate

fluxes that generally correspond well with current understanding of CO_2 sources and sinks. While the uncertainties are too large to make definite conclusions about the sign of the flux at the grid-scale resolution, especially given the limited measurement network used in this study, the main objective of estimating fluxes at this fine scale is to obtain a set estimates that can be aggregated to larger resolutions, in a manner that minimizes aggregation errors associated with estimating directly at coarser scales. As expected, areas of low uncertainty are generally located around measurement locations in regions defined in the TransCom analysis (DFB06) as Temperate Asia, Europe and Temperate North America (Figure 4.7).

Note that the inversion was designed to estimate fluxes everywhere, including ice-covered regions, which are generally assumed to have no significant sources or sinks of CO_2. Although these regions could easily have been left out of the inversion, including them provides an opportunity to assess the performance of the approach for areas where fluxes are considered well known. If estimates for Antarctica had shown significant fluxes at any spatial and temporal resolution, for example, this would have indicated a bias in the inversion setup or transport model. In the presented results, none of the grid-scale estimates for ice-covered regions are significantly different from zero at the $1\sigma_{\hat{s}}^2$ confidence level. This also holds true when estimates are aggregated to continental and/or annual scales, which lends support for the ability of the approach to accurately identify fluxes for these regions.

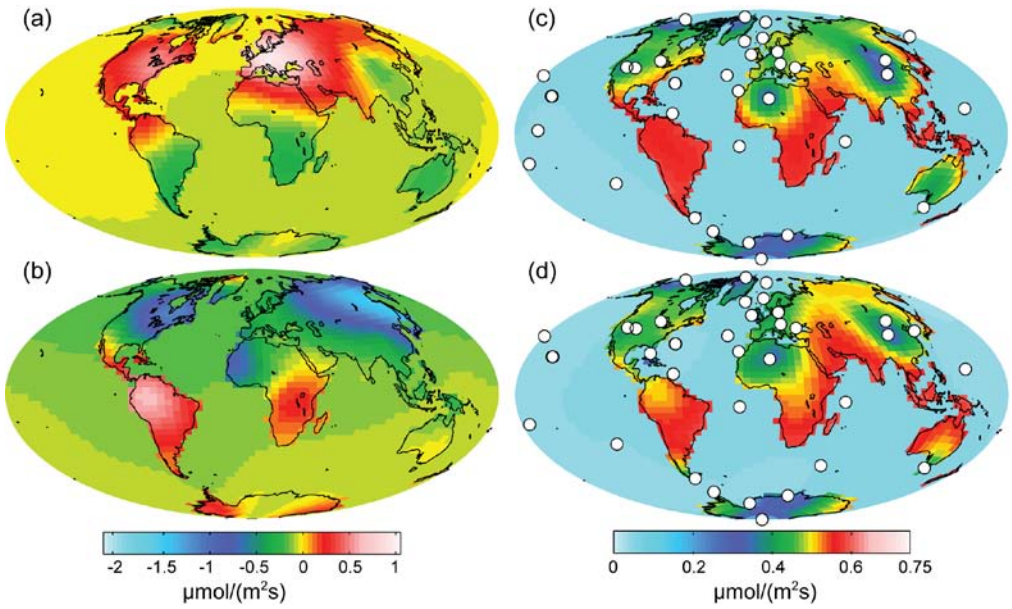

Figure 4.6: Flux estimates ($\hat{\mathbf{s}}$) for (a) January and (b) July, 2000, and (c, d) their associated uncertainties ($\sigma_{\hat{\mathbf{s}}}$). Observation locations for each month are shown as white dots. Note that the grid-scale fluxes should be interpreted together with their standard deviations, because many areas have high *a posteriori* uncertainties (e.g. Antarctica).

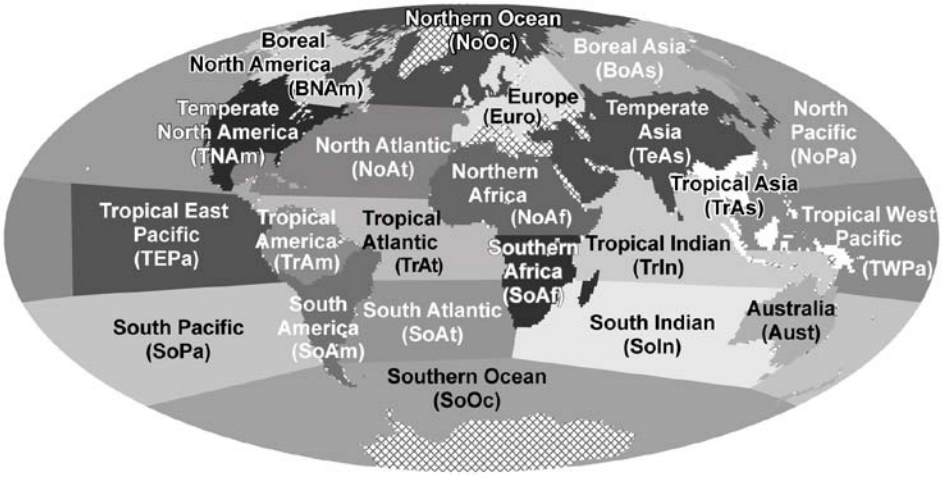

Figure 4.7: Locations of 11 land and 11 ocean TransCom regions (e.g. Gurney et al., 2003).

3.4 Aggregated comparison to existing CO_2 flux estimates

Fluxes and their associated uncertainties are aggregated to the regions used in the TransCom intercomparison study (Gurney et al., 2003, 2004; Law et al., 2003; DFB06) (Figure 4.7). The aggregated *a posteriori* fluxes from this application are then compared to estimates from previous studies in order to evaluate the ability of each method to constrain continental-scale fluxes, and to identify areas where estimates are consistent with results from other studies. Inferred fluxes are compared to (1) an aggregated set of bottom-up flux estimates (described in Chapter 2, Section 2.2) with regional corrections for deforestation and re-growth, (2) the TransCom 3 Level 3 intercomparison study (DFB06) where monthly flux deviations were recovered at the continental-scale using the set of bottom-up fluxes as *a priori* estimates, and (3) the CR03 study, which estimated monthly flux deviations at a 7.5° latitude by 10° longitude resolution from a different set of *a priori* fluxes (i.e., fossil-fuel component from (Olivier et al., 2001), NEP from (Sitch et al., 2000) and ocean fluxes from (Gloor et al., 2003)). Table 4.2 outlines the major components used in these top-down inversions compared to the geostatistical approach, in order to clarify the assumptions used in each study.

The geostatistical inversion method relies more heavily on the information content of the atmospheric CO_2 measurements relative to the other examined studies. Therefore, consensus among results would indicate regions where fluxes can be assumed to be relatively well understood, and therefore insensitive to the assumptions inherent in each study. In areas where the surface flux estimates vary, the impact of model assumptions on each estimate are explored. However, future research and/or more measurements may be required in order to reconcile flux estimates.

Table 4.2: Comparison of Inversion Setups.

	Geostatistical	DFB06	CR03
Resolution	3.75° latitude x 5° longitude, monthly fluxes (1997-2001).	22 TransCom regions, monthly fluxes (1988-2003). Monthly continental flux estimates assume pre-specified flux patterns as determined from a compiled set of bottom-up flux estimates [*Randerson et al.*, 1997; *Takahashi et al.*, 2003].	7° latitude x 10° longitude, monthly fluxes (1982-2001).
Measurement network	44 measurement locations from NOAA/ESRL sampling network [*Tans and Conway*, 2005].	78 measurement locations from *GlobalView-CO_2* [2004].	11-44 measurement locations from NOAA/ESRL sampling network [*Tans and Conway*, 2005].
Transport model	TM3 [*Heimann and Körner*, 2003] using National Centers for Environmental Prediction (NCEP) Reanalysis winds.	13 different transport models.	TM3 [*Heimann and Körner*, 2003] using National Centers for Environmental Prediction (NCEP) Reanalysis winds.
Model-data mismatch covariance	Scaling factor (c) applied to square of the residual standard deviations (RSDs) for each observation location, optimized using Restricted Maximum Likelihood (RML).	Sum of (1) transport model error determined from the spread of the *a posteriori* fluxes using different transport models, and (2) measurement error as described in DFB06.	Sum of (1) measurement error of variance 0.16/n where n is the number of data values per month (max n=8), and (2) model error as estimated from analysis of forward model run of prior flux estimates.
Prior flux distribution	No prior assumptions regarding flux distributions; a set of means and/or covariates are included *a priori* in the **X** matrix. For this application, **X** contains 24 columns representing an assumption of constant monthly means over land and oceans. The drift coefficients (**β**'s) that define the means are estimated as part of the inversion.	Prior estimates derived from (1) fossil fuel emissions (estimated from [*Brenkert*, 1998 and *Andres et al.*, 1996]), (2) CASA fluxes [*Randerson et al.*, 1997] and (3) ocean fluxes [*Takahashi et al.*, 2002] from pCO_2 measurements. Priors also include deviations from neutral biosphere based on knowledge of deforestation in the tropics and a upper mid-latitude sink.	Prior estimates derived from (1) fossil fuel emissions (based on EDGAR database [*Olivier et al.*, 2001]), (2) mean seasonal cycle LPJ biosphere modeled fluxes [*Stitch et al.*, 2000] and (3) ocean fluxes from *Gloor et al.* [2003] from an inversion of ocean carbon data, and from *Takahashi et al.* [1999] based on pCO_2 measurements.
Prior flux covariance	Based on correlation of flux residuals, modeled using an exponential covariance function. Parameters estimated separately for land and ocean regions using RML.	Seasonally varying land *a priori* uncertainty from *Gurney et al.* [2004]. Ocean uncertainty from *Gurney et al.* [2003] with an additional factor of $(0.5\ GtC/yr)^2$.	Based on correlation of residual flux values using an exponential covariance model. Correlation lengths based on statistical analysis of model intercomparisons. Variances based on global uncertainty estimates, downscaled for land areas using a flux intensity factor based on annual NPP.

3.4.1 Continental-scale seasonal flux comparison for year 2000

The estimated flux seasonality and uncertainties for the sample year 2000, shown in Figure 4.8, are comparable to the aggregated set of bottom-up estimates and estimates from DFB06. CR03 monthly flux estimates were not available and are therefore not shown. The figure demonstrates that the seasonality of fluxes from DFB06 and the geostatistical inversion agree particularly well for better-constrained regions (e.g. Europe and Australia), suggesting that the seasonality in these areas is relatively well understood. However, even in regions that are not well constrained by the current observational network, such as in Northern and Southern Africa, these two sets of flux results generally have similar magnitudes and seasonal variation. These results support the contention that a geostatistical inverse modeling approach can be used to recover fluxes with comparable accuracy and precision to existing synthesis Bayesian approaches, without relying on bottom-up flux estimates to define the magnitudes and spatial patterns of prior information.

In many under-constrained areas where there are differences between estimates, both the DFB06 and the geostatistical results tend toward their prior assumptions, which are respectively the bottom-up flux estimates and the geostatistical model of the trend ($\mathbf{X}\hat{\boldsymbol{\beta}}$). An example of this can be seen in the Tropical East Pacific, South Pacific, and Tropical West Pacific, where there is a lack of atmospheric observations. The geostatistical estimates for these regions covary strongly, principally because the fluxes themselves tend to revert to the model of the trend. In particular, flux estimates in many of these regions follow the seasonality reflected in the oceanic mean flux (Figure 4.5). The DFB06 estimates, in contrast, reflect their prior flux estimates, i.e. bottom-up estimates from Takahashi et al. (2002). Since Takahashi et al. (2002) fluxes are based on extrapolated ship-track data, the ocean uptake predicted by the geostatistical inversion for this region likely reflects a lack of observational data rather than a true departure from previous estimates. Overall, however, this result suggests that flux estimates for the Tropical East Pacific obtained by previous inversion studies were strongly determined by *a priori* fluxes, while those obtained from the geostatistical inversion tend to reflect the globally-averaged oceanic mean for this under-constrained region.

The continental-scale estimates for the Northern high latitude regions (e.g. Boreal North America, Boreal Asia, Northern Pacific, and Northern Atlantic) differ from past estimates, particularly in July, August and September. As mentioned in Section 3.2, the geostatistical *a posteriori* estimates may be affected by aliasing of a terrestrial photosynthetic signal onto adjacent ocean areas during the Northern Hemisphere summer months. This land-ocean aliasing cannot be directly measured, but it can be qualitatively seen most clearly in the North Pacific and North Atlantic, i.e. in ocean regions that are contiguous with land masses that exhibit strong flux seasonality. This aliasing can also be observed to a limited extent in past synthesis Bayesian inversion studies (e.g. DFB06), but tight *a priori* constraints on ocean fluxes limit the size of this effect, despite the fact that the atmospheric observations do not have sufficient information to accurately partition land and ocean fluxes. This observation points to difficulties in using an atmospheric transport model to correctly partition land and ocean signals during specific months in these regions. However, there is also a possibility that a portion of the anti-correlation between adjacent land and ocean regions observed in the current study is reflective of true flux variability. Note that the constant monthly mean assumption for land and ocean regions used in this study is not the cause of this aliasing, because results shown in the companion work (Gourdji et al. 2008) illustrate that using a more complex model of the trend to capture more of the expected spatial variability of fluxes over land reduces the observed anti-correlation between land and ocean fluxes, but does not eliminate it.

Because the geostatistical method accounts for spatial correlation in the flux distribution, which effectively allows the application to use the measurement information over larger scales compared to the DFB06 study, the uncertainty bounds on the geostatistical flux estimates ($\sigma_{\hat{s}}^2$) are also typically either comparable to, or narrower than, those from the previous work at this aggregated scale. The relatively small variability of the ocean fluxes, as inferred by RML and specified in the *a priori* spatial covariance matrix **Q**, also translates into narrower *a posteriori* uncertainty bounds on the geostatistical ocean flux estimates. Conversely, the geostatistical uncertainties are higher than those of the DFB06 study in a few well-constrained terrestrial regions (e.g. Europe

and Australia), principally because the TransCom study used more measurement locations in these areas.

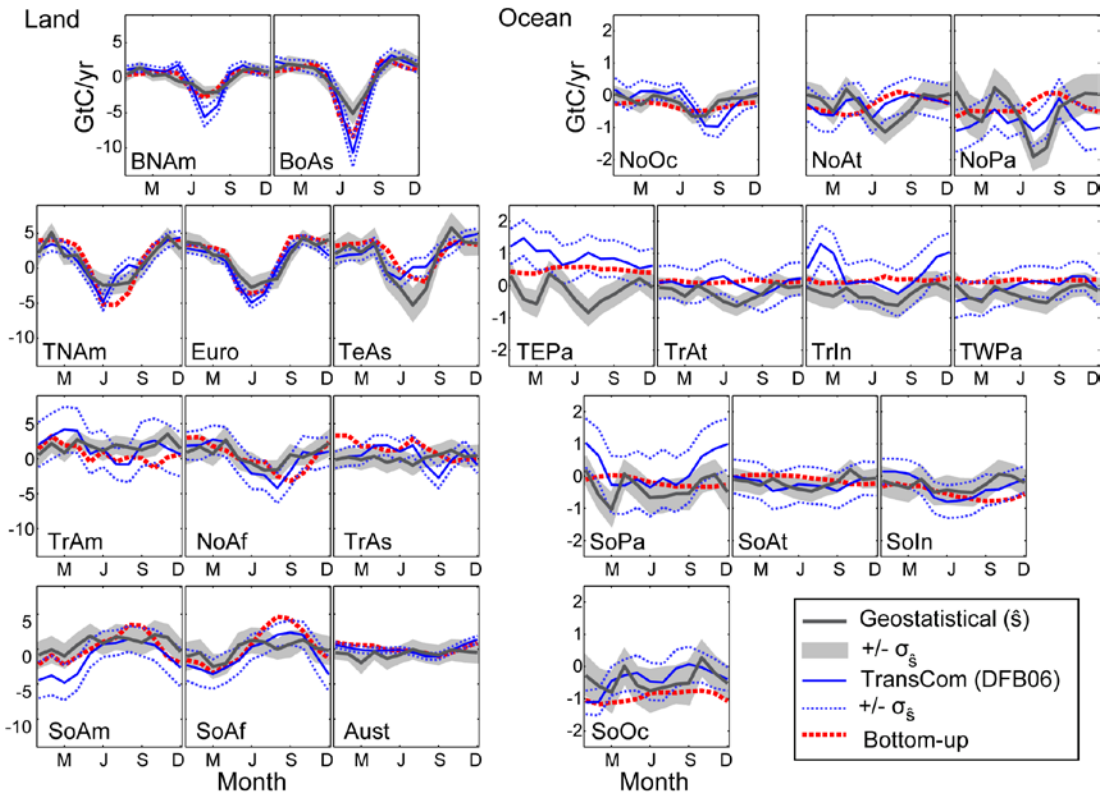

Figure 4.8: Monthly best estimates ($\hat{\mathbf{s}}$) aggregated to 22 TransCom regions with $1\sigma_{\hat{\mathbf{s}}}$ confidence intervals for year 2000 for geostatistical inversion, DFB06, and bottom-up estimates (Randerson et al., 1997; Takahashi et al., 2002; Brenkert, 1998) used as priors in DFB06. DFB06 estimates include fossil fuels from Brenkert (1998) for consistency.

3.4.2 Inter-annual flux variability comparison

Figure 4.9 presents mean-deviated annual moving averages of the *a posteriori* flux estimates for the geostatistical inversion, DFB06 and CR03. The estimates from the latter two studies include both fossil fuel emissions from Brenkert (1998) and an inter-annual fossil fuel component from DFB06 for consistency. The plot suggests that there is good agreement between the three studies with regard to the terrestrial inter-annual variability for most regions. One exception is Tropical America, where the CR03 fluxes display much more inter-annual variability relative to the other two sets of estimates. This may be due to the higher *a priori* uncertainty used by CR03 for this region relative

to both the DFB06 study and the amount of variability assumed by the *a priori* covariance for the geostatistical application. As a result, the inter-annual variability of the DFB06 and geostatistical inversion results for this area may be more realistic. For most other regions, the geostatistical inversion recovers inter-annual variability that is comparable to DFB06 and CR03, particularly in better-constrained regions.

For the ocean regions, the geostatistical mean-deviated fluxes show little inter-annual variability relative to fluxes from DFB06 and CR03. This difference is only significant in the Temperate East Pacific and South Pacific, where fluxes are highly influenced by the El Niño Southern Oscillation (ENSO). In these regions, the DFB06 results show a significantly greater CO_2 uptake than the others from the beginning of 1997 to the middle of 1998, and more outgassing in 2000. DFB06 used a richer measurement network in this region than either of the other two studies, which may have helped to inform fluxes during these years (e.g. Patra et al., 2005).

As with the seasonal results presented in Section 3.4.1, the geostatistical inversion flux estimates have comparable uncertainty bounds ($\sigma_{\hat{s}}^2$) to those from CR03 or DFB06, except in regions where TransCom used a more extensive observational network (e.g. Temperate Asia, Australia, Tropical Asia, and Europe). Differences in correlation length likely have little impact on the difference in *a posteriori* uncertainties between the geostatistical inversion and the CR03 study at this scale, because the geostatistical inversion was found to be relatively insensitive to this parameter (within the range examined by these two studies) for fluxes aggregated to continental resolutions. Instead, differences in the *a posteriori* uncertainty relative to CR03 are likely due to the *a priori* uncertainties used in the two studies, and the fact that CR03 assumed a spatially-variable *a priori* land uncertainty ($\sigma_{\mathbf{Q}_{land}}^2$) proportional to Net Primary Production (NPP). These results reinforce the fact that *a posteriori* uncertainties reflect not only the information provided by atmospheric measurements, but also the *a priori* covariance assumptions.

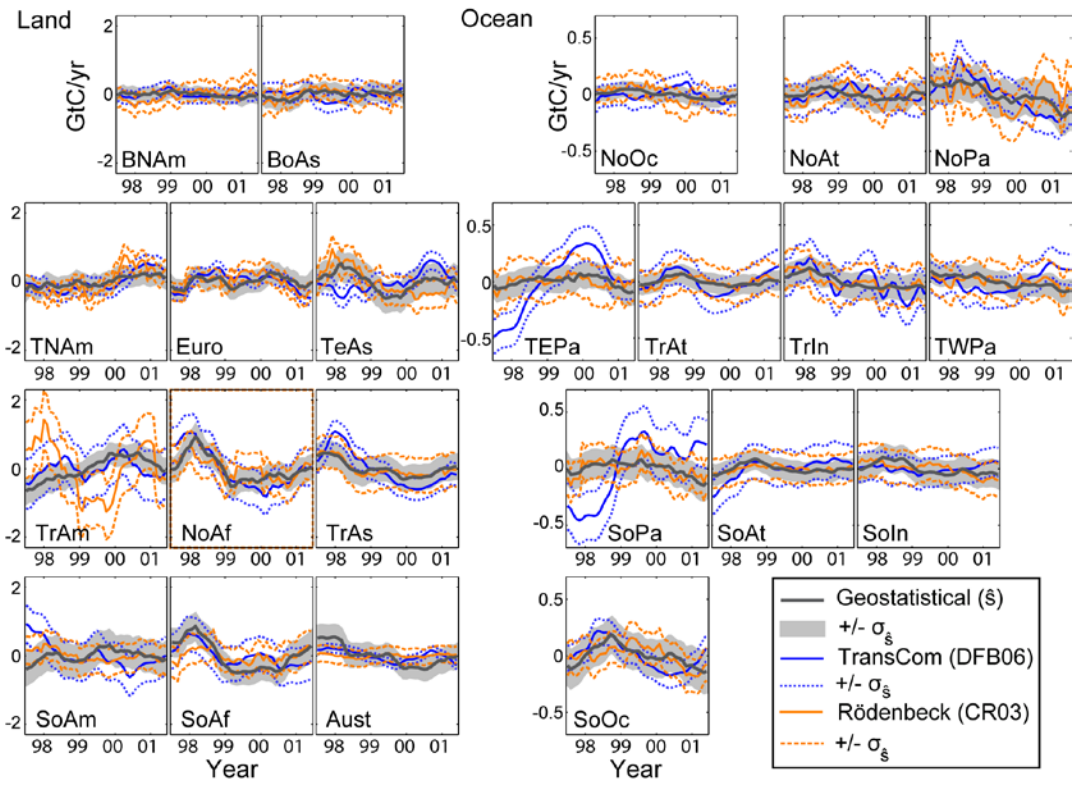

Figure 4.9: Mean-deviated de-seasonalized fluxes with $1\sigma_{\hat{s}}$ confidence intervals for 1997-2001 for geostatistical inversion, DFB06, and CR03. DBF06 and CR03 estimates include fossil fuels from both Brenkert (1998) and an inter-annual component as specified by DFB06 for consistency. Confidence intervals for all estimates are at $1\sigma_{\hat{s}}$. Estimates are presented for the 22 TransCom regions.

3.4.3 Annually averaged aggregated sources and sinks

Figures 4.10a and 4.10b present annually-averaged, aggregated land and ocean flux estimates for the 22 TransCom regions for the geostatistical inversion, DFB06, CR03, and the bottom-up fluxes. All fluxes represent averages for the period 1997 to 2001. Unlike other presented results, annual averages of fossil fuel emissions from Brenkert (1998) were subtracted *a posteriori* from the geostatistical estimates, in order to make them comparable to the biospheric fluxes reported by CR03 and DFB06. The uncertainty bounds, however, include the total uncertainty estimated for the sum of these two flux components. Because annually-averaged fossil fuel emissions are better understood than their seasonality (Gurney et al., 2005), subtracting inventory fossil fuel

emissions from the geostatistical estimates at the annual scale should provide an accurate estimate of the biospheric fluxes inferred using the presented approach.

For seven TransCom continental regions (Boreal North America, Temperate North America, Northern Africa, Boreal Asia, Temperate Asia, Tropical Asia and Australia), none of the three inverse modeling studies yield fluxes that are significantly different from zero, and the estimated fluxes vary among themselves by less than one GtC/yr. For three of the other continental regions (Tropical America, South America, Southern Africa), the large differences (significant at $1\sigma_s^2$ for the first region) in both sign and magnitude between DFB06 and CR03 may be due to their use of different terrestrial prior flux estimates (i.e. CASA estimates of net ecosystem exchange (NEE) (Randerson et al., 1997) in DFB06 vs. LPJ estimates of NEE (Sitch et al., 2000) in CR03). For example, whereas LPJ estimates a 0.1GtC/yr sink in Tropical America, CASA predicts a 0.56 GtC/yr source. In contrast, given that the geostatistical estimates better reflect the information content of the atmospheric data, results tend to show intermediate values for these regions.

Estimates for the final terrestrial region, Europe, also vary between studies. The use of different measurements for this relatively well-constrained region across studies most likely explains this discrepancy. For example, an additional measurement location (GOZ) was used in the geostatistical inversion compared to the CR03 study. The stronger European sink in the DFB06 study may also be related to their use of an expanded measurement network. However, Michalak et al. (2005) also showed that flux estimates for Europe were highly sensitive to the choice of *a priori* flux and model-data mismatch uncertainties for synthesis Bayesian inversions. Overall, the comparison points to the considerable influence of the choice of observations, inversion set-up and prior flux estimates on inferred fluxes, even for regions that are generally considered to be well-constrained by the measurement network. This is especially true when looking at net annual fluxes, which represent a relatively small residual between large seasonal sources and sinks.

For all ocean regions, the geostatistical annually-averaged fluxes show significant sinks with little variation between estimates. Particularly, the Tropical Indian and the Tropical East Pacific ocean estimates reflect more neutral results than those from the

other studies, with DFB06 and CR03 reporting a significant source of around 0.6 GtC/yr for the latter region. This is consistent with the seasonal results presented in Section 3.4.1, which suggests that the geostatistical oceanic fluxes tend to be influenced by the estimated monthly mean for poorly-constrained regions. An analysis of the off-diagonal *a posteriori* covariance terms ($\mathbf{V}_{\hat{s}}$) aggregated to the 22 TransCom regions shows that oceanic flux estimates in poorly-constrained regions rely on the long correlation lengths specified in the *a priori* covariance matrix (**Q**) due to the lack of atmospheric observations. The large positive *a posteriori* cross-covariances for adjacent ocean regions also suggest that the confidence bounds shown in Figure 10b may be underestimated for these regions.

Finally, note that the companion work (Gourdji et al., 2008) shows that the annually-averaged estimates presented here are consistent with those from an inversion that includes auxiliary environmental variables in the model of the trend for most continental-scale land regions.

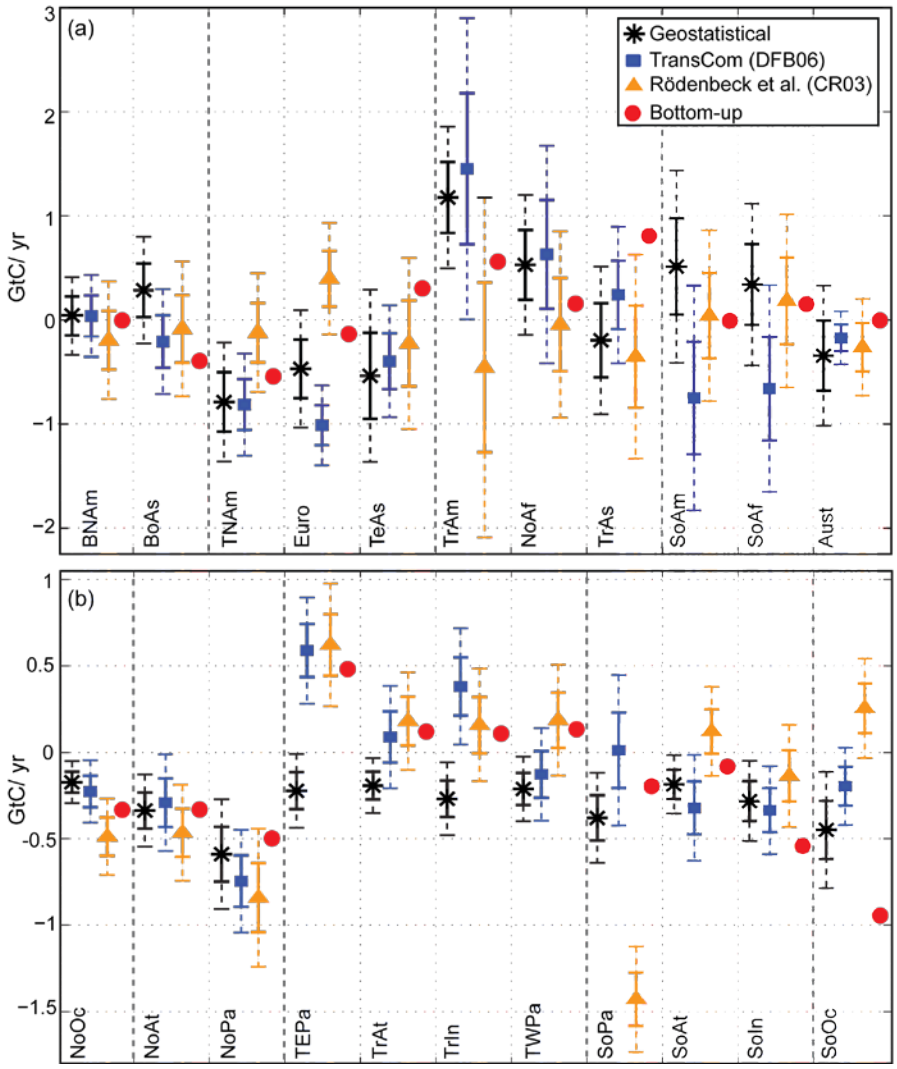

Figure 4.10a and 4.10b: Mean (a) biospheric and (b) oceanic flux (GtC/yr) for geostatistical inversion, DFB06, CR03, and bottom-up flux estimates (Randerson et al., 1997; Takahashi et al., 2002). Solid and dashed lines represent $1\sigma_{\hat{s}}$ and $2\sigma_{\hat{s}}$ respectively. Fluxes from all studies are averaged from 1997 to 2001. Estimates are presented for the 22 TransCom regions.

4.0 Conclusions

This research presents the first application of a geostatistical inverse modeling approach for estimating global monthly fluxes of CO_2 using atmospheric CO_2 concentration data, without the use of pre-defined flux patterns or *a priori* assumptions

about flux magnitudes. Results demonstrate that the existing atmospheric monitoring network can be used to estimate surface fluxes and their associated uncertainties at a 3.75° × 5° resolution, which limits aggregation errors inherent to inversions conducted at coarser scales. *A posteriori* fluxes aggregated to the 22 TransCom regions have uncertainties that are comparable to those reported by previous synthesis Bayesian inversions at monthly and inter-annual time scales. Overall, this work demonstrates that the presented approach provides a valuable data-driven alternative to synthesis Bayesian inversion methods, by avoiding many *a priori* assumptions inherent to aggregation, uncertainty estimation, and the magnitude and spatial patterns of flux distributions.

At the grid-scale, geostatistical flux estimates are most influenced by the limited information content of the available atmospheric measurements, and therefore have correspondingly large uncertainties. At this resolution, flux distributions reflect the assumption of a constant model of the trend, and rely more heavily on the inferred autocorrelation of the flux distribution, yielding smooth spatial variability. Conversely, synthesis Bayesian inversions tend to revert to their own prior assumptions about flux variability at this scale, but this variability is prescribed *a priori* and is also not derived from the information provided by atmospheric data.

The value in the presented approach is that it provides strongly atmospheric data-driven estimates of surface fluxes, which has several potential additional benefits. First, the flux estimates and uncertainties provide a valuable basis for comparison to estimates from other inverse modeling studies, which can help explain the influence of model assumptions on recovered fluxes. Second, by limiting the number of *a priori* assumptions, the geostatistical approach may highlight potential difficulties inherent to inverse modeling approaches that may otherwise go unnoticed. The observed possible land-ocean aliasing provides one example, suggesting that either this behavior had been previously undetected or that the limited atmospheric measurement network used here is not able to fully differentiate land and ocean fluxes in Temperate North America, Boreal Asia and adjacent ocean basins. In addition, results show that the limited atmospheric network does not provide independent information about ocean fluxes for large areas of the Earth, further highlighting the need for additional observations in the global oceans. Overall, the presented approach provides an ideal basis for further work towards

reconciling top-down and bottom-up estimates of fluxes, because, contrary to synthesis Bayesian inversions, it yields estimates that are independent of explicit prior flux assumptions based on bottom-up estimates.

CHAPTER 5

Use of the 2008 continuous measurement network to estimate regional fluxes for North America

This Chapter addresses objective 2 of the dissertation, by using atmospheric CO_2 observations to estimate 1° x 1° fluxes for the North American continent for 2008. The work assesses the ability of the expanding network of continuous CO_2 measurements to constrain monthly fluxes for North America.

1.0 Introduction

Atmospheric CO_2 inverse models, i.e. "top-down" approaches, have been used for carbon budgeting and to study carbon cycling at biome to continental scales at a variety of timescales. Top down approaches take advantage of the information available in atmospheric CO_2 concentration measurements to infer both the spatiotemporal variations and the magnitudes of CO_2 sources and sinks. Since there is a time delay between a time at which a flux occurs and when it can be detected by an observation, inversion models rely on an atmospheric transport model to link carbon exchanges at the earth's surface with atmospheric observations of CO_2. Thus, the transport model translates a rate of carbon exchange at the surface from a given area at a specific time into a mixing ratio as measured by atmospheric CO_2 concentrations at different tower locations. Traditionally, global Eularian transport models have been used with flask samples of CO_2 from mostly marine boundary sites representing background air in global inversions to infer continental scale fluxes (e.g. Gurney et al., 2003; Rödenbeck et al., 2003; Baker et al., 2006; Mueller et al., 2008; Gourdji et al., 2008).

More recently, regional inversions have used continuous data collection at continental sites to infer more fine-scale fluxes such as biome-scale sources and sinks (e.g. Carouge et al., 2010a, Carouge et al., 2010b,Schuh et al., 2010, Gourdji et al., 2010, Butler et al., 2010). Monthly 1°x1°, biome, and continental fluxes from regional inversions have also been compared to estimates from mechanistic models, which scale-

up process-based understanding of photosynthesis and respiration to larger scales (Gourdji et al., in prep.). Such comparisons hope to show which bottom-up models and at what spatiotemporal scales are most consistent to fluxes estimated primarily from the atmospheric data (Gourdji, in prep.). Hence, the use of continuous data within an inversion holds the promise of (i) quantifying carbon budgets and associated uncertainties at scales that may be informative for policy management and (ii) developing a means to reconcile CO_2 flux estimates from mechanistic models and top-down approaches.

The use of continuous measurements in an inversion requires careful consideration due to the unique characteristics associated with the towers and/or location of the towers that continuously sample atmospheric CO_2. Accurately linking measurements to fluxes via simulated atmospheric transport can be challenging for many of the tower locations. For example, measurement locations in regional networks tend to be located in highly productive areas. Towers also are more likely to be sited near major urban centers for easy accessibility. Therefore, the observations tend to be noisier (i.e., contain greater random variability) than flask measurements. Theses tower measurements also incorporate multiple scales of variability or both near and far-field fluxes (e.g. Gerbig et al., 2009; Gourdji et al., in prep).

Ascertaining long term temporal trends from small-scale measurement variability or fossil fuel spikes pose unique challenges to regional inversions that use continuous concentrations. In addition, many of the new towers are sited in areas with complex terrain or meteorology, (e.g., tops of mountains or at the coasts). These are regions were atmospheric transport modeling is most challenging, particularly in terms of accurately representing atmospheric mixing (i.e., convective turbulence and advective winds) and boundary layer heights. Finally, in 2007, some relatively short (less than 200m and in many cases less than 10m) AmeriFlux flux towers began to measure continuous CO_2, which raises questions regarding the spatiotemporal representation of the measurements. It is also uncertain whether an atmospheric transport model can appropriately link a measurement from heights of 10m or less to a distribution of fluxes at spatial scales of 1° x 1° or greater.

There are several studies (using both real and synthetic data) that have examined the relative impact of setup choices on the ability of a regional inversion to estimate

carbon flux (e.g., Carouge et al., 2010a; Carouge et al., 2010b; Lauvaux et al., 2008; Gourdji etal., 2010; Göckede et al., 2010). Although Gerbig et al. (2009) argues that continuous measurements can only "see" fluxes near a tower, in a synthetic data study in Europe Carouge et al. (2010a) found with additional observations the error associated with regional estimates was reduced substantially. However, these studies have only been able to use observations from a small number of tower locations given the limited size of continental networks. Hence, most of the estimation domain remained under-constrained by the observations, and, therefore, the inversions had to rely more on other constraints, such as the use of explicit prior flux estimates, to help constrain estimates. Thus, the conclusions regarding flux estimations drawn from previous works may have been more of a reflection of the specific *a priori* choices employed in each study rather than the ability of measurements to estimate regional fluxes. More importantly, regional flux estimates from previous inversions that were based on limited measurement networks are too inconsistent to provide reliable annual carbon budgets at the biome and continental scale.

Many earlier inversion studies have cited the lack of continuous measurements as one of the two the most important (along with simulated transport) limiting factors for carbon budgeting at regional scales using top-down methods (e.g. Cauroge et al., 2010a; Cauroge et al., 2010b; Schuh et al., 2010; Göckede et al, 2010; Gerbig et al, 2009). During 2008, the NA measurement network expanded from the 10 towers of 2004 (10TN) to 35 continuous CO2 measurement locations or towers (35TN). Many of these new sampling locations are located in previously unconstrained regions. Thus**,** for the first time certain areas of the continent are now relatively well covered by the network such as the Mid-Continent Intensive (MCI) region in Wisconsin, Iowa, and Minnesota. It is widely assumed that these additional measurements, along with improvements in modeling of atmospheric transport, will help improve the ability to locate and quantify terrestrial CO_2 sources and sinks at smaller spatial scales at a variety of timeframes. However, the extent to which these measurements will improve inversion results is not yet known. As such, there is a need to assess to what degree the continuous measurements from the expanded network can help constrain regional budgets at monthly and annual timescales for a range of spatial scales (e.g., from 1°x1° to the continental

scale). Without understanding the impact of these additional measurements have on estimating fluxes, especially in context of the other inversion choices of regional inversions, it is impossible to assess the incremental net benefit of expanding the network as opposed to focusing other limitations, such as improving boundary conditions or regional atmospheric transport.

2.0 Study objectives

The goal of this study is to assess the impact of the expansion of the regional measurement network of continuous CO_2 observations on top-down estimates, as opposed to other inversion choices known to have a large influence on inversion estimates. Specifically, this study tests the impact of the three choices: (1) selection of observations (in space and time); (2) the spatial and temporal scale at which to estimate fluxes, and (3) the selection of boundary conditions that specify atmospheric CO_2 contributions from fluxes outside of the regional domain. Geostatistical inverse model (GIM) is used to assess the influence of these three sets of choices, because GIM relies more directly on the atmospheric data to estimate fluxes at fine spatiotemporal scales, and optimize covariance parameters, relative to other Bayesian inversion approaches (e.g. Baker et al., 2006; Peters et al., 2007; Butler et al., 2010).

Thus, the analysis is designed to test two hypotheses. The first hypotheses is that including more measurements (both spatially and temporally) improves flux estimates and reduces their corresponding uncertainties, especially in areas that previously were under constrained by the measurement network. The second hypothesis is that including more measurements helps minimize the impact of other inversion choices. This stems from the idea that carbon budgets should be based more heavily on observations than assumptions. The results of testing these hypotheses will help determine how much information continuous measurements are able to provide in terms carbon budgeting at different spatiotemporal scales, and which setup choices are best to extract both the small and large scale variability from the additional observations.

The study assesses the influence of three inversion choices on the estimated fluxes post-aggregated to various spatial and temporal scales: (1) at the monthly grid-scale, (2) at spatially aggregated areas at the monthly timescale, (3) at annually averaged and spatially aggregated areas. Each of these spatiotemporal scales has relevance for

investigating carbon cycling dynamics. The spatial patterns represented in grid-scale flux estimates help to reconcile "top-down" and mechanistic understanding of carbon flux (Gourdji et al., in prep.). In addition, the monthly budgeting of regional areas at the size of states or biomes helps to improve our understanding of the behavior of ecosystem scale sources and sinks necessary both for predicting future flux scenarios developing carbon accounting schemes. Finally, annual budgeting for the continent and for specific regions within the continent has policy relevance in terms of complying with international treaties such as the Kyoto protocol.

Other setup choices, specifically the use of a particular atmospheric transport model and the choice of explicit prior estimates, are not considered in this study. Transport models are assumed to have a large impact on regional fluxes obtained from inverse models. As mentioned, simulated transport links measurements to fluxes via simulated atmospheric transport but accurately modeling transport is challenging. For example, atmospheric transport models have difficultly simulating rapid changes in planetary boundary height, advective winds, nighttime jets, and synoptic weather patterns, etc. However, the choice of which observations to use throughout the day is indirectly coupled to transport error. As such, the study aims to use measurements at times of day when transport can be trusted. The effect of the choice of an explicit prior is also not included in this analysis because GIM does not use explicit prior information to help constrain flux estimates, and thus avoids any potential biases associated with this assumption. Regardless, the outcome of the work can help inform all regional inversions modeling approach for CO_2 flux estimation so that estimates can more directly reflect the information content of available atmospheric measurements instead of the choices of selection of observations and the spatial and temporal scale at which to estimate fluxes.

Since the study assesses the information content of the measurements in the NA network for 2008, two networks are employed in the research, i.e. 35 towers (35TN) available in 2008 and 10 towers (10TN) available in 2004. Some of measurement sites in the NA network have been used previously, including observations from tall (greater than 300m), intermediate towers (between 30m and 300m) as well as marine boundary layer (MBL), to estimate fluxes for NA. For example, the measurement sites include the 10 tower network in Gourdji et al. (2008); Gourdji et al. (in prep) and the 19 tower network

used by National Oceanic Atmospheric Agency's (NOAA) Carbon-Tracker (CT) inversion (http://www.esrl.noaa.gov/gmd/ccgg/carbontracker/). These measurements are used in both a set of synthetic and real data inversion as will be explained in the following section.

3.0 Methods and data

This section provides the methods and data used to test the two hypotheses stated earlier, i.e. the extent to which more spatial and temporal observations improve inversion flux estimates as opposed to other inversion choices. The section outlines the inversion method used for the analysis, the observations used within the study, and the different setup choices employed within the analysis.

3.1 GIM approach

The geostatistical inversion method (GIM) has been shown to provide strongly atmospheric data-driven estimates of surface fluxes at the continental scale (Mueller et al., 2008, Gourdji et al., 2008). The method can also be used at regional scales to yield monthly carbon budgets. Two recent studies have proven the method at these finer scales. First, GIM was applied to a NA regional domain (Gourdji et al. 2010) using synthetic observations. The synthetic observations were created for 9 tower locations from meteorological data for 2004 along with a known set of biospheric fluxes. The results from this study demonstrated that GIM is able to infer relatively unbiased estimates of monthly net continental CO_2 surface fluxes at the biome scales (Gourdji et al., 2010) in the absence of transport model error. GIM has also been used in conjunction with real data to infer monthly and annual carbon budgets for NA for both the biome and continental scales for 2004 (Gourdji et al., in prep.).

GIM is used for the analysis presented herein precisely because it requires fewer assumptions known to influence estimates when compared to other Bayesian inversion methods, and is therefore better suited to extract the information content of the atmospheric observations. For example, GIM does not rely on an explicit set of prior flux estimates. Other Bayesian inversion approaches use explicit prior fluxes as derived from a biospheric model and combined with fossil fuel inventories and fire emission estimates to help constrain flux estimates due to atmospheric mixing and the temporal and spatial

limitations of the atmospheric observations. Instead, GIM employs a statistical trend where coefficients are optimized with the atmospheric data as part of the inversion. If the trend is as simple as a set of mean fluxes in both time and space (as used at the global scale in Mueller et al. (2008)), and the inversion relies almost exclusively on the information content in the CO_2 observations to budget fluxes. The flux estimates from this type of inversion set-up, therefore do not incorporate any errors inherent to the magnitude or structure of the explicit priors (Gourdji et al., in prep). In addition, the flux estimates and uncertainties provide a valuable basis for comparison to estimates from other "top-down" and mechanistic studies, because the budgets can be relatively independent of other methods. Finally, by limiting the number of assumptions, the geostatistical approach highlights potential difficulties inherent to the inverse modeling approach that may otherwise go unnoticed (Mueller et al., 2008).

There have been several applications of GIM at the global and regional scales. A full description of the method and algorithm can be found in Michalak et al. (2004), Mueller et al. (2008), Gourdji et al.(2008), Gourdji et al. (2010),and Gourdji et al. (in prep.). Chapter 3 also presented a summary of the method.

The GIM approach involves minimizing the following objective function:

$$L_{s,\beta} = \frac{1}{2}(\mathbf{z}-\mathbf{Hs})^T\mathbf{R}^{-1}(\mathbf{z}-\mathbf{Hs}) + \frac{1}{2}(\mathbf{s}-\mathbf{X\beta})^T\mathbf{Q}^{-1}(\mathbf{s}-\mathbf{X\beta}) \quad (5.1)$$

where the vector $\mathbf{z}$ $(n \times 1)$ represents the atmospheric CO_2 measurements, and $\mathbf{s}$ $(m \times 1)$ is the vector of unknown best estimates of surface fluxes. $\mathbf{H}$ $(n \times m)$ contains the sensitivity of CO_2 measurements to surface fluxes as derived from an atmospheric transport model (further described in Section 3.5), with units of $\mathrm{ppm}/(\mu\mathrm{mol}/(\mathrm{m}^2\mathrm{s}))$. $\mathbf{X}$ is a known $(m \times k)$ matrix which is the model of the trend. $\boldsymbol{\beta}$ is a vector$(k \times 1)$ of unknown drift coefficients, so that $\mathbf{X}\widehat{\boldsymbol{\beta}}$ is the resulting estimated trend. The two covariance matrices in the objective function, $\mathbf{R}$ $(n \times n)$ and $\mathbf{Q}$ $(m \times m)$, balance the relative weight of the atmospheric data and the trend in the flux estimate, $\hat{\mathbf{s}}$. The structure of $\mathbf{R}$ and $\mathbf{Q}$ covariance matrices are further described in Section 3.4.

Minimizing equation 5.1 with respect to the unknown fluxes, $\mathbf{s}$, and drift coefficients, $\boldsymbol{\beta}$, yields a linear system of equations presented in Chapter 3, equation 3.6. The geostatistical inverse problem involves estimating both $\widehat{\boldsymbol{\beta}}$ and $\hat{\mathbf{s}}$ (e.g. Michalak et al.,

2004) using equations 3.8 and 3.10 in Chapter 3. Thus, the best estimates of flux from the inversion can be regarded as a combination of a statistical trend ($\mathbf{X}\hat{\boldsymbol{\beta}}$) and a spatio-temporally correlated stochastic component. The *a posteriori* uncertainties associated with $\hat{\mathbf{s}}$ are a function of the covariance matrices, **R** and **Q**, the structure of **X**, and the transport matrices **H**, and are expressed by equation 3.9. The *a posteriori* uncertainties associated with $\hat{\boldsymbol{\beta}}$ as well are obtained from equation 3.10 in Chapter 3.

Equations 3.8 and 3.9 provided in Section 3 are used to estimate fluxes as well as associated *a posteriori* uncertainties at a 1°×1° resolution for 2008, with the domain including all land grid cells within the range of 10°N to 70°N and 50°W to 170°W, yielding 2635 estimations locations.

3.2 Temporal estimation scale

Regional inversions that use continuous data are more susceptible to temporal aggregation errors, because continuous measurements have strong diurnal and synoptic flux variability (Law et al., 2002; Carouge et al., 2010a; Gourdji et al., 2010). Temporal aggregation error results when the estimation resolution is too coarse and cannot properly account for the variability in either the transport of fluxes or the fluxes themselves.

Carouge et al. (2010a) suggested that 4-day flux estimates at a spatial resolution of 5° x 5° be post-aggregated to 10 days and approximately 10° x 10° to minimize temporal aggregation errors in a European synthetic data study. Gourdji et al. (2010) also showed the impact of temporal aggregation errors when estimating flux in a NA synthetic data study at different temporal scales (e.g., 8-day, 4-day, 3hr etc.). The Gourdji et al. (2010) study advocated for estimating 4-day fluxes that are divided into 3-hourly time blocks to account for the diurnal cycle (henceforward referred to as 4Ddiurnal). The study also noted that a 3-hourly flux resolution would additionally reduce temporal aggregation errors, but the gain in flux accuracy may not be worth the large computational expense.

Since many of the new tower sites in the NA network are located in areas with highly variable climate and synoptic weather patterns, the use of towers in the 2008 network may exacerbate problems associated with temporal aggregation errors. As such, this study employs two different estimation scales, 4Ddiurnal and 3-hourly, resulting in

the estimation of approximately 2 million and approximately 8 million flux estimations, respectively, for the entire year.

Given that we estimate not only the fluxes, but also their full *a posteriori* covariances, computational challenges arise in estimating covariance parameters, performing variable selection, and running the inversion itself at these estimation scales. The yearly real data inversion using the 4Ddiurnal scale can be run in a single batch inversion. However, the 3-hourly scale must be run monthly to obtain monthly *a posteriori* uncertainties. The monthly inversions are run with a two-week overlap on either end of the month to ensure that fluxes for the month are constrained by the monthly observations. Unfortunately, by running 12 monthly batch inversions, aggregated annual *a posteriori* uncertainties associated with the 3-hourly $\hat{\mathbf{s}}$ will be underestimated because the uncertainties do not consider covariance between flux uncertainties from different months. As such, annual aggregated uncertainties will not be shown.

3.3 Model of the trend (X)

The $\mathbf{X}$ $(n \times p)$ matrix defines the statistical model of the trend in GIM where each column of $\mathbf{X}$ is an individual component of the trend. The $\boldsymbol{\beta}$ values as estimated by the inversion define the linear statistical relationship between each component of the model of the trend and the estimated fluxes. In this study, the inversion associated with a 4Ddiurnal scale employs an $\mathbf{X}$ that accounts for an average monthly diurnal cycle defined by 8, 3-hourly blocks. Since the 4Ddiurnal inversion is run for a full year, $\mathbf{X}$ consists of 96 columns so that the diurnal cycle is allowed to vary monthly. For the inversions that involve estimating 3-hourly fluxes, the model of the trend has only 8 columns to represent the monthly average diurnal cycle as the inversion is run separately for each month. For both cases, the model of the trend is held constant in space for all times.

3.4 Covariance matrices (Q, R)

The covariance matrix $\mathbf{Q}$ is an $(m \times m)$ matrix representing the spatiotemporal correlation structure of the component of the fluxes not explained by the model of the trend $\mathbf{X}\boldsymbol{\beta}$, referred to henceforward as flux residuals.

For the synthetic data inversions, the $\mathbf{Q}$ matrix has off-diagonal terms representing the *a priori* spatial and/or temporal autocorrelation of the flux distribution following

recommendations from Gourdji et al. (2010). Conclusions from this earlier study showed that accounting *a priori* for both spatial and temporal covariance in the flux distribution is necessary for recovering accurate *a posteriori* uncertainty bounds on the estimated fluxes (Gourdji et al., 2010). The autocorrelation is modeled by the following covariance function:

$$\mathbf{Q}\left(h_x, h_t | \sigma_Q^2, l_Q, \tau_Q\right) = \sigma_Q^2 exp\left(-\frac{h_x}{l_Q}\right) exp\left(-\frac{h_t}{\tau_Q}\right) \quad (5.2)$$

where h_x and h_t are the separation distances between grid-cells in space and lag in time, respectively. The range of correlation between fluxes is three times beyond the correlation length parameter (l_Q) and the temporal correlation length parameter (τ_Q) in an exponential model. $\sigma_{\mathbf{Q}}^2$ is the asymptotic variance of fluxes at large separation distances. Cross spatial-temporal covariance is not considered.

For real data inversions, given the computational expense of accounting for temporal correlation with off-diagonal block terms for estimating the *a posteriori* uncertainties on the best estimates, only spatial covariance is considered. Therefore, equation 5.2 becomes:

$$\mathbf{Q}\left(h_x | \sigma_Q^2, l_Q\right) = \sigma_Q^2 exp\left(-\frac{h_x}{l_Q}\right) \quad (5.3)$$

It is assumed that the off-diagonal terms have more impact on the uncertainties than on the fluxes themselves, based on the work of Gourdji et al. (2010). When temporal correlation is not taken into account, **Q** is a block diagonal matrix, with the same block describing correlation between grid-cells repeated for each time period in the inversion. By not accounting for temporal correlations, it is expected that the uncertainty estimated for aggregated and $\hat{\mathbf{s}}$ will be underestimated.

For both synthetic and real data inversions, spatial covariance parameters are allowed to vary by month, given that the spatial variability of fluxes have been found to have a strong seasonal cycle, which, in turn, influences the inferred flux estimates (Huntzinger et al., 2010; Gourdji et al., in prep).

The other covariance matrix, i.e. the model-data mismatch covariance matrix (**R**), is diagonal where the diagonal entries characterize the uncertainty errors associated with atmospheric transport, the measurement instruments, and aggregation errors (Kaminski et al., 2001). These uncertainties determine the degree to which the transported flux

estimates ($\mathbf{H\hat{s}}$) should match the observations ($\mathbf{z}$). Following Gourdji et al. (2010) and Gourdji et al. (in prep), each tower has its own unique model-data mismatch covariance ($\sigma^2_{R_i,month}$) parameter. The optimized model-data mismatch is allowed to change monthly to account for seasonal transport variability, resulting in approximately 360 optimized covariance parameters, because some towers do not have any observations for a given month.

The covariance parameters in **Q** and **R** are obtained in a statistically rigorous manner through the application of a Restricted Maximum Likelihood (RML-Inv) approach using the observational data (equation 3.17 in Chapter 3). Using the observation data to obtain the covariance parameters in RML-Inv ensures that the inversion relies heavily on atmospheric data. Thus, the approach avoids any bias in the results associated with *a priori* assumptions regarding the flux distribution or the ability of the inversion to match the observations.

3.5 Atmospheric transport (H)

For this study, the Stochastic Time-Inverted Lagrangian Transport Model (STILT) is used in conjunction with high-resolution winds from the Weather Research & Forecasting (WRF), henceforward referred to as WRF-STILT. A detailed description of WRF-STILT is provided in Nekhorn et al. (2010). WRF uses a nested grid within the NA domain, with the inner nest having a 10 km resolution (Figure 5.1) and the outer nest having 40km spatial scale.

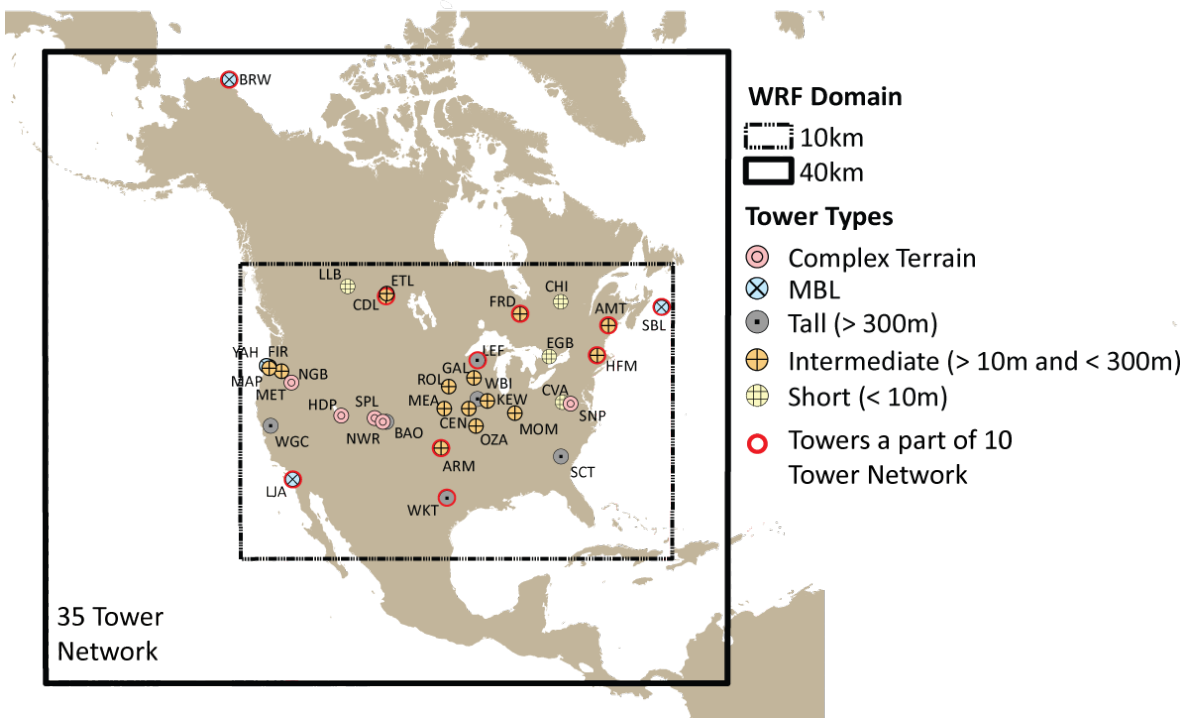

Figure 5.1: Locations of towers in the 35 and 10 tower networks with their associated classifications. Domains of the different nested WRF winds used in the WRF-STILT transport model are also shown.

STILT links the sensitivity of an observation to a flux more realistically than more coarsely defined Eulerian models, especially in areas near the tower (Lin et al., 2003). Previous studies have used STILT in conjunction with continuous measurements sited in areas with high CO_2 flux variability to estimate fluxes for regional areas in North America (e.g. Matross et al., 2006; Gourdji et al., in prep).

Sensitivities (in units of $\mathrm{ppm}/(\mu\mathrm{mol}/(\mathrm{m}^2\mathrm{s}))$) of observations to fluxes are estimated by releasing 500 particles from highest measurement location at each tower in the network for every measurement time period. The particle trajectories are tracked backwards in time and space for 10 days. The resulting sensitivities are the proportion of the 500 particles that reach a given flux estimation location (defined both in time and space). Thus, the resulting sensitivity footprints describe how unit fluxes in a particular gridcell of the domain at a particular time affect a CO_2 concentration at a particular tower location. Refer to Gourdji et al., (2010), Gourdji et al. (in prep), Nekhorn et al. (2010),

and Lin et al. (2003) for more details on WRF-STILT, including the physical schemes employed in the model and the derivation of sensitivities.

The concentration footprints, **H** ($ppm/(\mu mol/(m^2 s))$), provided by the WRF-STILT atmospheric transport model are used to understand what portions of the continent can be seen by a particular tower. To assess this, a method is adopted similar to Huntzinger et al. (in press) which assessed the ability of observations to detect differences in the spatial distribution of fluxes in the near- and far-field. For each tower and each hour in the month of June, the land cells are sorted in terms of how sensitive the tower measurements are to surface fluxes from that cell. Cells are ordered from those having the greatest influence to those having the least. The influences are cumulatively summed and divided by the overall or total sensitivity for that tower to the entire domain. The analysis provides a grid-cell percentage of coverage to show which areas of the continent are better constrained by observations from a given tower site.

The overall ability of an inversion to trace back observations from tower locations to surface flux locations is highly dependent on the ability of the transport model to simulate synoptic and seasonal weather variability. To identify areas where fluxes could be reliably interpreted throughout the year, the criterion used in Gourdji et al. (2010; in prep) is used. To meet the criterion, on average, a 4-day flux of $1 \mu mol/(m^2 s)$ must influence measured concentrations at all towers by a total of at least 0.1 ppm throughout the year 85% of the time. The well-constrained, i.e. high sensitivity, areas (henceforward referred to as HighSens areas) using a 10 tower network covered roughly 30% of the continent. With 35 towers in 2008, the well-constrained area is significantly larger, covering 70% of the NA domain (Figure 5.2). Thus, the monthly and annual 2008 carbon budgets for NA have the potential to be much better constrained by observations than for earlier years.

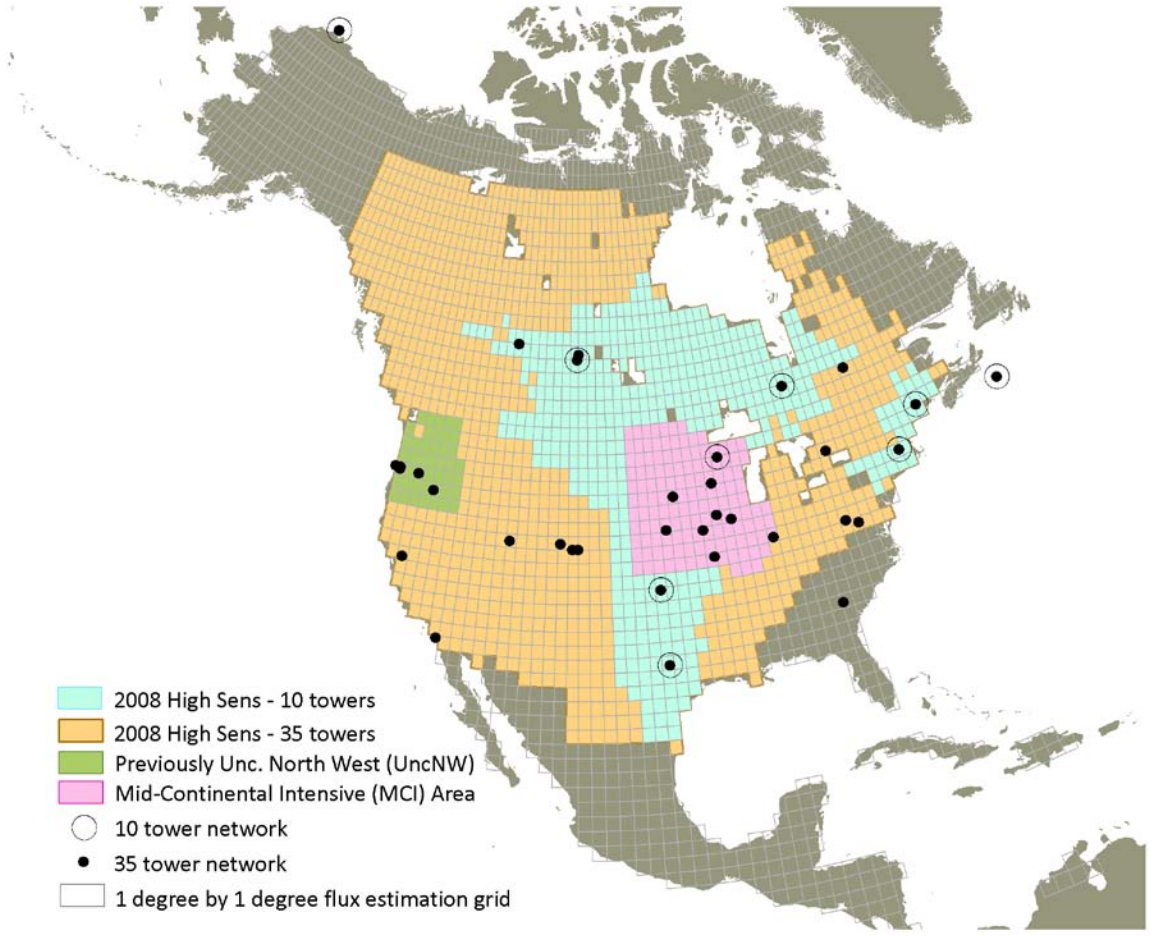

Figure 5.2: Regions used for the interpretation of flux estimates at spatially aggregated scales from both synthetic and real data inversions. Note high sensitivity from the 10 tower network is referred to as HighSens henceforward. The high sensitivity for the 35 tower network is shown to illustrate the additional constraint provided by the expanded network.

3.6 Atmospheric observations (z)

This study uses continuous calibrated CO_2 measurements from the locations shown in Figure 5.1 and listed in Table 5.1. The measurements are filtered to exclude data associated with any anomalous errors (measurement greater or less than 30 ppm over background air or observations associated with low-quality flags). As with Gourdji et al. (in prep.), data are also excluded if their sensitivity to ocean fluxes is greater than 85% of their total sensitivity to all land and ocean locations. The continuous measurements from all towers are averaged to a three-hourly timescale. No effort was made to fill the short

and long gaps in the concentration series for certain towers, although it is noted that these gaps may introduce discontinuities into the inversions that could influence final flux estimates.

Table 5.1: List of towers and the two different choices of times of the day for which to include observations for the real and synthetic data inversions (shortaft and 1pm/1am). Data providers include (a) Arlyn Andrews, (b) Matt Parker (c) Marc Fischer, (d) Colm Sweeney, (e) Doug Worthy, (f) Bill Munger, (g) Ken Davis, (h) Danilo Dragoni, (i) Britt Stephens, (j) Bev Law, and (k) Ralph Keeling.

Name	Location w/ data provider	agl (m)	Shortaft	1pm/1am
LEF	WI, Park Falls[a]	396	All 24 hours	1 pm
WKT	TX, Moody[a]	457	All 24 hours except 10am	1 pm
WBI	IA, West Branch[a]	379	All 24 hours	1 pm
BAO	CO, Boulder Atmospheric Obs.[a]	300	All 24 hours except 10am	1 pm
SCT	SC, South Carolina Tower[b]	305	All 24 hours except 10am	1 pm
WGC	CA, Walnut Grove[c]	483	All 24 hours except 10am	1 pm
AMT	ME, Argyle[a]	107	1, 4, and 7 pm	1 pm
BRW	AK, Barrow[d]	17	All 24 hours	1 pm
FRD	Ontario, Fraserdale[e]	40	1, 4, and 7 pm	1 pm
CDL	Saskatchewan, Candle Lake[e]	30	1, 4, and 7 pm	1 pm
SBL	Nova Scotia, Sable Island[e]	25	All 24 hours	1 pm
EGB	Ontario, Egbert[e]	3	1 pm	1 pm
ETL	Saskatchewan, East Trout Lake[e]	105	1, 4, and 7 pm	1 pm
LLB	Alberta, Lac LaBich[e]	10	1 pm	1 pm
CHI	Québec, Chibougamau	30	1 pm	1 pm
HFM	MA,Harvard Forest[f]	30	1, 4, and 7 pm	1 pm
ARM	OK, Southern Great Plains[c]	60	1, 4, and 7 pm	1 pm
CVA	WV, Canaan Valley[g]	7	1 pm	1 pm
MOM	IN, Morgan Monroe[h]	48	1, 4, and 7 pm	1 pm
OZA	MO, Ozark[g]	30	1, 4, and 7 pm	1 pm
KEW	IL, Kewanee[g]	140	1, 4, and 7 pm	1 pm
CEN	IA, Centerville[g]	110	1, 4, and 7 pm	1 pm
MEA	NE, Mead[g]	122	1, 4, and 7 pm	1 pm
ROL	MN, Round Lake[g]	110	1, 4, and 7 pm	1 pm
GAL	WI, Galesville[g]	122	1, 4, and 7 pm	1 pm
SNP	VA, Shenandoah National Park[g]	17	1 am	1 am
SPL	CO, Storm Peak Lab[i]	9	1 am	1 am
NWR	CO, Niwot Ridge[i]	5	1 am	1 am
HDP	UT, Hidden Peak Snowbird[i]	18	1 am	1 am
FIR	OR, Fir[j]	38	1, 4, and 7 pm	1 pm
MET	OR, Metolius[j]	34	1, 4, and 7 pm	1 pm
YAH	OR, Yaquina Head[j]	13	1, 4, and 7 pm	1 pm
MAP	OR, Mary's Peak[j]	8	1, 4, and 7 pm	1 pm
NGB	OR, NGBER[j]	7	1, 4, and 7 pm	1 pm
LJA	CA, LaJolla[k]	5	1pm and 1 am	1 pm

Gourdji et al. (in prep), partially validated the spatial pattern of the 2004 fossil fuel inventory dataset which was created from the version 1.4 Vulcan database for 2002 (Gurney et al., 2009) for the United States, information from British Petroleum fuel statistics, remotely-sensed night lights, and the existing Carbon Dioxide Information Analysis Center (CDIAC) fossil fuel emission estimates (Oda and Maksyutov, 2010) for Canada, Mexico, and Central America. The combined fossil-fuel dataset is scaled to 2008 based on published rates of anthropogenic CO_2 emissions (Raupach and Canadell, 2010). Given that the fossil fuel component is relatively well-known compared to the biosperhic component of flux, the fossil fuel dataset was transported from a 1°x1° monthly resolution to the observations using the WRF-STILT sensitivity matrices, and presubtracted from the 3-hourly averaged observations. In this manner, the resulting flux estimates best represent biospheric fluxes.

3.6.1 Selection of observations

Given the expansion of the measurement network of continuous observations from 10TN 2004 to 35TN in 2008, there are many options of which observations to use (both in space and time). However, given the tightly coupled nature of transport and measurements, it is important only to use observations when the simulated transport can be trusted. Analysis of footprints for the tall tower sites indicates that the midday data is well-mixed and retains a signature of the fluxes from the past several days (A. Andrews, personal communications). As a result, most regional inversions use only midday data but the times of day and averaging period varies per study (e.g. Peters et al., 2007; Butler et al., 2010). However, if simulated transport can be trusted during other time periods, then the additional atmospheric data can provide further constraints on flux estimates. Some inversions, therefore, have included either 24 hours of observations or nighttime data at tall towers (Gourdji et al., 2010; A. Andrews, personal communication). There are concerns, however, that the atmospheric transport models cannot properly simulate the height of the nighttime planetary boundary layer (PBL) or characterize the transition of the PBL during morning and early evening hours at most locations. Since the PBL has a large influence on the mixing of the CO_2, misrepresentation of its height or behavior can have a strong negative affect the flux estimates (Denning et al., 1996).

There are also concerns about using observations from complex terrain or coastal sites where transport is difficult to model (e.g. Ahmadov et al., 2009). For complex terrain sites, it is generally assumed that observations at 1am best represent background air as the variability of the topography results in the pooling of CO_2 into valleys and the measurement location are located on mountain peaks.

To better understand the behavior of the variability of measurements by tower, we analyzed the observational records, as well as the associated ΔCO_2 (i.e. the observations minus the influence of CO_2 variability originating outside of the examined domain, aka boundary conditions). Understanding the measurement variability assists in determining which times of the day to use observations for different tower locations, as hours associated with high variability likely correspond to complicated transport which is difficult to model. For tall towers, the measurements and corresponding ΔCO_2 have consistent variability throughout the day. However, for short and intermediate towers (Figure 5.3), a defined diurnal cycle is evident in both the observation records and corresponding ΔCO_2. The measurements associated with both the breakup of the night-time PBL during the morning and the onset of atmospheric stability at night have very large variability throughout the month of June as with all the growing season months. The variability in observations from the short towers is particularly strong (e.g. measurements can differ by more than 150ppm in the early morning hours at LLB in June). However, the measurements during the middle of the afternoon are more stable and display variability similar to observations from tall towers. The strong diurnal variability at both the short and intermediate towers warrants caution in choosing which observations to include within the inversion.

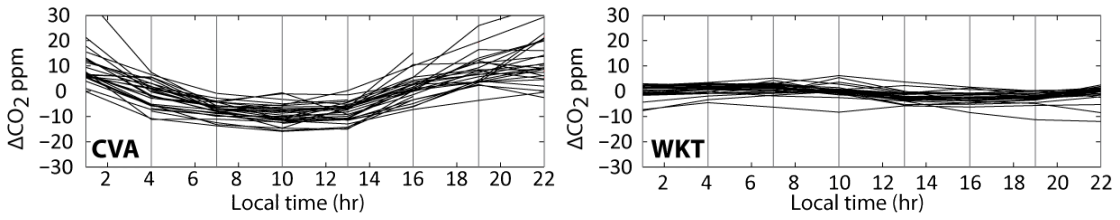

Figure 5.3: Daily June 3-hourly averaged concentrations as measured at CVA (a short tower) and WKT (a tall tower), with the influence of GV-BCs pre-subtracted (a.k.a. ΔCO_2). The daily ΔCO_2 records are overlaid on top of one another to highlight the diurnal variability. Note that the use of CT-BCs creates a systematic constant downward offset of ~1ppm, but no change to the diurnal variability.

The extra constraint from the addition of more measurements in space versus using more observations in time has not been previously investigated. To assess the impact of including more observations in space and time, both a 10TN and 35TN are used in the synthetic and real data inversions. In the synthetic data inversions, which assume close to perfect transport (i.e. $\sigma^2_{R_i,month}$ = 0.01 ppm^2), three choices of observations throughout the day are considered. Note all choices are using the 3-hourly averaged observations. The choices include: (1) 24 hours of data (all), (2) approximately one to four observations throughout the day (shortaft) (Gourdji et al., 2010), and a single observation, either 1pm or 1am (1pm) (based on CT choices). The specifics of the selection of data (i.e. shortaft versus 1pm) for each measurement location are defined by tower in Table 5.1. For the real data inversions, only the shortaft and 1pm selection of data is considered for the 10TN and 35TN inversions since simulated transport cannot be trusted at all times of the day for all towers.

3.6.2 Continental boundary conditions

The influence of fluxes from outside the NA domain on the measurements is accounted for in regional inversions by the use of boundary conditions for each tower location. In general, the boundary conditions are estimated by transporting the atmospheric concentration of CO_2 defined at the boundaries of the domain to measurement locations using WRF-STILT. These boundary conditions are pre-subtracted from observations and the resulting ΔCO_2 (i.e. **z**) are used in the inversion.

The choice of the specific set of boundary conditions to use in the inversion has a direct impact on the **z** vector used to estimate fluxes. Hence, many regional inversion studies have found flux estimates to be highly sensitive to the choice of boundary conditions (e.g. Schuh et al., 2010). This study uses two plausible sets of boundary conditions for inversions using a 1pm daily observation. The first is from NOAA's CT data assimilation system (CT-BCs) (Peters et al., 2007). CT-BCs have been used in several NA regional inversion studies (e.g. Schuh et al., 2010, Butler et al., 2010, etc.). In contrast, the second set of boundary conditions (GV-BCs) is more empirically based in attempt to correct known biases in the CT-BCs (A. Andrews, personal communication).

3.7 Outline of synthetic and real data experiments

The measurements are used in both a set of synthetic and real data inversion as will be explained in the following section to assess the measurement information of the expanded network as well as the influence of the temporal estimation scale and boundary conditions. Overall, several 1°x1° degree inversions are run using two different networks, i.e. 35 towers (35TN) available in 2008 and 10 towers (10TN) available in 2004. An outline of the specific inversions is presented in Figure 5.4.

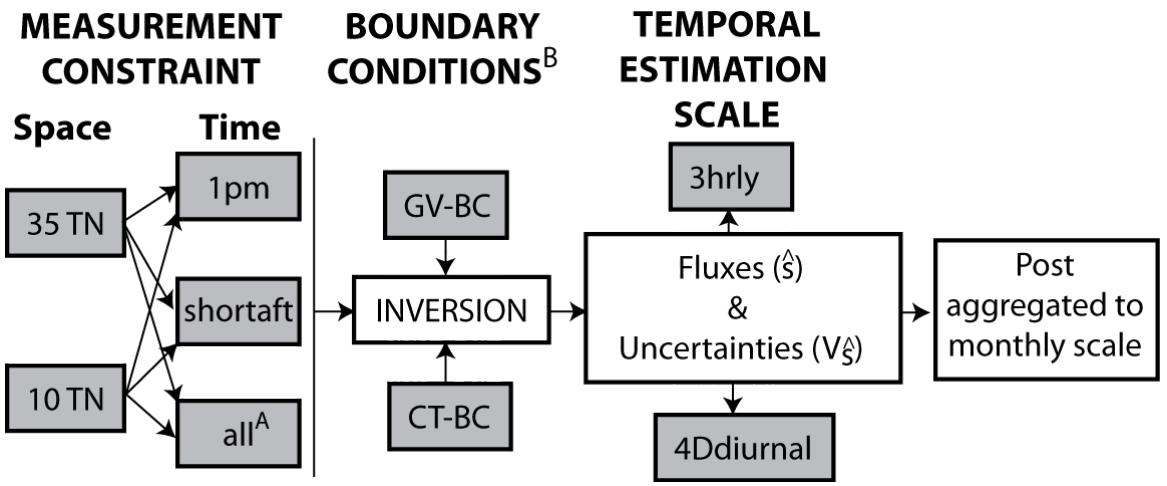

Figure 5.4: Schematic of the different geostatistical inversions for both the synthetic data and real data components of the research. Gray boxes indicate the different setup choices tested as part of the work. The shortaft and all data choices resulted in approximately three and eight times more temporal data coverage than 1pm respectively. Note that the all data choice (A) was only used in the synthetic data experiments, and boundary conditions (B) were only used in real data experiments. Overall, both the synthetic and read data experiments each involve 12 inversions.

Synthetic data studies help to isolate the impact of inversion setup choices by simplifying the problem because (1) $\mathbf{Hs}_{BM}$ are only influenced by fluxes occurring within the NA domain, and therefore there is no need to specify boundary conditions for the selected domain (Gourdji et al., 2010), and (2) are absent of any errors associated with transport. For this study, synthetic observations are generated by multiplying a vector of 3-hourly June2004 CASA-GFEDv2 (Randerson et al., 1997; Giglio et al., 2006) flux estimates by the sensitivity matrix **H** for each tower derived from the 2008 WRF-STILT particle trajectories. The multiplication results in modeled atmospheric CO_2 observations (i.e. $\mathbf{Hs}_{BM}$) for each tower. Note that June2004 CASA-GFEDv2 fluxes are used for the analysis given that 2008 CASA fluxes were not available. However, the choice of biospheric model is somewhat arbitrary for this analysis because the synthetic inversions are testing the ability of the inversion to recover a known "truth". As such, any plausible flux distribution could be used for this analysis.

The real data inversions are similar to the synthetic data inversions, but involve the use of actual measurements to estimate fluxes throughout 2008. Also, the real data

inversions employ two different selections of temporal observations as described in Section 3.6.1.

The results are analyzed for four different spatial areas: the entire NA domain (approximately 20 million km^2), an area considered well-constrained using the 10TN (i.e. HighSens previously explained in Section 3.4) (approximately 5 million km^2), the MidContinental Intensive (MCI) region, and the previously under-constrained area in the Pacific Northwest (UncNW). These areas are shown in Figure 5.2.

The MCI region is a region (approximately 1 million km^2) is located in the Midwest agricultural belt of the U.S. The MCI is not subject to the complexities and small-scale variability associated with microclimates, population density, topography that plagues other areas in the continent. In addition, the area is mostly flat and therefore atmospheric transport is easier to model in this region compared to others with mild to significant topographic relief. The area also constitutes a significant portion of the most intensively farmed region of the continent and hence, the carbon cycling dynamics of in the MCI has been highly studied in 2007 and 2008 (see http://www.nacarbon.org/cgi-nacp/web/investigations/inv_ic_profiles.pl for a list of ongoing projects).

In contrast, UncNW (~400,000 km^2) has significant small-scale to mesoscale variability in vegetation characteristics and complicated coastal transport that are difficult to model. The crest of the Cascade Mountains roughly splits that region into a western part dominated by dense, managed Douglas-fir forests and agricultural crops which are highly productive, and a semiarid eastern part mainly consisting of open ponderosa pine forest and juniper-sagebrush-grass communities (Göckede et al., 2010).

4.0 Results and discussion

The study assesses the influence of three inversion choices (selection of data, scale of estimation, and boundary conditions) on the estimated fluxes post-aggregated to various spatial and temporal scales: (1) at the monthly grid-scale, (2) at spatially aggregated areas at the monthly timescale, (2) at annually averaged and spatially aggregated areas. A sensitivity analysis is provided to show the observation coverage per tower, addressing concerns the extent of coverage provided by some of the new towers in the expanded measurement network. The study then relies on synthetic data inversions results to assess the biases and limitations associated with the inversion choices at the

different spatiotemporal scales. The inversions using real atmospheric data are then evaluated based the conclusions of the synthetic data experiments, to assess whether the conclusions are when robust using actual observations and real associated transport errors.

4.1 Footprint analysis

Over 50 percent of the total average June sensitivities for 1pm measurements are in areas that are approximately 700-1000 km away from most towers, indicating that observations contain more than just local information regarding sources and sinks (Figure 5.5). In fact, the sensitivities for the short towers cover areas similar to the intermediate towers. The extent of the short tower footprints indirectly suggest that WRF-STILT used in this study is able to simulate well-mixed times of the day at these tower sites as the locations of these towers were chosen, in part, to capture well-mixed air during midday. In other studies (e.g. CT, Peters et al., 2007), particles are released at an artificial height (~200m) when estimating the sensitivity of short towers to surface fluxes when simulating transport. For these other studies, the particles are released at a height much taller than the tower to avoid any problems with simulating transport associated with convective mixing. As such, it appears that WRF-STILT is able to circumvent errors associated with releasing particles at heights that are different than those corresponding with the actual observation.

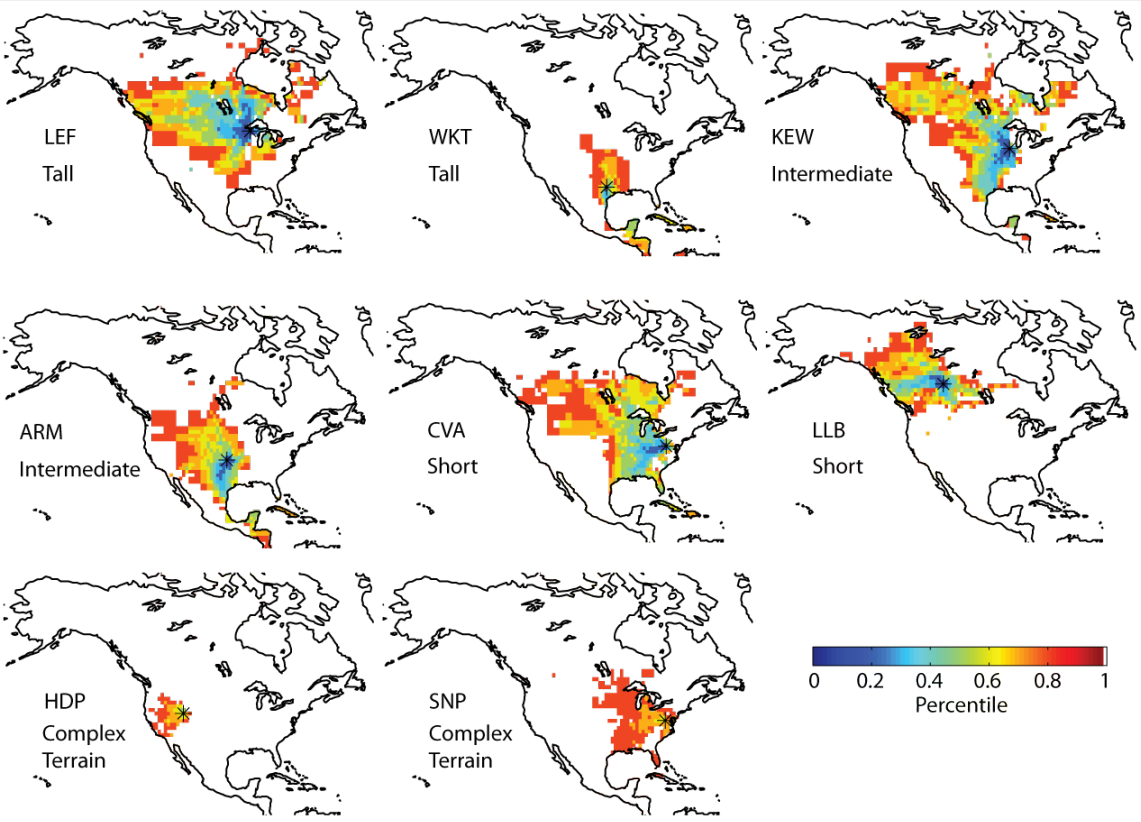

Figure 5.5: Average 3-hourly June footprint for different towers as percentiles of the total sensitivity for a given tower.

4.2 Synthetic data results for June 2008

The synthetic data experiments provide a baseline for the best achievable performance of real-data inversions, and help to highlight the impact of setup choices that may be obscured by the additional complexity associated with using real data.

4.2.1 Monthly grid-scale estimates

Including more observations both in time and space enables the inversion to better reproduce the true grid-scale fluxes when using a 3-hourly estimation scale (Figure 5.6, subplot a compared to Figure 5.6, subplot f). More importantly, when the number of towers is held constant, using observations from more times of the day substantially improves flux estimates relative to the use of measurements from more tower locations. Furthermore, the extra constraint from adding more observations in time is only apparent

with the use of the expanded network (refer to Figure 5.6, subplots d-f compared to subplots a-c). Hence, using more observations throughout the day at the 35 towers has the largest impact on the performance of the inversion in being able to reproduce both the spatial patterns and overall magnitudes (e.g. $\rho = 0.77$ with 1pm (subplot c) versus $\rho = 0.83$ (subplot a) with all using 35TN as shown in Figure 5.6). This is an important result as most inversions use only one or two measurements per tower per day representing a multi-hour average, and may not benefit as much from using more spatial data compared to inversions that incorporate more observations in time. Therefore, improving flux estimates using the expanded network involves incorporating observations from more times of the day, not just more towers.

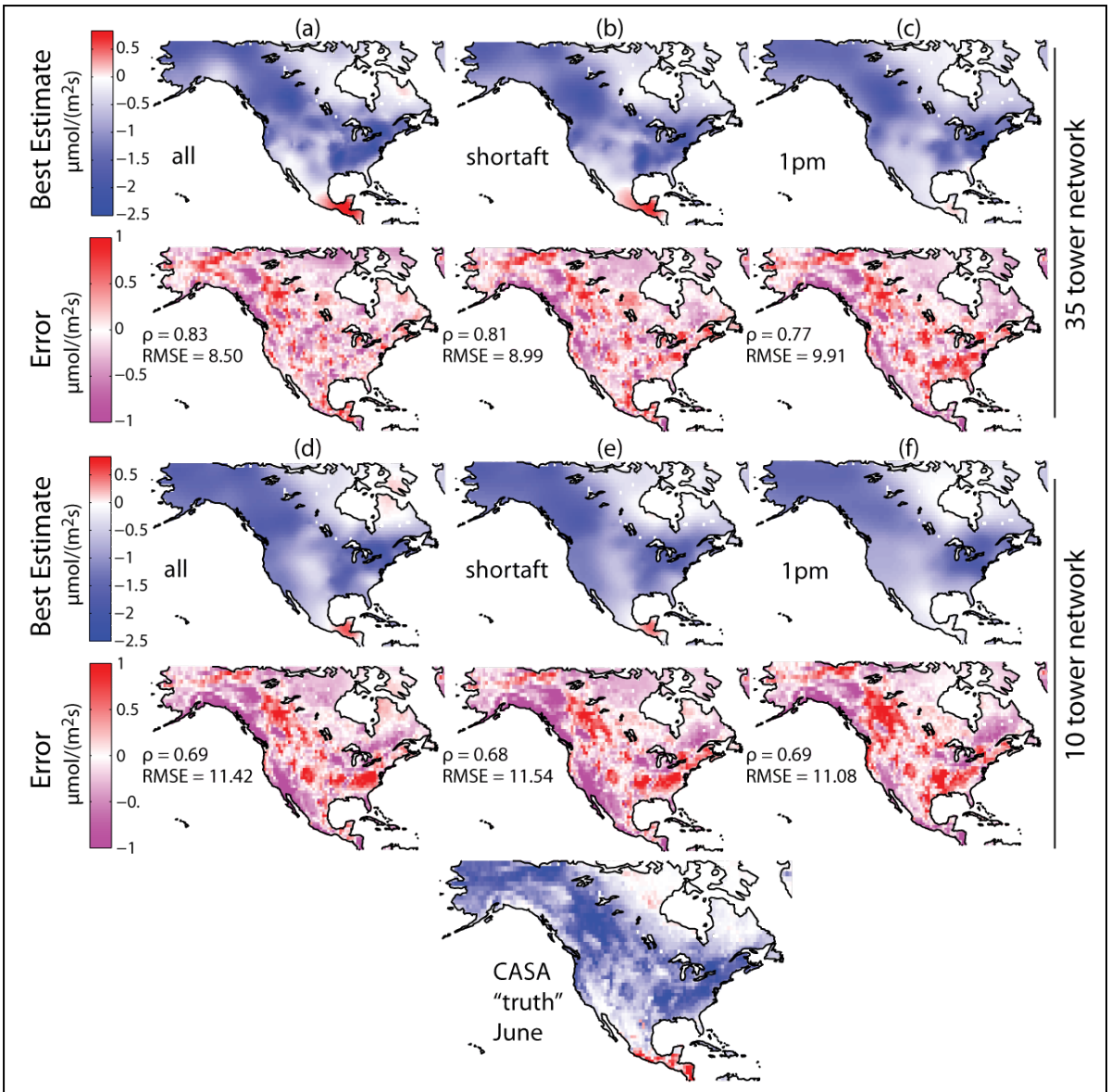

Figure 5.6: Average June grid-scale biospheric fluxes from the synthetic data inversions using a 3hr estimation scale. Also shown are the "true" CASA fluxes that were used to generate the synthetic data. The grid scale monthly correlation coefficient (ρ) and RMSE are provided next to each grid scale difference plot. Lower RMSE and higher correlation correspond to more accurate results.

Results show that estimating at finer temporal scales yields better flux estimates given the extent of the variability associated with regional synoptic transport. Comparing Figure 5.6 and Figure 5.7, shows that the highest accuracy grid scale-estimates is obtained with native timescales (i.e. the native resolution of the fluxes and sensitivities used to create the synthetic data). When using a coarser estimation scale (i.e. 4Ddiurnal),

the estimates are strongly affected by temporal aggregation error (Figure 5.7) as shown by the unrealistically strong sources and sinks in the recovered fluxes. As mentioned earlier, temporal aggregation error results when the estimation resolution is too coarse and cannot properly account for the variability in either the transport of fluxes or the flux distribution itself. Therefore an entire estimate is "shifted" up or down based on high variability associated with only a small portion of the estimate. In Figure 5.7, temporal aggregation error substantially reduces the ability of the inversion to reproduce the both the spatial patterns and magnitudes of the true flux, especially when including more data in time (e.g. $\rho = 0.62$ with 1pm (subplot c) versus $\rho = 0.46$ (subplot a) with all using 35TN as shown in Figure 5.7). By not taking into consideration temporal aggregation errors, one could come to the wrong conclusions and surmise that more spatial and temporal actually biases flux estimates when using the 35TN; a message directly opposed to that derived from the 3-hourly grid-scale results.

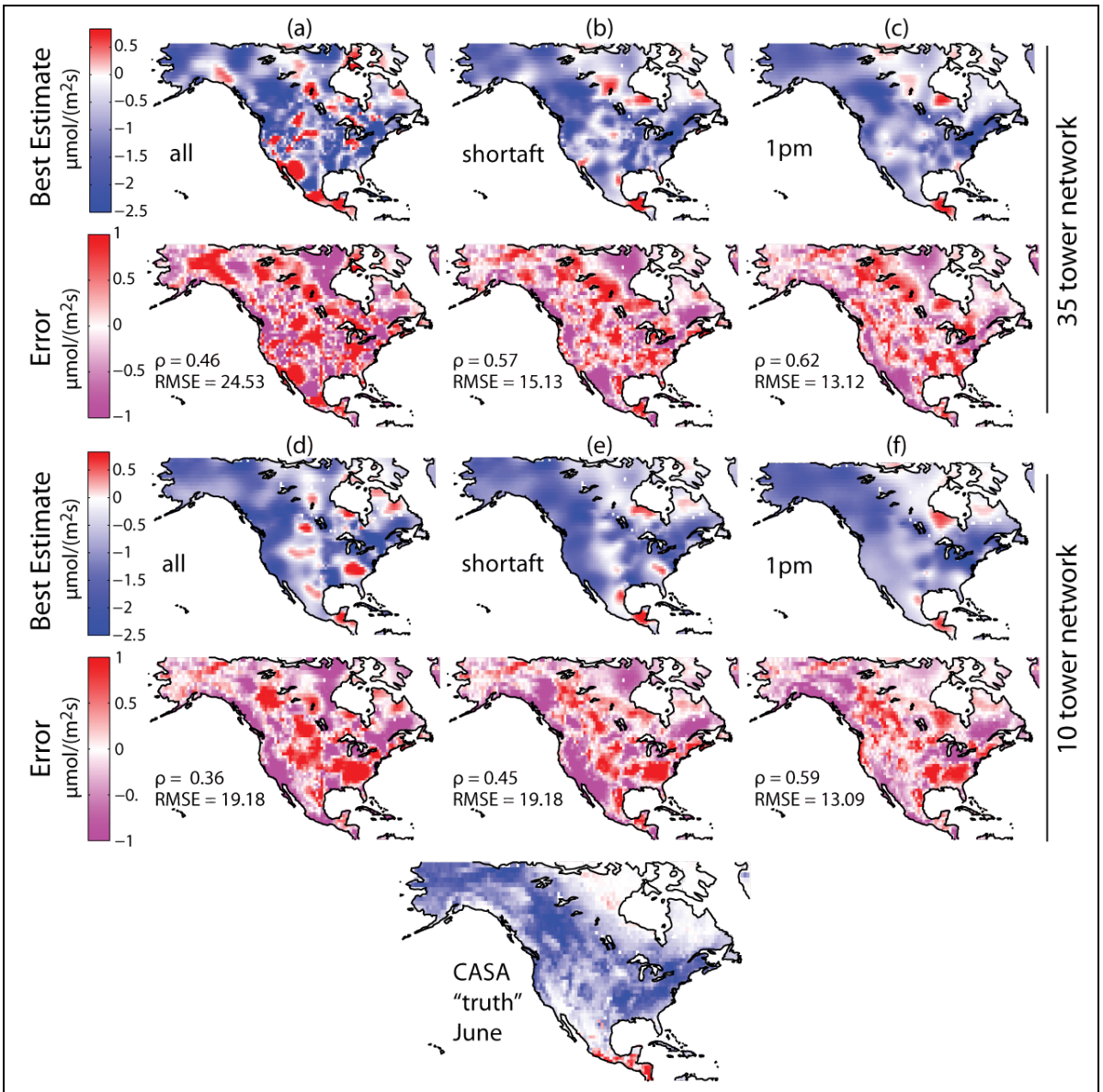

Figure 5.7: Average June grid-scale biospheric fluxes from the synthetic data inversions using a 4 day diurnal estimation scale. Also shown are the "true" CASA fluxes that were used to generate the synthetic data. The grid scale monthly correlation coefficient (ρ) and RMSE are provided next to each grid scale difference plot. Lower RMSE and higher correlation correspond to more accurate results.

The 4Ddiurnal results show that using an estimation scale of 4 days with a resolved diurnal cycle post aggregated to a monthly timescale cannot appropriately account for the underlying variability of either the fluxes or transport, which yields biased grid-scale fluxes. This is in contrast the conclusions drawn by Carouge et al. (2010a), and discussed above in Section 3.2, and is most likely due to the fact that the previous study

employed a daily observation which averaged out diurnal variability. Although the aggregation errors are significant for the choice of all 24 hours of data, they are less for the use of a single measurement per day at the 4Ddiurnal estimation scale. The danger for inversions that use a coarser estimation scale with a single daily observation is that there may be a tendency to interpret the grid-scale temporal aggregation error with a mechanistic argument (e.g. presence of a non-existent fossil fuel source or agricultural feedlots, etc.), such as errors shown in Figure 5.7, subplots e or f.

For the HighSens and MCI regions, adding in more data in time also helps the inversion reproduce both the spatial pattern and magnitudes of the "true" grid-scale flux estimates when using the expanded network (Figure 5.8). As with the average monthly grid-scale results for all of NA, temporal aggregation error also plays an important role in the grid-scale flux estimates within each of these smaller regions. In terms of the UncNW, it is assumed that the large variability in underlying fluxes in this region make it difficult for the inversion to reproduce the grid-scale fluxes even with the maximum data coverage using the finest estimation scale (Göckede et al., 2010).

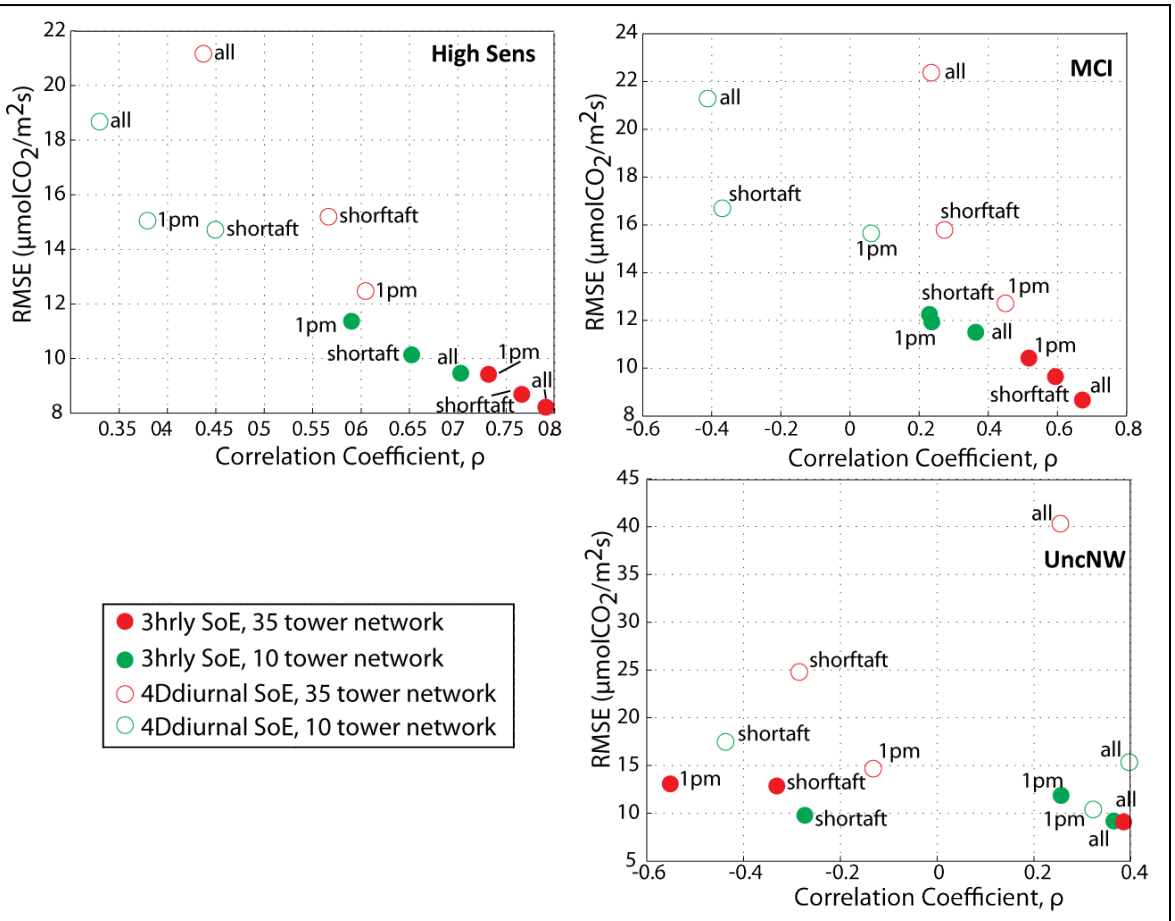

Figure 5.8: Root Mean Squared Error (RMSE) and correlation coefficient (ρ) between June grid-scale flux estimates for different regions from the synthetic data inversions and the "true" CASA fluxes. Lower RMSE and higher correlation correspond to more accurate results.

Note, that because the synthetic data inversion assumes perfect transport, it is expected that including all data for the 35TN would yield the best results. However, the synthetic data results also show that accurate carbon budgeting at different spatiotemporal scales can be achieved using the 35TN if we are able to trust transport for more time of the day. In a real data inversion, the atmospheric transport models errors are diurnally dependent and thus may negate the advantages shown in Figure 5.6 and 5.8.

4.2.2 Spatially aggregated monthly flux estimates

As can be seen in Figure 5.9, the conclusions drawn from the synthetic grid-scale results (Section 4.2.1) generally continue to apply at spatially aggregated scales. That is,

with more observations in space and time, the better the inversion is able to reproduce the aggregated fluxes, but the ability of the inversion to replicate the "truth" diminishes as the size of the region decreases (e.g. Figure 5.9, UncNW region). At the NA scale, the accuracy of the estimates from the inversion that uses the most measurements in time or in space is almost identical to those from the inversion that use the least amount of observations. As the size of the region gets smaller, the additional measurements has a larger influence by allowing the inversion to better reproduce the truth.

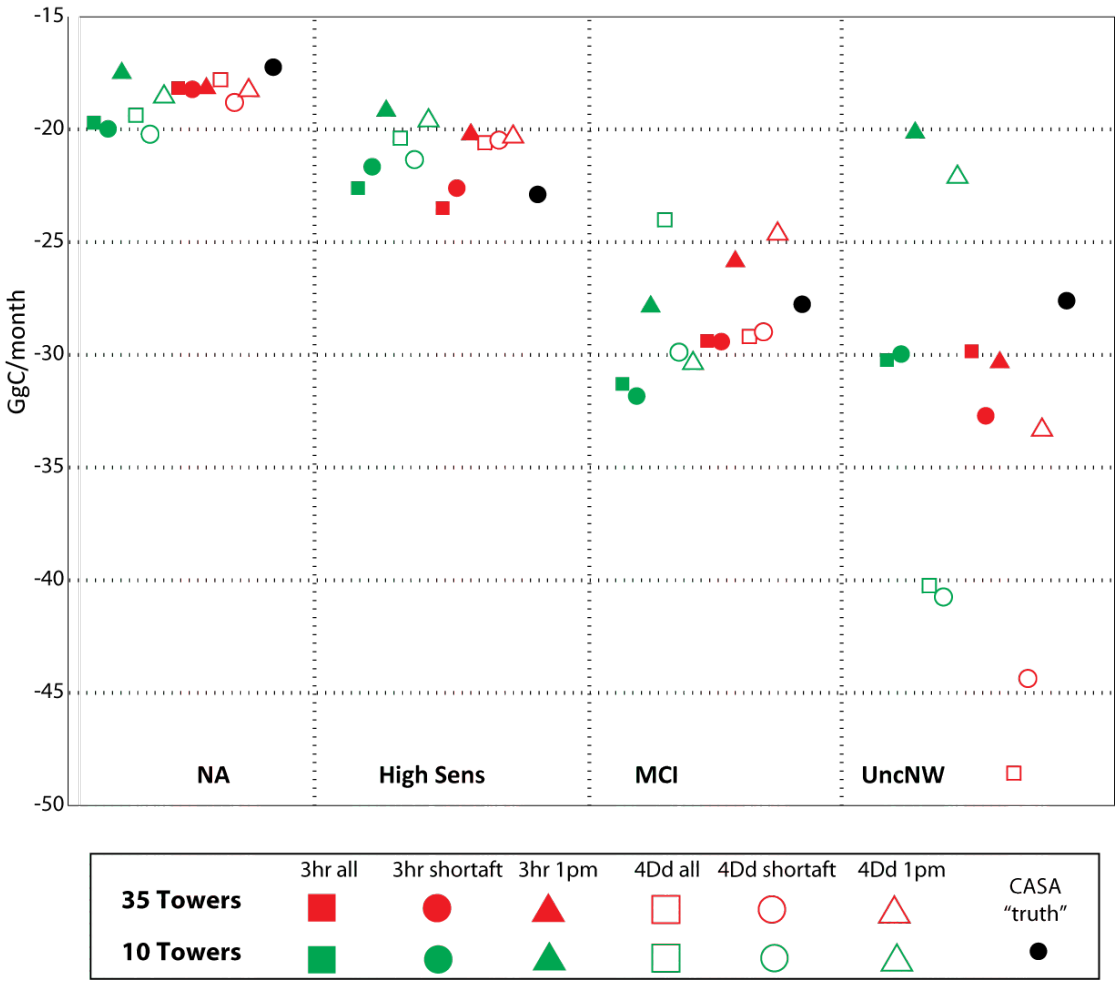

Figure 5.9: **S**patially post-aggregated June fluxes estimates from the synthetic data inversions along with the "true" CASA fluxes. The June fluxes are post-aggregated to NA, High Sens, MCI, and UncNW.

As with the grid-scale results in Section 4.2.1, estimating at a fine temporal resolution is a better choice for obtaining accurate fluxes at spatially aggregated scales

because this limits temporal aggregation error, but the extent of the influence also depends upon the size of the region. Therefore, the influence of the estimation scales and, hence, the presence of temporal aggregation is seen most clearly in the UncNW. Other studies have concluded that temporal aggregation is negligible when fluxes are post aggregated to large regional areas (~5°x 5° grid-cells, Carouge et al. (2010a)). However, as seen here, even at larger regional scales, temporal aggregation can have a large impact, especially if the region contains highly variable fluxes or experiences significant shifts in transport such as UncNW at monthly timeframes.

4.3 Real Data Results for January – December, 2008

With real data inversions, there is no means to directly assess CO_2 flux estimates because there is no "truth" for comparison. However, by performing a series of real data inversions with different setup choices, the sensitivity of flux estimates to a particular setup choice can be assessed in light of simulated transport errors.

4.3.1 Monthly grid-scale flux estimates

At the 3-hourly estimation scale, using atmospheric CO_2 concentration data, adding more measurements at a given tower (i.e., more times of the day) has a greater influence on the grid-scale flux estimates than adding more observation locations (spatially) to the inversion. As with the synthetic data results, the extra constraint provided by the additional observations is most apparent for flux estimates in both June and October using the 35TN using shortaft (Figures 5.10 and 5.11). The impact of using more measurements per day on flux estimates is most obvious in areas that were previously under-constrained. For example, the use of 24 hours of data at tall towers such as BAO, WGC, and BRW results in lessening of sinks in Northwestern states in the US and in the northern parts of Alaska. In contrast, the expanded network appears to have little influence compared to the 10TN when using only a single measurement per day. Although the synthetic data experiments did show small improvements in flux estimates with the use of a single measurement per day with the expanded network, the uncertainty associated with real data and transport (as inferred by RML), may weaken the flux signal in the observations. As such, with real data, there are less benefits of including more spatial observations with limited temporal coverage.

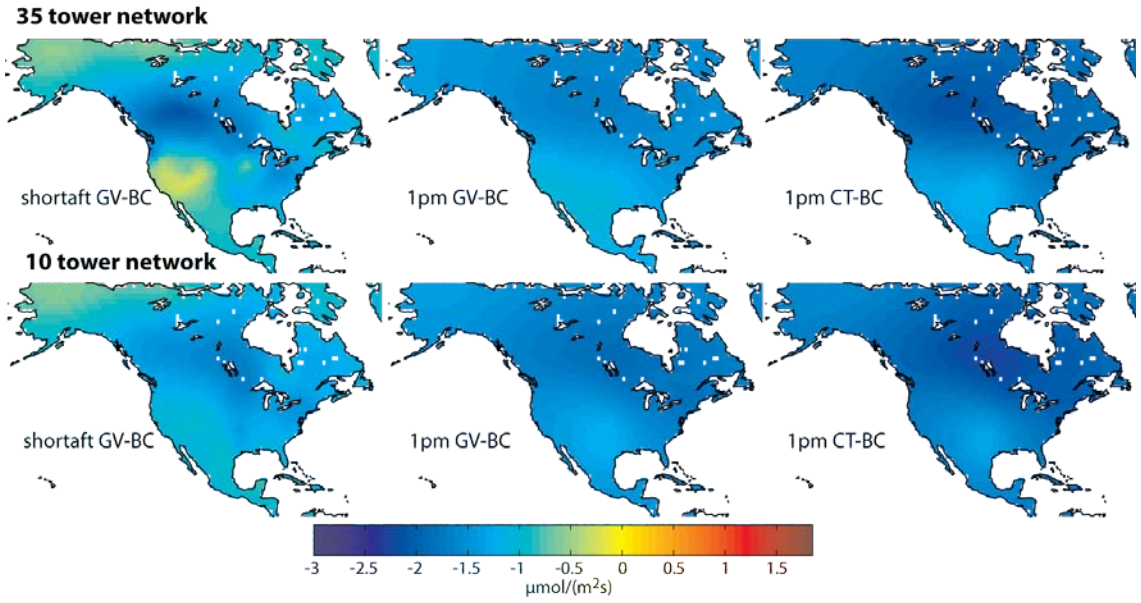

Figure 5.10: Average June grid-scale biospheric fluxes from the real data inversions using a 3-hourly estimation timescale.

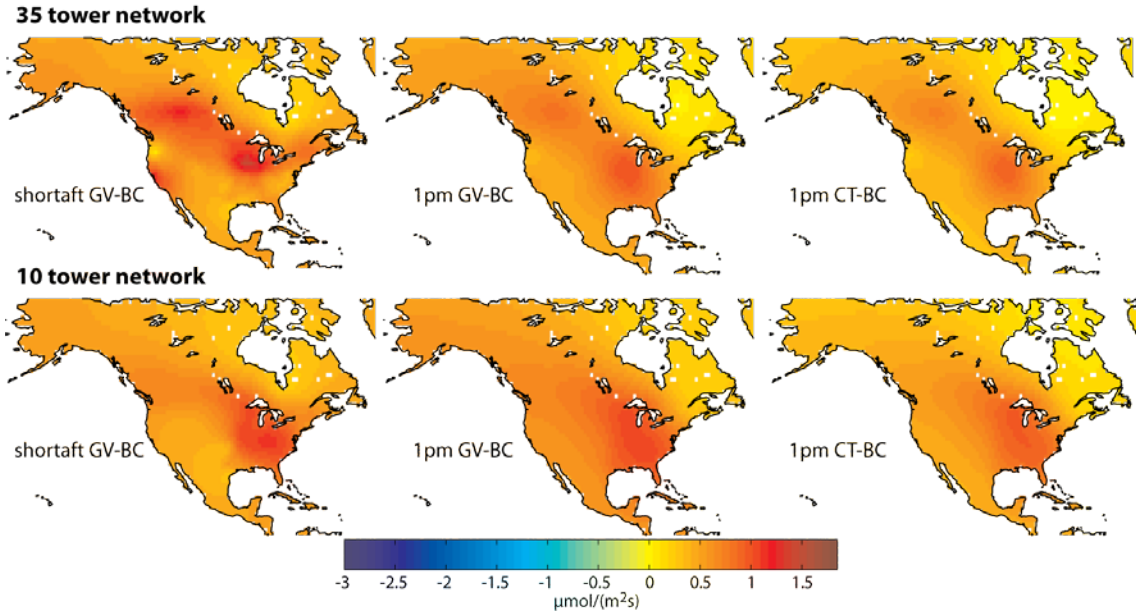

Figure 5.11: Average October grid-scale biospheric fluxes from the real data inversions using a 3-hourly estimation timescale.

At the 4Ddiurnal estimation scale, the strength of the grid-scale sources and sinks compared to the 3-hourly estimates indicates that the 4Ddiurnal fluxes are influenced

significantly by temporal aggregation errors (e.g. shortaft GV-BC results in Figures 5.12 and 5.13 specifically in Midwestern states and northern Canadian provinces). Including more observations throughout the day with the 35TN also impacts the 4Ddiurnal estimates but to a lesser extent than the scale of estimations. Given the parallels between the flux estimate results from the synthetic and real data inversions, it can be concluded that inversions that estimate 3-hourly fluxes using more observations throughout the day are able to extract the most out of the expanded network in terms of estimating monthly grid-scale fluxes.

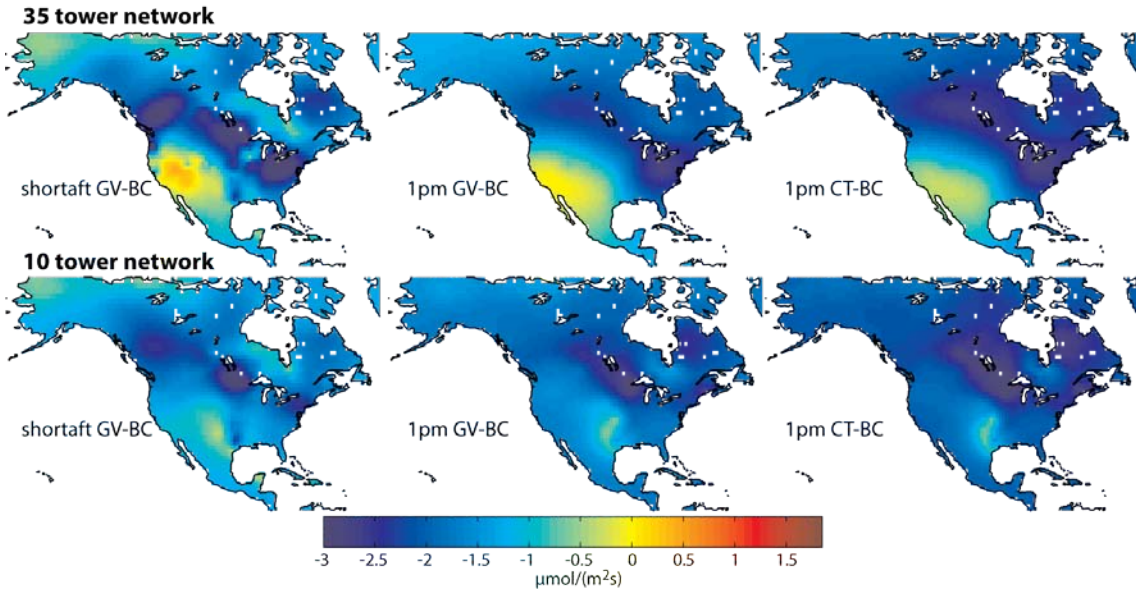

Figure 5.12: Average June grid-scale biospheric fluxes from the real data inversions using a 4- day diurnal estimation timescale.

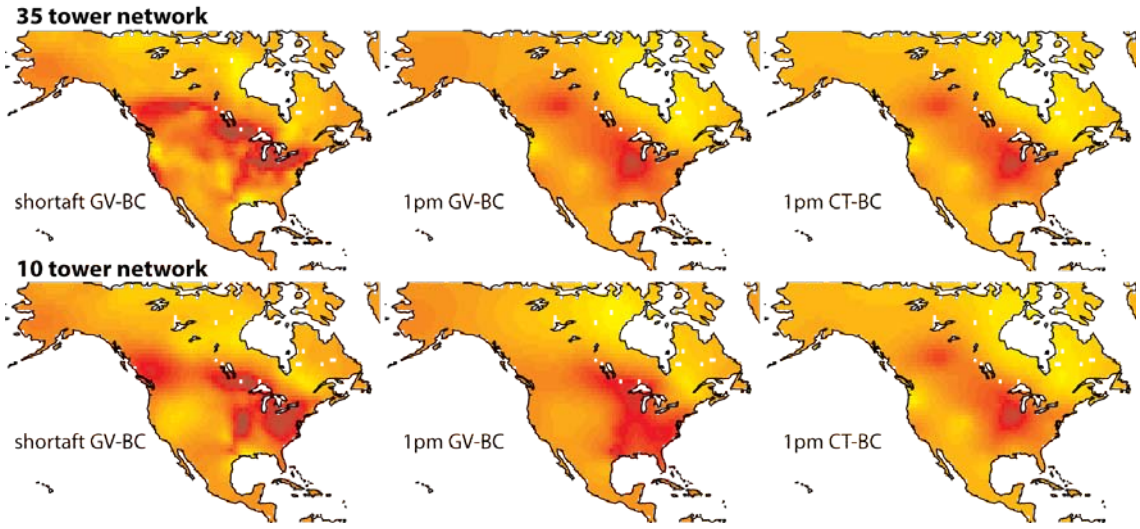

Figure 5.13: Average October grid-scale biospheric fluxes from the real data inversions using a 4-day diurnal estimation timescale.

In contrast to the selection of observations, the choice of boundary conditions has negligible impact on the spatial patterns of the grid-scale fluxes at both the 3-hourly and 4Ddiurnal estimation scale. The CT-BCs result in slightly stronger sinks in June or weaker sources in October in the boreal areas compared to the flux estimates using GV-BCs (Figures 5.12 and 5.13) most likely due to the limited tower coverage in these northern areas. As such, the fluxes in these areas would be mostly constrained by the northwesterly inflow of air. The minor impact of the boundary conditions suggest any errors associated with the choice of boundary conditions do not contribute to the inconsistencies in grid-scale flux estimates from different inversion studies.

From these results, estimating 3-hourly fluxes using more spatial and temporal observations is the best setup to recover monthly grid-scale estimates. Although results are shown for both the 3-hourly and 4Ddiurnal fluxes for June and October for 2008, the conclusions regarding inversion setup choices (i.e. selection of observation, the spatial and temporal scale at which to estimate fluxes, and boundary conditions) also apply to the grid-scale flux estimates from all other months in 2008 and therefore, are not seasonally dependent

4.3.2 Spatially aggregated monthly flux estimates

The use of the 35TN yields flux estimates that have a weaker seasonal cycle, as can been seen especially in mild uptake of CO_2 during the height of the growing season for NA (Figure 5.14). This decreased sink is reasonable given the extra coverage of the 35TN which constrains areas such as the Southwest and the Central West that are less productive than Midwestern areas constrained by the 10TN (shown in Figure 5.2). Note that the inferred $\widehat{\boldsymbol{\beta}}$ using a 10TN indicates stronger uptake during the growing season than the inferred $\widehat{\boldsymbol{\beta}}$ using the 35TN (results not shown for brevity) as the inferred $\widehat{\boldsymbol{\beta}}$ is mainly influenced by the smaller more productive areas of the continent sampled by the smaller measurement network. The inversions use the model of the trend, $\mathbf{X}\widehat{\boldsymbol{\beta}}$, to help further constraint estimates in areas that are poorly covered by the atmospheric data which explains why the seasonal cycle of all of NA appears to be weaker using the expanded network. Thus, inversion studies that use a limited network to infer carbon cycle dynamics, particularly in areas that are only partially constrained by the atmospheric network, may be influenced more by inversion assumptions (e.g., explicit prior flux) rather than the information contained in the atmospheric data.

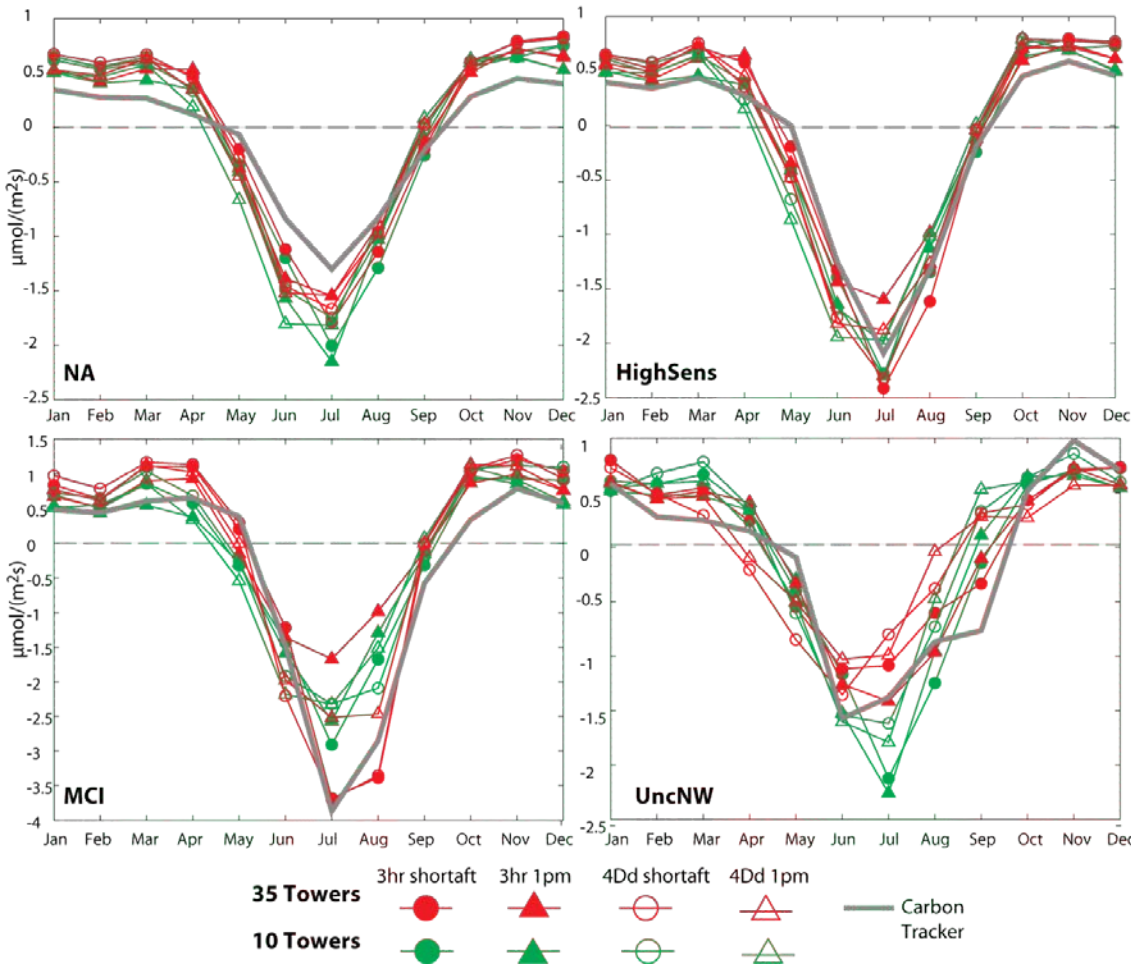

Figure 5.14: Seasonal cycle of monthly fluxes aggregated to NA, HighSens, MCI, and UncNW from real-data inversions. Estimated fluxes are shown for two different choices of observations to include, two estimation timescales, and two networks. All results are shown with the use of GV-BCs as the use of CT-BCs provides only a systematic downward offset for all regions of 0.1 to 0.5 µmol/m^{2}s. The shift is most prevalent during the growing season. Carbon Tracker fluxes also shown only for comparison.

The number of observations (both in space and time) has the largest influence on the monthly budgets for each region in Figure 5.14 during the growing season compared to the other setup choices. Observations from more times of the day from the 35TN yield the greatest uptake at the height of the growing season in all areas except for the UncNW. In contrast, the use of a single measurement per day with the 35TN at the height of the growing season yields the weakest sink. The variation between the flux estimates from different choices of observations throughout the day is particularly apparent in the MCI.

The information contained within a single daily afternoon measurement may be too small when combined with the errors associated with synoptic and diurnal transport to provide much information regarding the seasonality of regional fluxes particularly during the growing season.

During the non-growing season for all regions, the timescale of estimation has the most impact on the spatially aggregated fluxes as can be seen in Figure 5.14 during January through March and October through December. As with the synthetic data results, temporal aggregation error has less of an impact at the NA scale but the impact increases as the size of the region decreases. As such, the UncNW exhibits the largest difference in flux estimates from 3-hourly and 4Ddiurnal estimation scale inversions. This implies that during the non-growing season, temporal aggregation errors may cancel out at larger spatial resolutions at the monthly timescale.

Note that results with CT-BCs were not shown in Figure 5.14 as the inversion using CT-BCs yielded flux estimates that are marginally smaller in magnitude than those from the inversion using GV-BCs. The difference was ~0.1μmol/m^2s in the non-growing season months. During the growing season, the difference was slightly greater (~0.3μmol/m^2s). The choice of boundary conditions did not change the seasonal behavior of the fluxes which is consistent with the findings of Schuh et al. (2010). Even though the differences are small, they have the same magnitude and follow the seasonal pattern of the fluxes in each region. This result is unexpected for the MCI region. For the MCI, it was assumed that the flux would be constrained mostly by the differences in the ΔCO_2 measurements among the towers in the area.

4.3.3 Spatially aggregated annual flux estimates

The choice of boundary conditions plays the largest role in the overall annual budgeting of CO_2 for the NA continent (Figure 5.15). In addition, the use of more observation throughout the day also has an impact on the NA budget (approximately 0.35 PgC/yr), but it is minor compared to the choice of boundary conditions (approximately 1.25 PgC/yr). The strong agreement of estimates at smaller regional areas is likely an artifact of the units (PgC/yr) as the annual contribution to the overall NA carbon budget is marginal from regions such as the MCI and UncNW. Given that the choice of BCs only have a minor influence at the seasonal aggregated scale, results from Figure 5.14

and 5.15 indicate that small differences at the monthly estimates can yield large differences at the annual scale. As such, improving the seasonality of flux estimates is important for obtaining accurate annual budgets.

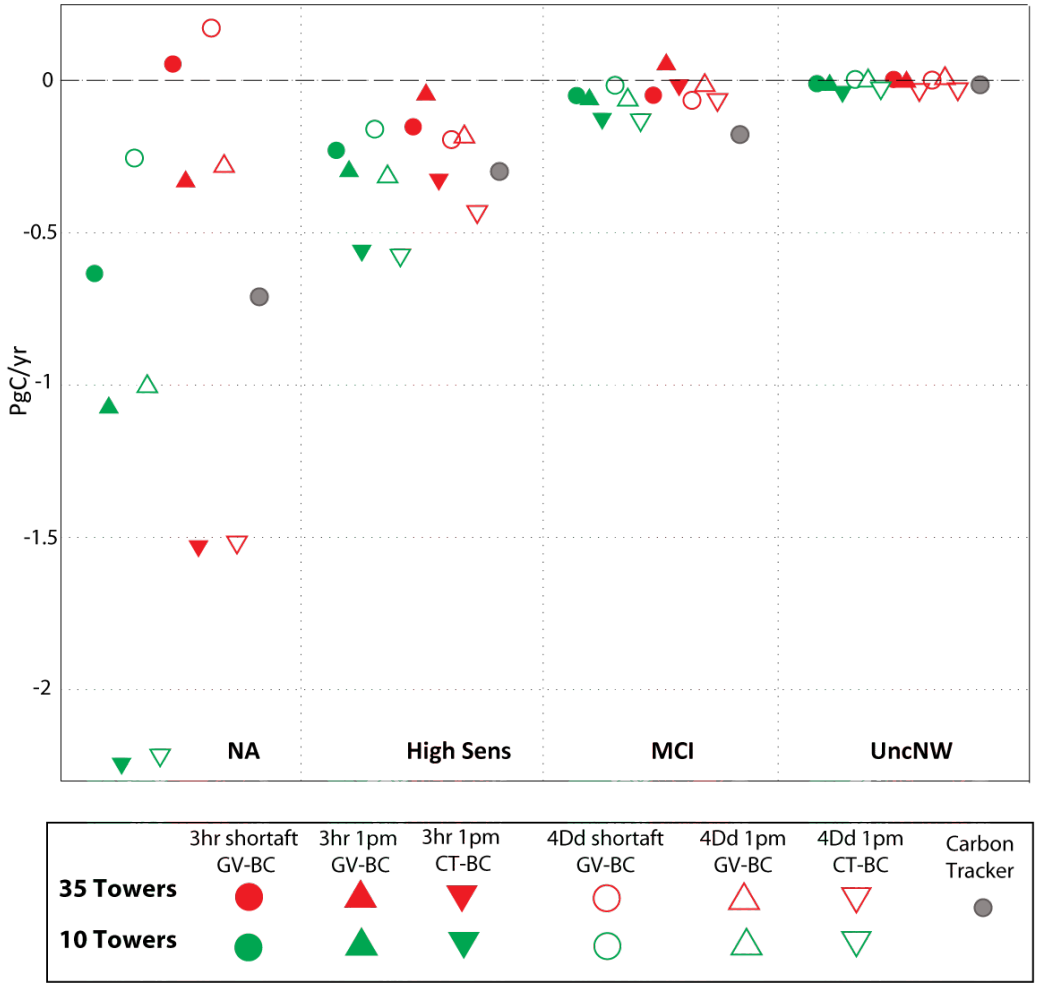

Figure 5.15: Spatially and temporally post-aggregated flux estimates from the real data inversions, together with Carbon Tracker fluxes shown for comparison. Unlike the "true" CASA fluxes in Figure 5.9, the Carbon Tracker fluxes are presented simply to provide another set of possible flux estimates.

Figure 5.15 points to the fact that the community must reach a consensus on boundary conditions before regional inversions can be used to provide reliable budgets given that the choice of boundary conditions has such a large impact on the estimates (greater than 1ppm difference for NA). For each area, the choice of boundary condition contributes to a difference of more than 50%. Although GV-BCs are more empirical, and

therefore assumed to be a better choice, CT-BCs have synoptic and longitudinal variability that is not present in the GV-BC product. More importantly, the GV-BCs are currently only defined as a single curtain at the longitudinal boundaries of the domain. By comparison, CT-BCs are defined in four dimensions (latitude, longitude, altitude and time). As a result, in estimating the CT-BCs using WRF-STILT, particles that have been released from a measurement location that have not completely exited the domain after the 10 days are assigned a CO_2 value at their exact location. In contrast, using WRF-STILT, these particles are assigned a CO_2 value associated with the nearest latitudinal curtain. It is assumed that the errors associated with the calculation of GV-BCs is marginal compared to the biases in the CT-BCs because they are more empirically based (Andrews et al., personal communication). Regardless, improving continental boundary conditions is an active area of research and is beyond the scope of this dissertation.

4.3.5 Average monthly reduction in uncertainty using 35TN relative to the 10TN

The average monthly reduction in uncertainty at the grid-scale resulting from the expansion of the observation network is calculated by comparing the results of the 10TN relative to the equivalent setup using a 35TN. Thus, the term "reduction in uncertainty" is not used here in the same sense as in Bayesian studies, which calculate the percent reduction in the *a posteriori* uncertainties relative to the *a priori* uncertainties within the context of a single inversion. The results in Table 5.2 indicate that adding data at new observation sites significantly reduces the uncertainty on the *a posteriori* flux estimates for both the grid-scale and spatially aggregated fluxes. The largest relative reduction at the grid-scale is associated with using a single measurement per day. However, by comparison, the reductions of uncertainties corresponding with inversions that use more observations throughout the day (i.e. shortaft) are less for both the grid and aggregated scales. The result suggests that the use of more temporal measurements may already provide more constraint on monthly grid-scale estimates, and therefore adding more towers locations into the network.

Table 5.2: Average monthly grid-scale and aggregated-scale reduction in uncertainty. The percent reduction is calculated as the reduction in the a posteriori variance for inversions using the 35 tower network relative to those using the 10 tower network. Results are shown at the 3-hourly estimation scale with the use of GV-BCs since the results for 4-Ddiurnal and CT-BCs were similar.

Spatial scale	Estimation scale	Temporal observations	NA	HighSens	MCI	UncNW
gridscale	3hr	shortaft	14%	13%	22%	43%
		1pm	83%	84%	83%	86%
aggregated	3hr	shortaft	58%	44%	56%	71%
		1pm	77%	75%	80%	86%

4.3.6 Comparison of grid-scale monthly fluxes to other flux estimates

The choice of more spatial and temporal measurements in conjunction with a 3-hourly estimation scale not only helps the inversion yield more realistic seasonal spatially aggregated fluxes, but more importantly, the use of additional observations helps to inform more realistic grid-scale spatial patterns. These conclusions are partially validated by the synthetic data results. Visually, the grid-scale 3 monthly mean grid-scale results for the growing season (July, August, and September) and non-growing season (October, November, and December) (Figure 5.16) for 2008 using additional data in space and time is most similar to grid-scale variability shown in mechanistic models (represented by CASA-GFED in Figure 5.18). The grid-scale variability is also more similar to flux estimates from a 2004 application of GIM that uses auxiliary variables in **X** to further constrain estimates (see details in Gourdji et al. (2004)). Although Figure 5.15 compares flux estimates from different years, we expect the seasonal flux grid-scale patterns to be similar from year to year and thus a check on flux results. The large sinks in the agricultural belt during the growing season exhibited in the 2008 GIM using shortaft is consistent with Crevoisier et al. (2010) which pointed to the Midwest as the location of the largest regional sink in NA. The arid Southeastern United States is also more flux neutral as is expected. As such, we are more confident that the flux estimates from more spatial and temporal data is providing more realistic monthly grid-scale flux estimates.

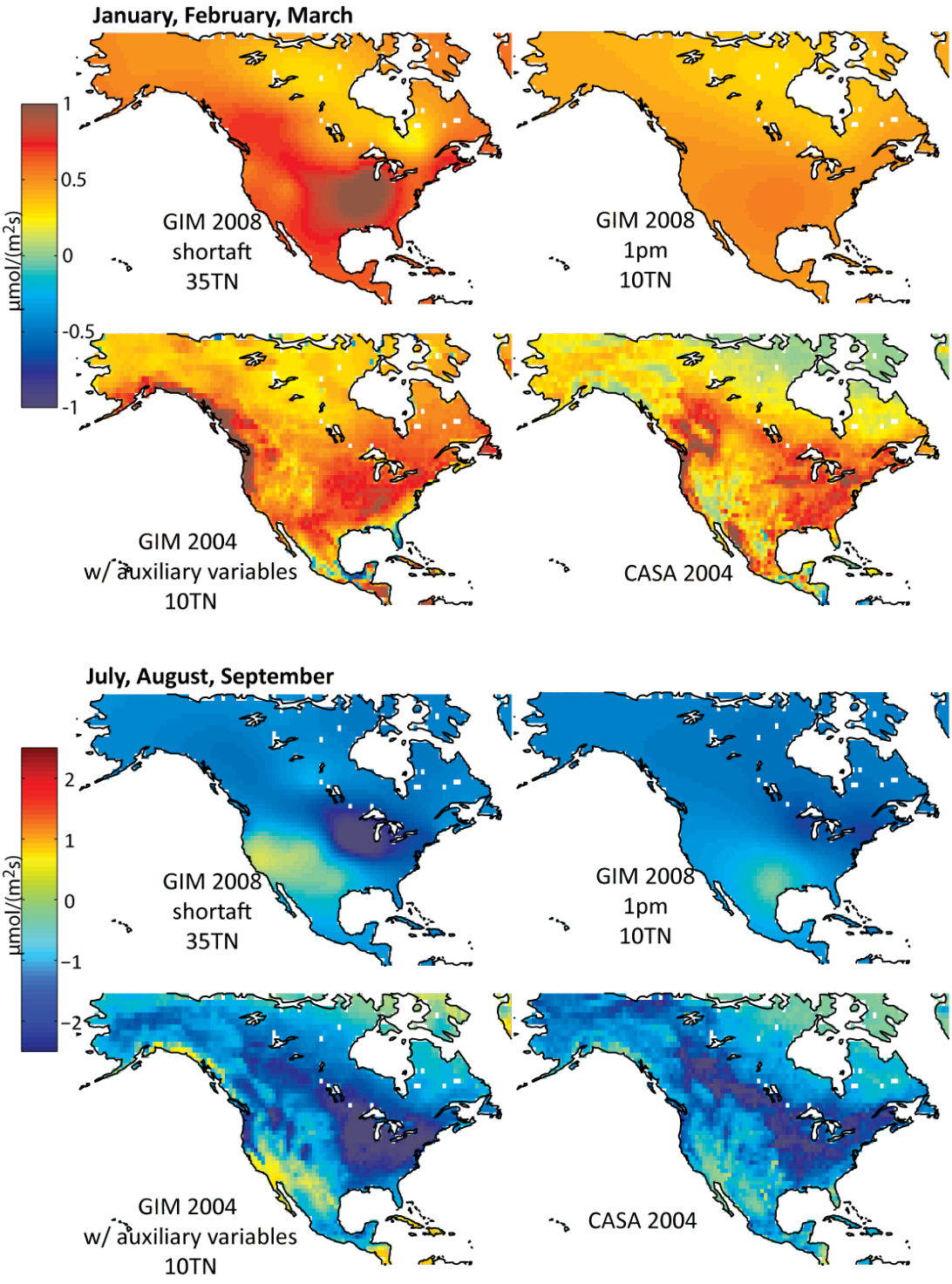

Figure 5.16: Three-monthly average grid-scale biospheric fluxes from the 3hrly shortaft 35TN inversion as compared to 3hrly 1pm 10TN using GV-BCs. Also shown are 2004 GIM inversion fluxes that use a 10TN, similar data choices as the 1pm, as well as NARR auxiliary variables in (**X**) to help further constrain grid-scale flux estimates. Grid-scale fluxes from CASA-GFED are also shown for comparison. Please note the different scales for each season.

5.0 Conclusions

The results of this study support the first stated hypothesis: including more measurements spatially appears to improve flux estimates and reduce their corresponding uncertainties, especially in areas that previously were underconstrained by the measurement network. However, in order to extract the most out of the additional spatial coverage provided by the 35TN, it is necessary to include observations from more than one time of the day (e.g., 1 p.m. or a measurement representing an average of multiple hours in the afternoon) as in conventionally done in most Bayesian inversion studies. Although simulated transport may be more trustworthy when using an afternoon measurement during well-mixed conditions, measurements associated with these times may only contain a diffuse signal and thus, only may only be able to constrain very large areas. Using observations from more times throughout the day helps to inform spatial patterns of sources and sinks that, when aggregated to larger spatial and temporal scales, impact flux estimates. However, regional transport models need to be improved to make it possible to increase the number of observations per day within an inversion.

Until regional transport models are improved, the number of observations to be used per day may need to be selected for each location on a case by case basis, and may need to be seasonally refined. While the study demonstrates the advantages of using more data throughout the day with the 35TN, there is a potential of including observations that correspond to times when we expect systematic errors in simulated transport (e.g. the misrepresentation of the height of the night-time planetary boundary layer (PBL), transition of the convective PBL, nighttime jets, etc.) that can also bias inversion results. However, if more observations can be used, there is a potential to significantly improve flux estimates at both the grid and aggregated scales. New observational screening technique (Maki et al., 2010) may provide means to select observations to include into the inversion without biases the results with transport errors associated with times of the day that are difficult to model atmospheric transport.

In addition, this study has demonstrated that fluxes should be estimated at the 3-hourly scale to account for the variability of the underlying fluxes and atmospheric transport. If the estimation scale is too coarse, as is the case with many Bayesian inversion applications, the estimations are subject to temporal aggregation errors even if

the estimates are post-aggregated to large spatial and temporal resolutions confirming findings in Gourdji et al. (2010). The issue of temporal aggregation error is best illustrated with a geostatistical inversion because the shape of the diurnal cycle is not specified *a priori*. However, temporal aggregation error will be problematic for estimates obtained from Bayesian inversions if the diurnal cycle of their explicit prior flux estimates is misrepresented. This is likely to be of at least some concern, given the differences in the diurnal cycles predicted by different biospheric models. Note, that it is recognized that a sub-daily estimation scale has large associated computational costs, but it is feasible to estimate monthly 3-hourly fluxes as shown in this application in a timely manner for an entire year with a 35TN network.

Finally, this work has shown that boundary conditions play a large role budgeting annual sources and sinks at the continental scale, although their impact is less at the monthly scale. The role of boundary conditions on even very well-constrained areas has some impact on monthly budgeting, partially disproving the second hypothesis, i.e. including more measurements helps minimize the impact of other inversion choices. It was assumed that the 35TN would correct any inconsistencies in flux estimates associated with the choice of boundary conditions, since flux estimates would be based primarily on the difference between ΔCO_2 from different tower locations. The offset of the boundary conditions on observations would therefore be cancelled out in areas constrained by many towers. A much larger measurement network would be needed to correct the offsets from currently available boundary conditions.

Since more temporal measurements are essential for elucidating regional flux estimates, there is a possibility that the addition of other atmospheric data streams (such as aircraft observations, flask measurements, or even future XCO_2 estimates from satellites based on a 1pm sampling time) may not improve regional grid-scale flux estimates as much as expected. Given the results from this study, other atmospheric data streams might only constrain large areas unless there are improved means to leverage the data. However, the atmospheric information within the continuous measurements is still limited and therefore, inversions will most likely require additional data to recover realistic fluxes at finer spatial resolutions until regional transport models are improved to use more temporal data. As shown in Gourdji et al. (in prep.), GIM can use grid-scale

environmental datasets with a mechanistic relationship to CO_2 flux to further improve the grid-scale pattern of flux estimates if incorporated into the inversion in a statistically rigorous manner (e.g. Gourdji et al. 2008; Gourdji et al., in prep.).

CHAPTER 6

Attributing the variability of eddy-covariance CO_2 flux measurements across temporal scales using a geostatistical regression

This Chapter addresses objective 3 of the dissertation using direct estimates of flux to infer the drivers of CO_2 variability at a landscape scale, as inferred by a statistical regression model at daily, weekly, and monthly timescales.

1.0 Introduction

The eddy covariance (EC) method estimates the flux of CO_2, i.e. net ecosystem exchange (NEE), as the covariance of the deviations in atmospheric CO_2 concentrations and vertical wind speed from their mean concentrations at a given flux tower site (e.g. Canadell et al., 2000; Baldocchi et al., 2001). The eddy covariance (EC) method provides the opportunity to study relationships between environmental datasets and surface flux exchange at a ~1km^2 at various timeframes because it provides the most direct measurement of the flux density between vegetation and the atmosphere (Baldocchi at al., 2008). At present, the AmeriFlux network contains approximately 100 active sites (http://public.ornl.gov/ameriflux/site-select.cfm) located in various ecosystems (e.g. deciduous forests, agricultural areas, grasslands, wetlands etc.) (Hargrove et al., 2003). With this established network, a large amount of terrestrial ecosystem CO_2 exchange data now exist, along with many other micrometeorological and biometric variables for different types of land cover. Eddy-covariance measurements are generally continuous in time providing ample temporal coverage (e.g. 30 minute averages) for long durations (e.g. greater than 5 yrs). As such, NEE measurements provide the opportunity to improve the understanding of the temporal variability of CO_2 surface flux of a particular ecosystem through statistically inferred relationships (Law et al., 2002).

One of the benefits of using eddy-covariance data to investigate the relationship between fluxes and environmental factors is that both long and short term trends can be

inferred from the data because measurements are reported at a high frequency. Statistical regression methods are commonly employed to understand the climatic controls of both the inter-annual and seasonal variability of carbon cycling (e.g. Law et al., 2002; Hui et al., 2003). However, these approaches are limited by (1) assumptions regarding the dependent variable (i.e., how to best decompose NEE into photosynthetic uptake and respiration), (2) the approach used to select the variables to include in the regression, and (3) the assumption of independent and identically distributed residuals.

This work in this Chapter involves the application of a geostatistical regression (GR) approach that can be used with eddy-covariance data to investigate the relationships between carbon flux and environmental variables at multiple timescales, ranging from monthly to daily. The approach uses an adaptation of the Bayes Information Criterion to identify an optimal set of environmental variables that are able to explain the observed variability in carbon flux. In addition, GR quantifies the temporal correlation in the portion of the flux signal that cannot be explained by the selected variables, and directly accounts for this correlation in the analysis. This GR approach was applied to data from the University of Michigan Biological Station (UMBS) AmeriFlux site to identify the dominant explanatory variables for Net Ecosystem Exchange (NEE), Gross Ecosystem Exchange (GEE) and heterotrophic and autotrophic respiration (R_{h+a}) at different temporal scales. The GR approach was also used to evaluate whether environmental variables can be used to isolate the GEE and R_{h+a} signals from the NEE measurements and to determine the impact of temporal scale on the inferred relationships between environmental variables and CO_2 flux for the forest surrounding the University of Michigan Biological Station flux tower site.

2.0 Site description

UMBS is located in the northern portion of Michigan's Lower Peninsula (45^o 33' 35.0" N, 84^o 42' 49.6" W). The station is home to a flux tower (Schmid et al., 2003; Curtis et al., 2002 & 2005; Gough et al., 2007 & 2008), part of the FLUXNET and AmeriFlux networks (Baldocchi et al., 2001), where NEE is measured at 10Hz and averaged to reported hourly estimates. Data have been collected since 1999, together with many other environmental datasets.

The tower is located on lake-border plains in the transition zone between mixed hardwood and boreal forests (Curtis et al., 2005). Within this footprint, big-toothed and trembling aspen (*Populus grandidentata, P. tremuloides*) are the dominant tree species, and red oak (*Quercus rubra*), American beech (*Fagus grandifolia*), red maple (*Acer rubrum*), white pine (*Pinus strobus*), and hemlock (*Tsuga canadensis*) are also present. Brackenfern (*Pteridium aquilium*) comprise the majority of the understory vegetation (Schmid et al., 2003; Curtis et al., 2005).

UMBS is one of the few sites where concurrent biometric and meteorological measurements have been conducted along with annual assessments of carbon storage based on accounting methods (e.g. Curtis et al., 2002; Gough et al., 2008). These data suggest that temperature and solar radiation exert strong controls on carbon exchange (e.g. Curtis et al., 2005; Gough et al., 2007 & 2008) at the site, similarly to other Northern deciduous forests. It is assumed that these constraints vary seasonally and depend on leaf phenological period (Gough et al., 2008), although this has not been fully evaluated at sub-annual time-scales. The extensive research that has been conducted at UMBS provides a unique context for interpreting the results of the GR analysis.

3.0 Study period, setup, and data

The presented analysis explores the linear relationship between NEE, GEE and Rh+a, and environmental variables (a.k.a. auxiliary variables) at daily, 8 day, and monthly time scales. The examined period spans February 2000 to December 2004. The study uses auxiliary variables collected at UMBS as well as data from the Moderate Resolution Imaging Spectrometer (MODIS) on the TERRA satellite (Schmid et al., 2003; Curtis et al., 2005) (http://ladsweb.nascom.nasa.gov/), listed in Table 6.1. Note that two sets of LAI and fraction of photosynthetically active radiation (fPAR) data are used in this study. Site-specific LAI data were derived from Vegetative Area Index (VAI) measurements using a Licor LAI 2000 Plant Canopy Analyzer and leaf litter trap estimates. In addition, the MODIS LAI data set was used (Myneni et al., 2002). Two fPAR data sets were also collected: one from MODIS and another by transforming site-specific LAI using Beer's Law (e.g., Campbell and Norman, 1998). Both MODIS LAI and fPAR data were provided at 8 day 1 km scale, and the pixels within a 1 km

radius of the tower were averaged on the basis of the area of the pixel within this radius. All data in Table 6.1 were quality controlled and averaged to daily, 8 day, and monthly scales. For variables with coarser than daily resolution (e.g., MODIS data sets), data were downscaled using linear interpolation. Day and night averages of NEE were estimated using PAR values greater than zero as an indicator of daytime measurements. The auxiliary variables were categorized into groups representing controls on surface CO_2 flux as shown in Figure 6.1. Note that most variables have very similar seasonal cycles (Figure 6.2)

Table 6.1: Variables considered for the geostatistical regression analysis. The first superscript indicates the timeframe for which measurements are available, where 1 : 1999-2004; 2 : 2000-2004; 3 : 2003-2004. The second superscript indicates the principal investigator responsible for compiling and/or sourcing the data, where a : Chris Vogel, Peter Curtis and HaPe Schmid (AmeriFlux Tower): b : Kim Mueller (data compilation only); c : Mary Anne Carroll (PROPHET Tower); d : NASA & Oak Ridge National Laboratory.

Parameter	*Units*
Wind Speed[1,a]	*m/s*
Friction Velocity[1,a]	*m/s*
Soil Temperature @ 7.5cm[1,a]	*°C*
Daytime Soil Temperature @ 7.5cm[1,a]	*°C*
Nighttime Soil Temperature @ 7.5cm[1,a]	*°C*
Vapor Pressure Deficit[1,b]	*kPA*
Photosynthetically Active Radiation (PAR)[1,a]	$\mu mol/m^2 s$
Leaf Area Index (LAI, site-specific)[2,a]	m^2/m^2
fraction of PAR (fPAR) derived from site specific LAI[2,b]	*unitless*
fPAR (from PAR sensors)[3,b]	*unitless*
Ozone Concentration[2,c]	*ppbv*
Normalized Vegetative Index (NDVI) from MODIS[2,d]	*unitless*
Enhanced Vegetative Index (EVI) from MODIS[2,d]	*unitless*
LAI from MODIS[2,d]	m^2/m^2
fPAR from MODIS[2,d]	*unitless*
Soil Moisture @ 102cm[1,a]	*%H2O*
Air Temperature[1,a]	*°C*
Daytime Air Temperature[1,a]	*°C*
Nighttime Air Temperature[1,a]	*°C*
Precipitation[1,a]	*mm*
Albedo from MODIS[2,d]	*unitless*
Daily Accumulative PAR[1,b]	*µmol*
Net Radiation[1,a]	W/m^2
Shortwave Radiation[1,a]	W/m^2
Shaded Air Temperature[1,a]	*°C*
Soil Heat Flux[3,a]	W/m^2
fPAR x Accumulative PAR[2,a]	*µmol*
Average Bole Temperature[2,a]	*°C*

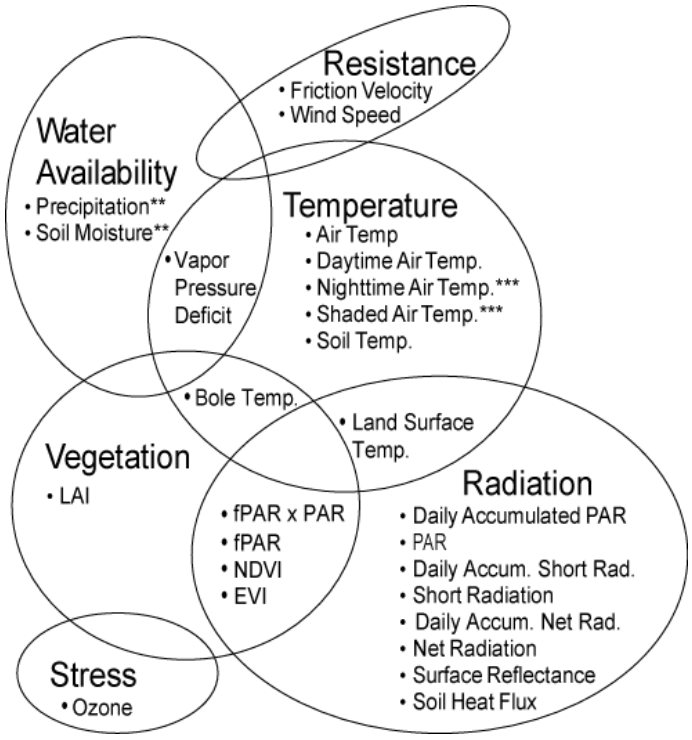

Figure 6.1: Groups of auxiliary variables. Sensitivity tests were run where the starred variables were allowed to be selected in addition to another variable in their category, but these tests showed that more than one variable per category were never selected.

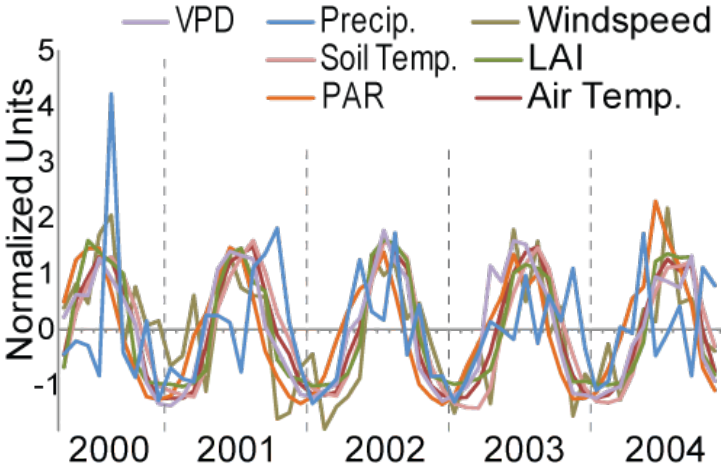

Figure 6.2: Sample of monthly averaged normalized auxiliary variables.

The hourly NEE data have many nonrandom gaps due to the lack of vertical air motion (e.g., atmospheric stability), or due to rain obscuring sensors. A gap-filled data product available for UMBS (Schmid et al., 2003) was used as the primary data stream in the presented analysis. Note that the gap filling methods used at UMBS include (1) short-term ensemble averages of hourly fluxes over the course of a day during leaf-out periods and (2) parametric models during the growing season that define the relationship between ecosystem respiration and soil temperature and gross primary ecosystem uptake to PAR (Schmid et al., 2003). Because of the large proportion of data gaps at this site (>40%), the analysis was also repeated using non-gap-filled data for comparison to ensure that results are not reflecting assumptions used in the gap-filled model.

The GR analysis was conducted separately on NEE, GEE, and R_{h+a}. To obtain the GEE and R_{h+a} signals, the daily averaged nighttime observations of NEE were used to represent daily ecosystem respiration (i.e. average(NEE_{night}) = daily R_{h+a}), similar to the approach in Urbanski et al., (2007). Daily GEE was then derived by subtracting the averaged NEE night measurements from the daily NEE average (i.e. GEE = average(NEE) – average(NEE_{night}). Although this approach may under-predict GEE because daytime temperatures are higher than nighttime temperatures, alternative methods for separating GEE and R_{h+a} are based on assumed relationships between these flux components and auxiliary variables such as temperature. Such parametric relationships may have biased our results where the selected variables may have solely mirrored the prescribed relationships used to separate fluxes. For the non-gap-filled NEE analysis, if more than 50% of the nighttime NEE measurements were missing, then NEE, R_{h+a}, and GEE were not considered separately.

Random gaps occurring in the environmental data sets within a day were not filled unless they were large (>50% of missing data for a given day). For such large data gaps, all data were excluded from the analysis. The averaged monthly, 8 day, and daily variables were evaluated against coincident gap-filled data sets available from the Carbon Dioxide Information Analysis Center (ftp://cdiac.esd.ornl.gov/pub/AmeriFlux/data/), and no substantial differences were observed.

4.0 The geostatistical model

As explained in Chapter 3, geostatistical regression (analogous to multiple linear regression (MLR) in classical statistics) expresses the dependent variable (in this case, NEE, GEE, and R_{h+a} measurements), $\mathbf{z}$, as the sum of a deterministic component ($\boldsymbol{\mu}$) and a stochastic term, ($\boldsymbol{\varepsilon}$), representing the residuals between the observations and the deterministic component. However, instead of assuming that these regression residuals are independent (i.e. "white noise"), $\boldsymbol{\varepsilon}$ is modeled as a vector of correlated zero-mean residuals. The deterministic component represents that part of the observations that can be explained using a set of covariates (i.e. auxiliary variables) (Huang et al., 2007), while the stochastic component describes the variability in $\boldsymbol{z}$ that is not explained by the deterministic component:

$$\boldsymbol{z} = \mu + \boldsymbol{\varepsilon}. \tag{6.1}$$

The deterministic component takes the form of a model of the trend or expected drift (i.e. $\mu = \mathbf{X}\boldsymbol{\beta}$). This model can be as simple as a single overall mean, or can include any linear combination of variables related to $\boldsymbol{z}$. The $\mathbf{X}$ matrix contains vectors of k covariates that are scaled by the vector of unknown drift coefficients ($\boldsymbol{\beta}$). Even though the individual columns in $\mathbf{X}$ are linearly related to $\boldsymbol{z}$, the columns themselves can potentially contain transformations of one or more auxiliary variables, e.g. exp(*temperature*) or lagged data. GR (Section 3.4) is used to obtain the best estimates of the drift coefficients, $\widehat{\boldsymbol{\beta}}$, which represent the relationship between CO_2 flux and each covariate, and their corresponding uncertainties, $\sigma^2_{\widehat{\boldsymbol{\beta}}}$.

The covariance of the regression residuals, $\boldsymbol{\varepsilon}$, is modeled as:

$$Q(h_{i,j}) = E[\varepsilon(t_i)\varepsilon(t_j)], \tag{6.2}$$

where $h_{i,j}$ is the time lag between times t_i and t_j, $Q(h_{i,j})$ is the covariance for points with a lag $h_{i,j}$, and $E[\,]$ denotes the expectation operator. Equation (6.2) assumes that the flux residuals are homoscedastic, although a model where the variance changes seasonally could be implemented if needed.

As outlined in Chapter 3, Section 2, many covariance functions can be used to model the behavior of the residuals in equation (6.2) (e.g. Cressie, 1993), but a

combination of a nugget and exponential covariance function was found here to aptly model the temporal covariance of NEE, GEE, and R_{h+a} observations and residuals:

$$Q(h_{i,j}) = \begin{cases} \sigma_{n,Q}^2 + \sigma_{s,Q}^2 & h_{i,j} = 0 \\ \sigma_{s,Q}^2 exp\left(-\frac{h_{i,j}}{\tau_Q}\right), & h_{i,j} > 0 \end{cases} \quad (6.3)$$

where the practical temporal range of correlation is approximately 3τ. Beyond 3τ, the covariance between residuals is close to zero. The nuggets, $\sigma_{n,Q}^2$, represents variability at time scales below the averaging time used for the observation and measurement error. These parameters are estimated using Restricted Maximum Likelihood as discussed in Chapter 3, equation 3.17.

4.1 Model of the trend, X

As explained in Chapter 3, Section 4, to identify environmental variables to include in the model of the trend, Bayes Information Criteria (BIC) is modified so that equation that can account for correlated residuals becomes:

$$BIC_j = \ln|\boldsymbol{\Omega}| + [\boldsymbol{y}^T(\boldsymbol{\Omega}^{-1} - \boldsymbol{\Omega}^{-1}\mathbf{X}(\mathbf{X}^T\boldsymbol{\Omega}^{-1}\boldsymbol{X})^{-1}\mathbf{X}^T\boldsymbol{\Omega}^{-1})\boldsymbol{y}] + k\ln(n). \quad (6.4)$$

For the special case of independent residuals, $\mathbf{Q} = \sigma^2\mathbf{I}$, where $\mathbf{I}$ is an identity matrix, and equation (7) reduces to the more conventional form, where RSS is the residual sum of squares:

$$BIC_j = -n\ln\frac{RSS}{n} + k\ln(n) \quad (6.5)$$

In this study, most of the variables are highly correlated (more than 15 of the 27 variables considered for the trend had a pair which yielded a correlation coefficient greater than 0.75). This is not surprising given that many of the datasets represent similar quantities, such as temperature, radiation, and vegetation. Therefore, these similar datasets are grouped into categories as presented in Figure 6.1, complementing the BIC with scientific understanding regarding their relationship to flux. The BIC is then run by restricting the number of variables from each category to at most one, to avoid problems with excessive collinearity among the auxiliary variables, which could lead to large and opposing regression coefficients that do not reflect expected relationships to flux, and that have overly wide associated uncertainty bounds (Faraway, 2005). Note that fully automated model building procedures are not recommended as a means for identifying the best

interpretable model, because such procedures can potentially select models that represent only spurious relationships, and therefore can fail when applied to comparable datasets (Judd and McLelland, 1989). A condition number is used to diagnose collinearity (Faraway, 2005). Finally, because correlation coefficients for variables in the trend provide a measure of the relationship among themselves and not the relative independence of the relationship of a variable into $\mathbf{X\beta}$ flux, the correlation coefficients of the drift coefficients, $\widehat{\boldsymbol{\beta}}$, for the selected variables are also estimated and compared.

4.2 The geostatistical regression equations

As shown in Chapter 3, equations 3.10 and 3.11, estimates of the drift coefficients, $\hat{\boldsymbol{\beta}}$, and their uncertainty covariance ($\mathbf{V}_{\hat{\boldsymbol{\beta}}}$) (e.g. Cressie, 1993) are calculated as:

$$\widehat{\boldsymbol{\beta}} = (\mathbf{F}^T\boldsymbol{\Omega}^{-1}\mathbf{F})^{-1}\mathbf{F}^T\boldsymbol{\Omega}^{-1}\boldsymbol{y} \tag{6.6}$$

$$\mathbf{V}_{\widehat{\boldsymbol{\beta}}} = (\mathbf{F}^T\boldsymbol{\Omega}^{-1}\mathbf{F})^{-1} \tag{6.7}$$

where all variables are as previously defined, and the diagonal elements of $\mathbf{V}_{\hat{\boldsymbol{\beta}}}$ are the variances representing the uncertainty of the drift coefficients. The coefficient of determination R^2 is calculated as:

$$\mathrm{R}^2 = 1 - \frac{(\boldsymbol{z}-\boldsymbol{X}\widehat{\boldsymbol{\beta}})^T(\boldsymbol{z}-\boldsymbol{X}\widehat{\boldsymbol{\beta}})}{(\boldsymbol{z}-\bar{\boldsymbol{z}})^T(\boldsymbol{z}-\bar{\boldsymbol{z}})}, \tag{6.8}$$

to quantify the portion of the observation variability explained by the model of the trend.

5.0 Results

The GR was performed for a 5 year time period, as well as for three distinct seasons (growing season, spring green-up, and non-growing season). The goal was to identify the dominant variables that explain the variability in NEE, GEE, and R_{h+a} at different temporal scales. The study also investigated the feasibility of using auxiliary data to statistically separate flux components (i.e., GEE and R_{h+a}) in NEE measurements. Finally, this work explored the sensitivity of results to the use of remote-sensing versus site-based LAI and fPAR data and to the assumption of linearity between the auxiliary variables and flux observations.

Several sensitivity tests were performed to ensure that (i) the model selection was not unduly influenced by data from a particular year, (ii) using gap-filled data did not affect results, and (iii) the regression residuals were symmetric and close to Gaussian. Excluding individual years from the analysis negligibly impacts the presented results, as did the substitution of non gap-filled data in the analysis. More importantly, the results using gap-filled data do not mirror the assumed relationships used in the NEE gap-filling algorithm (in particular, soil temperature was never selected as an important variable for respiration) (Section 2.2). Finally, regression residuals are symmetric. As such, results of these sensitivity tests are not shown for brevity. However, the outcome from these tests provides evidence for the statistical validity of the results presented in the following sections.

5.1 Explanatory variables in the monthly, 8-day, and daily NEE, GEE, and Rh+a trends

Auxiliary variables were selected using the BIC algorithm outlined in Section 3.2 for regression models for NEE, GEE, and R_{h+a}. Drift coefficients and associated uncertainties were estimated for the resulting 9 models (3 dependent variables $\times$ 3 temporal scales) using equations 3.10 and 3.11 presented in Chapter 3 (Table 6.2). The correlation coefficients of the drift coefficients ($\widehat{\boldsymbol{\beta}}$) for all models are less than 0.7 (unless noted otherwise in the text) with condition numbers less than 30, indicating that the BIC method, complemented with the grouping of variables, is able to avoid problems with excessive collinearity. Note that a positive sign on the estimated drift coefficients indicates a positive correlation with CO_2 flux (i.e. a source or a reduction in sink), while a negative sign indicates a negative correlation (i.e. a sink or reduction in source).

Table 6.2: Selected Variables and Associated Drift Coefficients ($\hat{\boldsymbol{\beta}}$) as Estimated From the GR Algorithm at the Monthly, 8 Day, and Daily Temporal Scales. Units are mmolCO2/m2s. All drift coefficients as estimated by GR are significant at the 95% confidence level unless italicized in the table. Numbers in brackets indicate the reduction in explanatory power when the associated variables are removed from the model (ΔR_i^2) where a higher number signifies a more dominant variable. The variance explained (R^2) and condition number of the trends are provided for each model. Note that other variables in Table 6.1 were never selected and are therefore not listed here. Dashes indicate categories of variables that were not selected for a particular model.

		Monthly			8-day			Daily		
Category	**Variable Name**	**NEE**	**GEE**	**R_{h+a}**	**NEE**	**GEE**	**R_{h+a}**	**NEE**	**GEE**	**R_{h+a}**
	Constant Comp.	*0.23*	*-0.32*	0.39	-2.15	-2.89	0.38	-2.14	-2.95	*0.12*
Resistance	Friction Velocity	-----	-----	-----	-----	-----	-----	-----	-0.14 [~0]	-----
Temperature	Air Temp.	-----	-2.32 [0.01]	-----	1.48 [~0]	-----	-----	-----	-----	-----
	Night Air Temp.	-----	-----	1.50 [0.03]	-----	-----	1.52 [0.16]	0.83 [~0]	-----	1.42 [0.13
Water/Temp	VPD	-----	-----	-0.39 [0.01]	-0.41 [~0]	-----	-0.36 [0.02]	-----	-----	-0.27 [0.04
Water Avail.	Precipitation	-----	-----	-----	-----	-----	-----	0.12 [~0]	0.25 [~0]	
Radiation	Soil Heat Flux	-----	0.44 [0.01]	-----	-----	-----	-----	-----	-----	-0.15 [0.01
Vegetation	LAI (MODIS)	-4.81 [0.27]	-4.72 [0.09]	-----	-----	-----	-----	-----	-----	-----
	LAI (site specific)	-----	-----	-----	-7.30 [0.11]	-7.35 [0.06]	-----	-6.76 [0.14]	-7.16 [0.09]	-----
Veg/Rad	fPAR (MODIS)	2.79 [0.09]	3.19 [0.03]	-----	-----	-----	-----	-----	-----	-----
	fPAR (site specific)	-----	-----	0.45 [0.01]	5.56 [0.05]	5.26 [0.02]	-----	5.25 [0.06]	4.94 [0.02]	0.52 [0.02
	fPAR x Accum. PAR	-----	-----	-----	-1.31 [0.13]	-1.37 [0.09]	0.43 [0.02]	-1.40 [0.18]	-1.22 [0.11]	-----
	R^2 =	0.92	0.97	0.98	0.83	0.91	0.97	0.77	0.82	0.92
	K =	8	13	11	21	16	7	19	13	6

All selected models of the trends explain over 75% of the variability in measured fluxes ($0.77 \leq R^2 \leq 0.98$, Table 6.2). Note that the high R^2 values are not solely reflecting the predictability of the seasonal cycle, because using a trend derived for a coarser timescale (e.g. monthly) to explain variability at a finer timescale (e.g. 8-day or daily) yielded a substantially lower R^2 relative to the case where the timescale-specific trend was used. For example, the monthly trend explains only 61% of the variability in the daily measurements compared to 77% explained by the daily trend.

Overall, the variance explained is particularly high for R_{h+a}, which suggests that respiration can be more easily represented than photosynthetic uptake. Photosynthetic uptake is also captured well, except for periods with exceptionally strong uptake, such as in July 2003 (Figure 6.3) and for the 8-day and daily cases in July 2001 (not shown), indicating that key variables needed to explain this anomalous uptake may be missing, or that nonlinear effects become important in these cases.

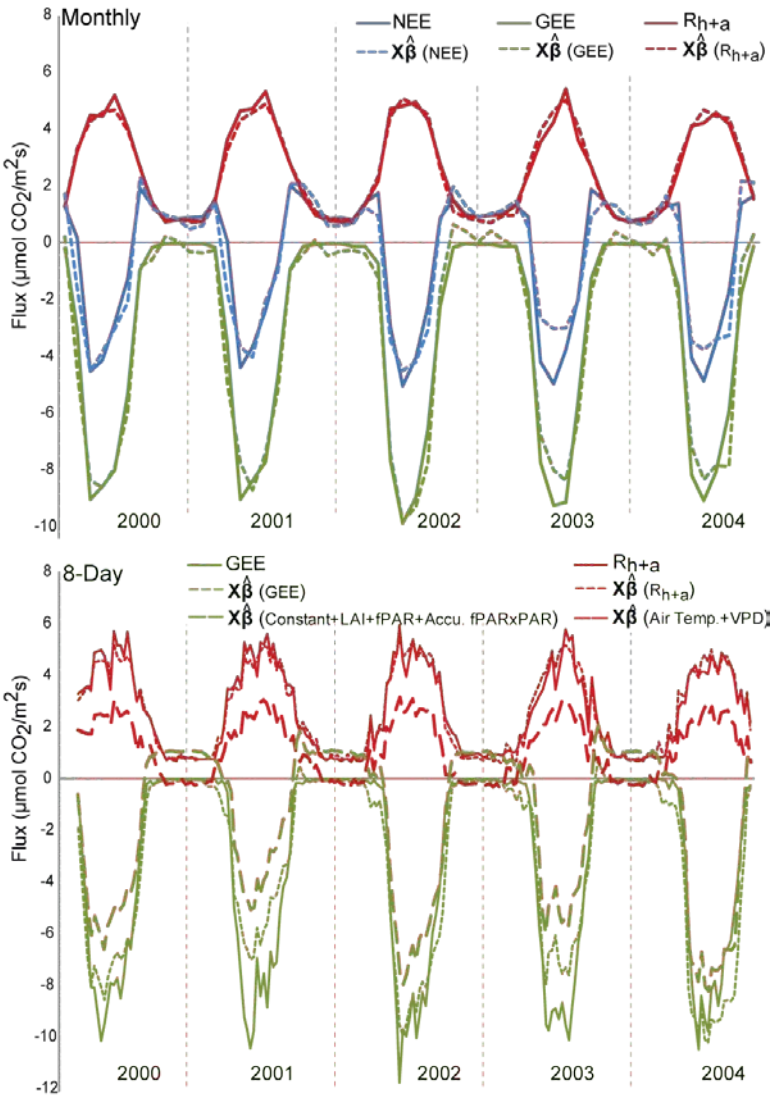

Figure 6.3: Monthly flux measurements (solid lines) with estimated trends (dashed lines). Eight day averaged Gross Ecosystem Exchange (GEE) and Rh+a measurements, their associated trend $\mathbf{X}\widehat{\boldsymbol{\beta}}$, and the components of the Net Ecosystem Exchange (NEE) trend associated with carbon uptake (negative $\widehat{\boldsymbol{\beta}}$) or loss (positive $\widehat{\boldsymbol{\beta}}$).

Vegetation (as represented by the sum of the LAI and fPAR contributions) has the strongest correlation to seasonal carbon cycling at UMBS across all temporal scales. This finding is expected given that the morphological, physical and chemical properties of vegetation have been shown to affect most processes of carbon and nutrient cycling in deciduous forests (e.g. Dorrepal, 2007). This result is also expected because the UMBS

forest is an overall net sink of CO_2, such that variables associated with carbon uptake are expected to be important in explaining the overall signal. At the finer (daily and 8-day) time scales, on the other hand, the influence of the amount of PAR intercepted and/or absorbed by the canopy (APAR = fPAR x Daily Accumulated PAR) also becomes significant in explaining carbon uptake, as represented by both the NEE and GEE measurements (Table 6.2). As noted by Anderson et al. (2000), many other studies have demonstrated the linear relationship between the increase in canopy biomass and the amount of visible light intercepted or absorbed in the canopy (e.g. Monteith, 1966). However, as expected, these results indicate that Light Use Efficiency (LUE) plays a more important role at synoptic scales, whereas vegetation better explains seasonal carbon cycling.

In addition to examining the regression coefficients associated with individual variables and their associated uncertainties, the explanatory role of selected variables was further examined by successively eliminating each variable from the trend, and quantifying the resulting reduction in R^2 (Table 6.2), or ΔR_i^2. Variables that result in a larger reduction in R^2 explain more variability in the flux measurements. For example, when LAI was excluded from the model of the trend for NEE at the monthly scale and regression coefficients were recalculated for the remaining variables, the ΔR_i^2 associated with LAI is 0.27. Removing fPAR at this scale has much less of an impact (ΔR_i^2 is 0.09). Thus, LAI is a more important variable at this scale, and fPAR appears to be adjusting LAI to help fit the NEE measurements. The magnitude and sign on the regression coefficients for these variables further confirm this result, because the drift coefficient of LAI is negative, corresponding to a sink of CO_2, and explaining the main seasonality of carbon uptake.

Conversely to NEE, the variables that best explain respiration, and their significance, are relatively scale independent (Table 6.2). In terms of carbon sources at UMBS, Curtis et al. (2005) noted that losses from soils account for approximately 70% of the carbon respired between 1999 and 2003. These losses include both root respiration and microbial respiration, which are, in turn, influenced by factors including photosynthetic supply to roots, substrate quality and availability, temperature and moisture (Hibbard et al., 2005). In addition, Curtis et al. (2005) noted only small inter-

annual variation (< 6%) in soil respiration at UMBS, suggesting that there is little variation in these primary controls from year to year. This finding at UMBS, coupled with results presented herein, suggests that the respiration signal is more consistent both spatially and temporally than previously understood (e.g. Hanson et al., 2000; Hibbard et al., 2005) for mixed Northern hardwood forests.

The specific variables selected for the R_{h+a} model of the trend (including nighttime air temperature, vapor pressure deficit (VPD), and site-specific fPAR) are different from those identified as important controls in previous work (including soil temperature and moisture, substrate availability and quality, soil carbon decomposition and microbial growth dynamics, and soil hydraulic properties) (e.g. Davidson et al., 2002; Reichstein et al., 2005). Although many of these variables were either not available or provided at scales that rendered them unsuitable for this analysis, the exclusion of soil temperature and moisture from the R_{h+a} model of the trend is unexpected. These results may reflect the fact that the soil moisture data was collected at 1m depth, which tends to be less temporally variable than soil moisture closer to the surface. Given that the soils at this site are well-drained spodosols (92% sand, 7% silt, and 1% clay) (Gough et al., 2008) with a shallow O horizon, a shallower soil moisture dataset might reflect moisture dynamics in the root zone. Unfortunately, this data was also not available for the study. In addition, nighttime air temperature (or air temperature) may be more representative of the actual temperature influencing heterotrophic respiration than soil temperature (which is measured at a depth of 7.5 cm).

The significance of VPD in the respiration model may indicate that this variable acts as a proxy for the moisture available in the canopy where larger values indicate drier conditions that physiologically impede carbon efflux. The effects of water stress on plant respiration often are mediated through loss of tissue turgor and stomatal closure (Aber et al., 1991), which can result in substantial reductions in respiration per plant (Davidson et al., 2006).

The significance of fPAR in the R_{h+a} model of the trend (Table 6.2) is more difficult to interpret. fPAR is likely acting as a proxy for another variable that was not included in the analysis. For example, fPAR might be representing the amount of substrate available for heterotrophic respiration. Other studies have found that using LAI

(which is closely related to fPAR) as a surrogate for site productivity across a range of temperate forests could help explain differences in annual respiration, hypothesizing that the larger the site LAI, the more substrate is produced for respiration (Reichstein et al., 2003). Otherwise, as discussed in Section 4.3, site-specific fPAR may simply act as a better proxy for overall seasonality than other available variables because it is a temporally smoother dataset. Note that removal of fPAR from the model results in a smaller ΔR_i^2 relative to the removal of nighttime temperature, indicating that temperature explains more of the respiration variability.

In addition to reflecting the general findings noted previously, the daily-scale analysis yields some unexpected results for all examined dependent variables. For example, precipitation is associated with a source or a decrease in sink at the daily scale in the NEE and GEE trend models, but was not significant for the R_{h+a} model where it might be associated with soil moisture. While this result may seem counterintuitive for this ecosystem type, precipitation may in fact be acting as a proxy for periods with significant cloud cover, and therefore for times with reduced sunlight for photosynthesis. This would have a larger impact at synoptic scales, whereas this effect may be averaged out at 8-day or monthly time resolutions. Note that precipitation may have a lagged effect on carbon uptake by affecting water availability on different time scales, which could be investigated using a shallower soil moisture dataset, or by adding a lagged precipitation variable to the superset of variables considered for model selection. Variables such as friction velocity may also be helping the model of the trend capture some of the small scale flux variability that cannot be represented by the other variables that were collected at larger time scales, rather than informing some mechanistic understanding. In all cases, these variables are associated with a smaller ΔR_i^2 relative to LAI, fPAR, and APAR, making conclusive attribution of their impacts more difficult.

Note that at 8-day and daily time scales, accounting for correlation among the residuals using GR yields different models of the trend, regression coefficients, and uncertainties relative to a setup where such correlation is ignored (analogous to MLR), specifically for the NEE and GEE. When temporal correlation was ignored, at least 2 or 3 more variables are identified for the trend, because the underlying temporal correlation is misattributed to one or more of the candidate variables. In addition, the significance of

the regression coefficients is reduced when MLR was applied. These results further emphasize the need to account for the covariance of residuals in regression analysis of flux data at sub-monthly resolutions.

5.2 Isolating photosynthesis and respiration from NEE measurements

The auxiliary variables selected for the NEE model can be used to partially isolate carbon uptake and release at the sub-monthly temporal scales. At the monthly scale, none of the variables identified as being important for R_{h+a} are selected for the NEE model, indicating that R_{h+a} cannot be derived from the NEE observations using auxiliary variables. This is likely due to the fact that the seasonality at UMBS dominates the monthly signal, which is primarily controlled by the seasonal cycle of photosynthetic activity at this site. At the 8-day and daily time scales, however, results are more promising (Table 6.2), with air temperature (a variable similar to nighttime temperature important for R_{h+a}) also being selected for NEE. Overall, the covariates that are associated with carbon uptake and release in the NEE model explain 90% of the GEE variability and 94% of the R_{h+a} variability at the 8-day scale (Figure 6.3), and 83% and 86% at the daily scale (Figure 6.4), respectively. This result indicates that NEE measurements at fine time scales can be used to identify variables that are important for photosynthesis and respiration separately. This suggests that selected auxiliary variables can potentially be used to separate NEE observations and/or geostatistical inverse modeling total CO_2 flux estimates (e.g. Michalak et al., 2004; Gourdji et al., 2008) into component fluxes.

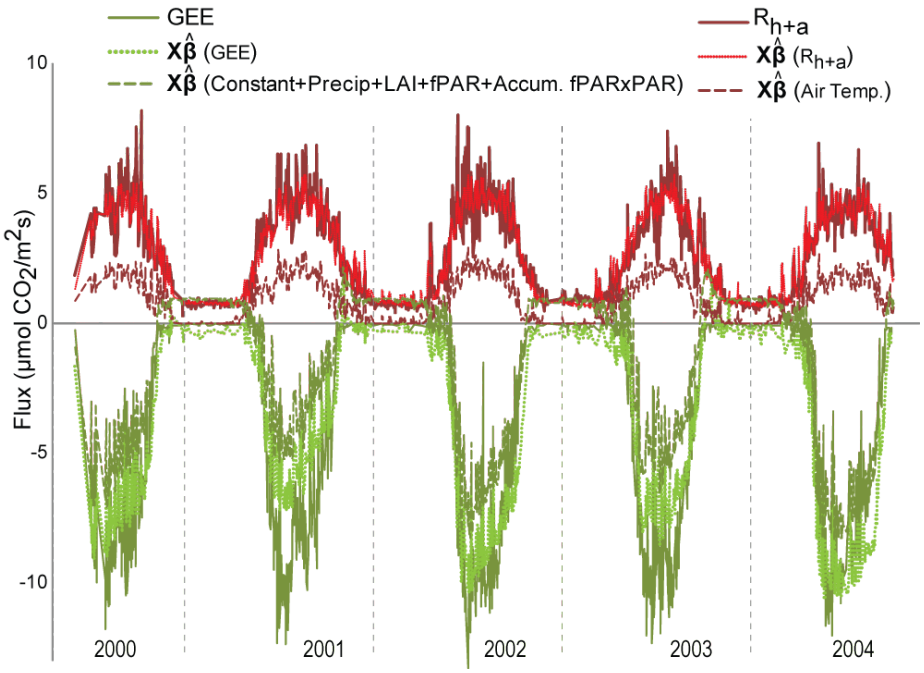

Figure 6.4: Daily-averaged GEE and R_{h+a} measurements, their associated models of the trend ($\mathbf{X}\hat{\boldsymbol{\beta}}$), and the components of the NEE model of the trend associated with carbon uptake (negative $\hat{\boldsymbol{\beta}}$) or loss (positive $\hat{\boldsymbol{\beta}}$).

5.3 Regression analysis for growing Season, spring green-out, and non-growing season

The forest at UMBS is a net carbon source from early fall (late September) until late spring (mid May) (Gough et al., 2008), and this strong seasonality may be associated with changes in the significant auxiliary variables and/or their relationship to flux for the current analysis. To investigate this question, the daily GR analysis was repeated for (1) the growing season, approximately day of year (DOY) 140-276, a period of increasing leaf density defined by the period for which soil temperature is above 5ºC (Schmid et al., 2003), (2) spring green-up in May, a period of rapid leaf growth coinciding with dramatic shifts in atmospheric humidity, surface energy balance and the balance between respiration and photosynthesis, and (3) the non-growing season, approximately DOY 295-117, a period of leaf senescence and limited growth due to lack of sunlight and cold temperatures, with an average air temperature below -1ºC.

The amount of available sunlight is found to drive photosynthesis during the growing season, consistent with current understanding (e.g Gough et al., 2007) (Table 6.3). Net radiation, the daily variation of which is similar to that of PAR during this time of the year (Oliphant et al., 2006) explains the majority of the variability in NEE and GEE, with some adjustments provided by vegetative indices (i.e. site-specific fPAR and site-specific LAI in the NEE and GEE trends respectively). The selection of vegetation indices is reasonable, because seasonal changes in leaf area strongly affect the light environment of forest canopies, especially those dominated by aspen (Roden, 2003). However, it is unclear whether site-specific LAI or site-specific fPAR is most strongly associated with carbon uptake during this time period, because the fPAR dataset was derived from the LAI data, as described in Section 2.2. The other variables play a more minor role, but are generally consistent with those from the analysis presented in Section 4.1. The only notable exception is the absence of site-specific fPAR in the R_{h+a} model of the trend, which suggests that temperature controls are more dominant on respiration during this time period.

Table 6.3: Selected variables and their associated drift coefficients ($\hat{\boldsymbol{\beta}}$) in $\mu molCO_2/m^2s$ as estimated from the geostatistical regression algorithm at the daily temporal scale for the 3 seasons (Growing, Green leaf-out, Non-growing). All drift coefficients are significant at the 95% confidence level unless italicized in the table. Numbers in brackets indicate the reduction in explanatory power when the associated variable is removed from the model (ΔR_i^2) where a higher number signifies a more dominant variable. The variance explained (R^2) and condition number (K) of the trends are provided for each model. Note that other variables in Table 6.1 were never selected and are therefore not listed here. Dashes indicate categories of variables that were not selected for a particular model.

		Growing season			Non-growing season		May		
Category	**Variable Name**	**NEE**	**GEE**	**R_{h+a}**	**NEE**	**R_{h+a}**	**NEE**	**GEE**	**R_{h+a}**
	Constant Component	35.95	13.44	1.29	*0.34*	*-0.15*	*-0.71*	-69.10	*-0.16*
Resistance	Friction Velocity	-----	-0.20 [~ 0]	0.11 [0.01]	-----	-----	-----	-----	-----
Temperature	Air Temperature	0.47 [~ 0]	-0.31 [0.08]	-----	-----	-----	0.50 [0.10]	-----	-----
	Land Surface Temp.	-----	-----	-----	-----	-----	-----	0.43 [0.05]	-----
	Nighttime Air Temp.	-----	-----	1.06 [0.43]	0.29 [0.30]	0.32 [0.23]	-----	-----	0.64 [0.19]
Water/Temp.	VPD	-----	0.45 [0.01]	-0.42 [0.12]	-----	-0.07 [0.01]	-----	0.38 [0.15]	-0.13 [0.01]
Radiation	Accum. PAR	-----	-----	-----	-----	-----	0.57 [0.03]	-----	-----
	Soil Heat Flux	-----	-----	-0.24 [0.03]	-----	-----	-----	-----	-0.21 [0.02]
Water Avail.	Precipitation	0.28 [0.07]	0.34 [0.07]	-----	-----	-----	-----	-----	-----
Radiation	Accum. Net. Rad.	-2.03 [0.12]	-1.43 [0.33]	-----	-----	-----	-----	-----	-----
Vegetation	LAI (MODIS)	-----	-----	-----	-----	-----	-1.54 [0.02]	-1.22 [0.06]	-----
	LAI (site-specific)	-----	-1.56 [~ 0]	-0.06 [0.01]	-----	-----	-----	-----	-----
	NDVI (MODIS)	-----	-----	-----	*0.06 [~ 0]*	0.15 [0.05]	-----	-----	0.39 [0.13]
	EVI (MODIS)	-----	-----	-----	-----	-----	*1.09* [0.04]	-----	-----
Veg./Rad.	fPAR (site-specific)	-1.07 [~ 0]	-----	-----	0.10 [0.10]	0.17 [0.08]	-----	-----	-----
	fPAR x Accum. PAR	0.71 [~ 0]	-----	0.17 [0.02]	-----	-----	-1.35 [0.09]	-0.87 [0.18]	-----
	R^2 =	0.63	0.53	0.63	0.74	0.80	0.73	0.83	0.79
	K =	6	3	4	2	3	12	4	4

In May, on the other hand, the rapid change brought about by leaf-out in the spring results in the largest changes in both selected variables and estimated variables from the overall seasonal relationships presented in Section 4.1 (Table 6.3). However, the amount of PAR absorbed or lost within the canopy remains the dominant explanatory variable of carbon uptake during this time period (i.e. ΔR_i^2 is largest when fPAR x Accumulated PAR was removed from the NEE and GEE May trends, among variables

with an associated negative regression coefficient). As with the growing season, air temperature (or nighttime temperature) captures the majority of the respiration signal in both the NEE and R_{h+a} models of the trend.

Only NEE and R_{h+a} were evaluated for the non-growing season, because there is little growth during this period. Nighttime air temperature remains the dominant variable in the R_{h+a} model, and also becomes an important variable for NEE, providing further evidence that temperature controls carbon efflux for this forest ecosystem. The other dominant variable, fPAR, appears to help the model of the trend better fit the seasonality of the respiration signal, and is therefore likely not directly acting as a proxy of some mechanism controlling respiration (Figure 6.5).

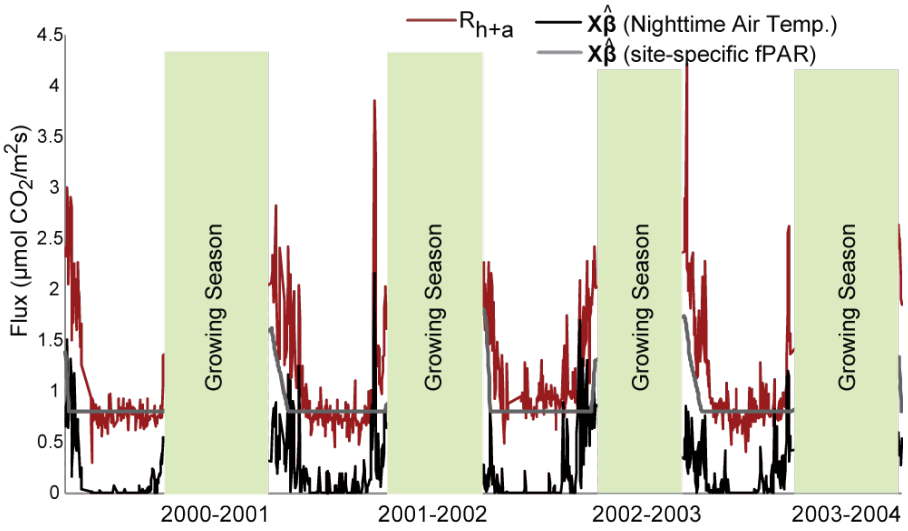

Figure 6.5: Daily non-growing season R_{h+a} measurements and contributions ($\mathbf{X\hat{\beta}}$) of nighttime temperature and fPAR.

Note that the regression residuals from the seasonal analysis are homoscedastic, whereas those in the full-year analysis showed some differences in variance with seasons. Given that the results of the seasonal analyses are generally consistent with those presented in Section 4.1 for the full year, heteroscadicity of these residuals does not appear to play an important role in the year-round analysis.

5.4 Sensitivity analysis of LAI and fPAR

A sensitivity analysis was performed to assess the impact of using site-specific versus remote-sensing-derived LAI and fPAR on the results presented in Section 4.1. This analysis is particularly important given the significant roles that LAI and fPAR play in the models of the trend at all temporal resolutions. In addition, the fact that site-specific LAI and fPAR are selected over the remote sensing data products at smaller temporal scales (and at all scales for R_{h+a}) raises questions about the use of satellite data products for eddy-covariance studies. Figure 6.6 shows that the MODIS LAI appears to overestimate site specific LAI during the growing seasons, while the fPAR measurements are relatively consistent, although the onset and subsidence of the growing season differ. In addition, the MODIS LAI and fPAR datasets are inherently noisy, especially in the non-growing season when there is no vegetation activity at UMBS. In the sensitivity analysis, the "preferred" LAI and fPAR datasets (defined as the LAI and fPAR selected for those models in Table 6.2), were removed from the analysis, the BIC was rerun, and the impact on the selected variables and their relationship to NEE, GEE and R_{h+a} was reevaluated (Table 6.4).

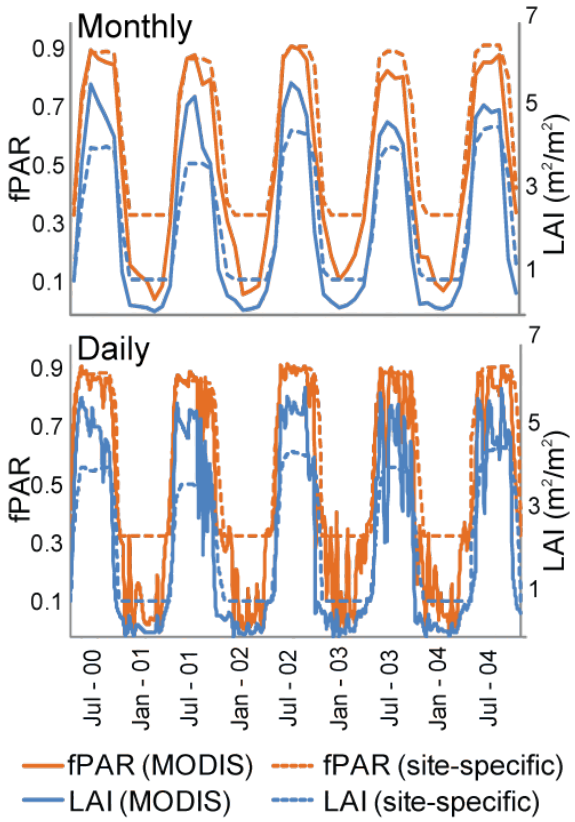

Figure 6.6: LAI and fPAR data sets from MODIS and from VAI field measurements scaled by total annual leaf area as estimated from site leaf litter traps at the (a) monthly and (b) daily time scales.

Table 6.4: Selected variables and their associated drift coefficients ($\hat{\boldsymbol{\beta}}$) in $\mu molCO_2/m^2s$ as estimated from the geostatistical regression algorithm when the preferred sources of LAI and fPAR (Table 6.2) are removed the analysis. All drift coefficients are significant at the 95% confidence level unless italicized in the table. Bold values identify variables that were not selected in the original analysis (Table 6.2). The variance explained (R^2) and condition number (K) of the trends are provided for each model. Note that other variables in Table 6.1 were never selected and are therefore not listed here. Dashes indicate categories of variables that were not selected for a particular model.

		Monthly			8-day			Daily		
Category	**Variable Name**	**NEE**	**GEE**	**R_{h+a}**	**NEE**	**GEE**	**R_{h+a}**	**NEE**	**GEE**	**R_{h+a}**
	Constant Component	0.20	0.48	0.81	2.83	1.81	0.74	1.94	1.52	0.41
Resistance	Friction Velocity	-----	-----	-----	-----	-----	-----	-----	-0.15	0.05
Temperature	Air Temperature	-----	-1.69	-----	0.85	-----	-----	-----	-----	-----
	Nighttime Air Temperature	-----	-----	1.59	-----	-----	1.53	0.68	-----	1.37
	Soil Temperature	-----	-----	-----	-----	-0.93	-----	-----	-----	-----
Radiation	Accum. Shortwave Rad.	-1.20	-----	-----	-----	-----	-----	-----	-----	-----
	Surace Reflectance (MODIS)	-0.83	-0.77	-----	-----	-----	-----	-----	-----	-----
	Soil Heat Flux	-----	-----	-----	-----	-----	-----	-----	-----	-0.14
	Accum PAR	-----	-----	-----	-----	-----	-----	0.23	-----	-----
Water/Temp.	Vapor Pressure Deficit	-----	-----	-0.41	-----	-----	-0.36	-----	-----	-0.26
Water Avail.	Precipitation	-----	-----	-----	-----	-----	-----	0.74	0.25	-----
Vegetation	LAI (site-specific)	-7.80	-4.72	0.38	-----	-----	0.43	-----	-----	0.56
	EVI (MODIS)	-----	-----	-----	-1.26	-1.06	-----	-1.05	-1.63	-----
Veg./Rad.	fPAR (site-specific)	6.09	2.99	-----	-----	-----	-----	-----	-----	-----
	fPAR x Accum. PAR	-----	-1.28	-----	-1.65	-1.45	0.43	-2.22	-1.22	-----
	R^2 =	0.88	0.96	0.98	0.78	0.90	0.96	0.74	0.77	0.91
	K =	20	24	10	5	16	7	9	3	7

Although all models of the trends have slightly less explanatory power without the "preferred" LAI and fPAR datasets, MODIS and site specific LAI and fPAR explain similar seasonality in the monthly NEE and GEE measurements. As the temporal scale decreases, however, MODIS EVI becomes a better substitute for site-specific LAI ("preferred" dataset) and site-specific fPAR (also a "preferred" dataset) over MODIS LAI and fPAR. Since EVI is also inherently noisy, this substitution may be due to the difference in the resolution of these MODIS products, where LAI and fPAR were provided at the 1km scale, whereas the EVI data was available at a 250m resolution. These results suggest that the representativeness of the MODIS 1km products of a flux tower site may be adequate at monthly scales, but less so at finer temporal resolutions. In addition, these results indicate that site-based estimates of LAI and fPAR based on

relatively few measurements appear to be able to adequately represent properties of large areas (~1km^2) at flux tower sites for the purposes of studying carbon cycling, which would be contrary to suggestions cited in previous work (e.g. Beerling and Quick, 1995).

For R_{h+a}, when site-specific fPAR was removed from the analysis, site-specific LAI was always selected as a substitute, with minor changes to the overall fit of the model, indicating that the process characterized by fPAR is best represented by site-specific vegetation variables at all temporal scales.

For all models (NEE, GEE, and R_{h+a}), most other variables remain consistent with those selected in Section 4.1, suggesting that the relationship between these parameters and flux is relatively independent of the representativeness of the LAI and fPAR datasets. The fact that their associated inferred drift coefficients are similar both in signs and magnitudes further supports this finding, supporting the robustness of the results presented in Section 4.1.

5.5 Testing the linearity assumption

The GR models built in this work assume a linear relationship between NEE, GEE, or R_{h+a}, and the selected auxiliary variables. This assumption was tested by examining scatter plots of flux as a function of individual selected variables for the monthly, 8-day, and daily analyses. An example of 8-day averaged GEE and R_{h+a} plotted against a subset of auxiliary variables is presented in the top row of Figure 6.7. These scatter plots reveal possible non-linear relationships. However, these nonlinear relationships either vanish, or are significantly reduced in the residuals from the GR models (bottom row of Figure 6.7). This result indicates that relationships that appear to be nonlinear when fluxes are regressed against individual variables can in fact be explained using linear relationships when multiple auxiliary variable are considered, due to the co-variability among the key auxiliary variables. The analysis presented in Figure 6.5 also supports the use of a linear model for the analyses presented in this work, and further cautions against using single variable statistics to infer relationships with NEE, GEE, or R_{h+a}, because such single-variable regressions may lead to incorrect conclusions about the nonlinearity of the relationship between environmental variables and flux.

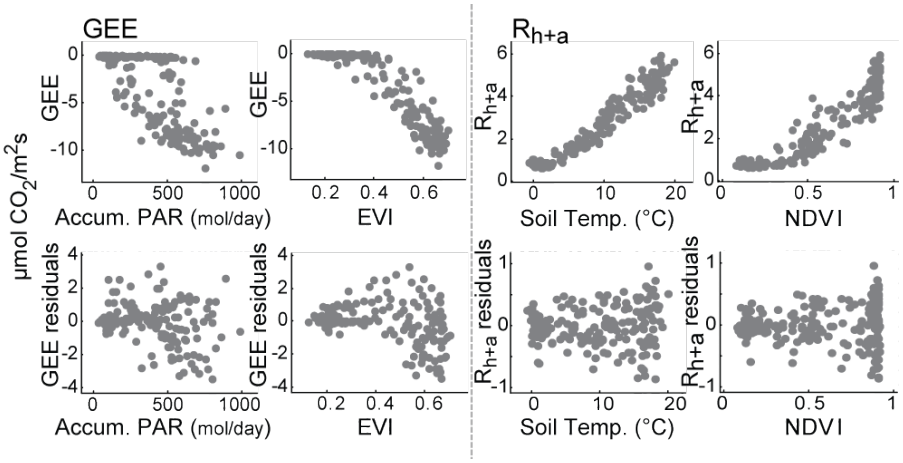

Figure 6.7: Scatterplots of GEE and R_{h+a} as a function of a representative sample of auxiliary variables. All variables are 8 day averaged. (top) GEE and R_{h+a}; (bottom) GEE and R_{h+a} residuals from the estimated trend.

6.0 Discussion and lessons learned

6.1 Are results consistent with existing understanding of the controlling factors of photosynthesis and respiration at UMBS? Do they provide new insight into carbon cycling at this site?

In general, the results of this study are consistent with current understanding of carbon cycling for this forest ecosystem, including the strong correlation between respiration and temperature, and the influence of solar radiation on carbon uptake during the growing season (Gough et al., 2008).

However, this study has also identified additional variables to the expected ones mentioned above, that explain variability in GEE and R_{h+a}. First, fPAR appears to act as a proxy for other important variables that were not considered in this analysis to capture the overall seasonality in R_{h+a}, such as potentially the amount of litter substrate available for heterotrophic respiration, or the amount of substrate available for root respiration. This finding is consistent with the fact that the UMBS soil is nutrient poor, making substrate availability important in terms of respiration (Gough et al., 2008). Second, light and LAI are important for explaining, and therefore potentially controlling, sink processes at UMBS. APAR is more important at fine temporal scales, although LAI and fPAR remain the most important auxiliary variables. This suggests that, despite the

complexity of this ecosystem, CO_2 uptake is regulated mostly by vegetation response to large scale energy input (Albertson et al., 2001), and, therefore, can be represented using simple linear relationships to a few key environmental variables. Third, the variance explained for the R_{h+a} models is higher than those for NEE and GEE for all examined cases. This is an unexpected result given the current relative lack of understanding of processes controlling respiration, and implies that unexplained variability in GEE may contribute to large uncertainties in annually averaged predicted uptake.

Finally, site-specific and remote-sensing LAI and fPAR data do not appear to be interchangeable, especially at finer temporal scales. This is likely due to either the poor spatial representativeness of coarser remote-sensing data products relative to site-specific data, or to noise within these MODIS datasets. These results are important because the choice of data, especially for vegetative indices, in empirically-based models, is the subject of much debate, with some studies electing to use EVI (e.g Sims et al., 2006) while others prefering LAI (e.g. Lindroth et al., 2008), fPAR (e.g. Running et al., 2004) and/or Land Surface Water Index (LSWI) (Mahadevan et al., 2008), all generally provided or derived from MODIS products, as proxies for gross productivity. This work suggests that the spatial representativeness of data at relevant spatial and temporal scales may be as important as the choice of the specific vegetative indices to be used.

6.2 To what extent can NEE be used to understand processes controlling photosynthesis and respiration at UMBS? Are results applicable at other sites?

If the variables selected for the NEE model of the trend were consistent with those selected for GEE and R_{h+a}, then the NEE signal could be used directly to understand the processes controlling component fluxes. Conversely, if there were no relationship between variables selected for NEE, GEE, and R_{h+a}, this would indicate that NEE contains little direct information about component fluxes. Because sink activity dominates at UMBS, the monthly NEE model of the trend contains similar variables to those selected for GEE, and does not include variables that capture R_{h+a}. However, at smaller resolutions (8-day and daily), results suggest that auxiliary variables may provide an alternative means to separate photosynthesis and respiration from the NEE measurements.

The relative amount of sink and source activity should be considered in assessing the ability of the geostatistical algorithm to partition the NEE signal using auxiliary variables. Given that the relationship between respiration and primary production would be different at every flux site, it is difficult to determine whether estimated NEE models would yield similar results at other sites. However, it seems reasonable that at longer scales, the dominant activity (i.e. sink or source) would be better represented by the selected variables within a model.

6.3 To what extent does GR provide insight into factors that influence carbon cycling?

One advantage of statistical approaches for studying carbon cycling is that they can identify key relationships among available observations and environmental datasets, with relatively little reliance on assumptions about controlling processes. This can lead to the identification of important variables that would otherwise be overlooked. Statistical approaches can also be seamlessly applied across temporal scales, thereby providing a method for evaluating the validity of mechanistically-derived relationships at different temporal resolutions.

This study suggests that simple linear regression methods used in previous flux studies relying on relationships between carbon flux and individual auxiliary variables, yield derived relationship may be a result of the correlation in the seasonal cycles of flux and individual auxiliary variables, rather than a true explanatory relationship. Such a correlation could eclipse the true relationship between an auxiliary variable and flux. This work confirms conclusions from other studies (e.g. Stoy et al., 2009) that concluded that the statistical relationship between an auxiliary variable and flux can be scale-dependent, as well as seasonally-varying. These results emphasize the need to explicitly interpret statistical models only at the scales at which relationships were derived. Similarly, studies that use biospheric models that 'scale-up' or 'scale-down' relationships inferred at one resolution to another resolution should verify whether the processes and parameterizations used by the model are scale-dependent.

This study also demonstrates the need to account for temporal correlation in residuals in statistical regressions, especially for analyses at fine temporal scales (i.e. sub-monthly), where residuals have correlation lengths that span multiple time periods (e.g.

the τ_Q for the NEE and GEE 8 day residuals was 6 and 6.5 8-day periods, respectively, compared to a τ_Q for R_{h+a} residuals of 1.25). Correlation is quantified using the Restricted Maximum Likelihood (RML) method, further limiting model assumptions that could otherwise bias estimates.

This work relied on an assumption of linearity between the examined auxiliary variables and flux. Although this is contrary to the functional forms of the relationships between these variables and flux as implemented in many biospheric models (which are applicable at a physiological level), results presented in Section 4.4 show that a linear model is able to reproduce what initially appear to be nonlinear dependency when variables are examined individually. Note that there is a possibility that the linear assumption in the model could eclipse a "true" nonlinear relationship between a variable and flux (such as the Q_{10} exponential relationship between temperature and heterotrophic respiration), as mentioned in Section 7.0, Chapter 3. However, this work suggests that the linearity assumption is justified for this analysis, and further emphasizes the potential for inferring erroneous relationships between variables and flux when examining variables individually.

Finally, although statistical methods can be powerful tools for studying complex systems such as carbon cycling, these analyses do not in and of themselves prove causality. Instead, they highlight dominant relationships and patterns that can, when reaffirmed with additional results and scientific knowledge, illuminate process-based understanding. One limitation of the approach presented in this work is that the BIC method used here selects a single "best" model of the trend. In some cases, multiple similar sets of auxiliary variables provided comparable fits to the available observations, although dominant variables remained consistent. Approaches for accounting for the uncertainty associated with the form of the model of the trend are explored in related work (Yadav et al., in press).

Note that although the focus of this work is on statistical inference, a further analysis was performed to see how well the GR method could perform in predicting daily NEE for a given year, relative to multiple linear regression. In this analysis, data from one year were removed from the analysis, and the remainder of the data were used to (i) select variables, (ii) estimate regression coefficients, and (iii) predict fluxes for the

missing year. The results show an improvement in prediction (as evaluated using R^2) over multiple linear regression. The majority of the improvement is attributed to the more representative set of variables that are selected by the BIC method when temporal correlation is considered in the GR approach.

7.0 Conclusions

This research presents a GR approach for studying the complex biosphere-atmosphere exchange of CO_2 at eddy-covariance measurement sites, and applies the proposed approach to the AmeriFlux site at UMBS. The GR approach is shown to be a useful method for exploring the relationships between auxiliary variables and NEE, GEE, and R_{h+a} at this flux tower site across temporal scales.

Overall, conclusions about carbon cycling from this study at UMBS are consistent with current understanding, including the strong correlation between respiration and temperature, and the influence of solar radiation on carbon uptake during the growing season. However, the study also highlights the influence of other variables such as precipitation, VPD, and fPAR on both carbon uptake and release across multiple temporal scales. Results also confirm that many relationships between flux and auxiliary variables are scale-dependent. In addition, the study showed that site-specific and remote-sensing LAI and fPAR data are not interchangeable at finer temporal scales, indicating that the choice of the specific vegetative indices used in an analysis is as important as their spatial and temporal representation. Finally, results show that a linear GR model is able to capture what initially appear to be nonlinear relationships, due to the co-variability among individual auxiliary variables in the model.

In addition, GR is found to be able to identify variables that partially isolate GEE and R_{h+a} from the NEE signal at smaller time scales. Therefore, GR can be used to infer process-based information from observations of NEE using other available datasets, without having to separate the signal into component fluxes, thereby avoiding a possible source of error. This result also suggests that a similar approach may be useful for geostatistical inversion studies (e.g. Michalak et al., 2004; Gourdji et al., 2008) that use atmospheric measurements along with auxiliary data and an atmospheric transport model to infer CO_2 surface fluxes, because the auxiliary data used in such studies may help isolate the photosynthetic and respiration signals.

The GR model as presented herein could be extended to account for the uncertainty of selecting a single "best" model of the trend when multiple sets of auxiliary variables provide comparable fits to the available observations (Yadav et al., 2010). In addition, instead of separating the data by seasons, heteroscedasticity in the residuals could be modeled using a more complex temporal covariance matrix,**Q**. Finally, nonlinear or lagged relationships could also be included to further improve the fit of the model to the data.

CHAPTER 7

Conclusions and Future Directions

This section summarizes the objectives and findings of the contributions of this dissertation, provides a synopsis of the collaborations with fellow researchers connected to this work, and also suggests directions for future work.

1.0 Contributions

The overarching goal of this dissertation is to infer carbon cycling dynamics that more directly reflect the information content of the available atmospheric measurements. To achieve this goal, the dissertation involved applying and further developing two different geostatistical methods: an inversion (GIM) and a regression (GR) applied at different spatial and temporal resolutions. GIM uses the variability in atmospheric CO_2 concentrations to infer the most likely distribution of surface CO_2 fluxes while GR uses direct NEE measurements to infer relationships between carbon flux and environmental variables. The following sections summarize the major contributions from each of these objectives.

1.1 Objective 1: Global geostatistical inversion study

Objective 1 involved estimating global monthly CO_2 surface flux at a 3.75° latitude × 5° longitude resolution for 1997-2001 to quantify the degree to which the global observational network can inform the distribution of CO_2 fluxes at various spatial and temporal scales with limited model assumptions. The main conclusions and contributions from Objective 1 are listed below.

<u>Conclusions:</u>

- Contrary to assumptions in the carbon cycle community, the existing atmospheric monitoring flask network can be used to estimate surface fluxes and their associated uncertainties at a 3.75° × 5° resolution. The grid-scale fluxes reflect the general knowledge of the seasonality of surface flux exchange;

- The geostatistical gird-scale flux estimates are most influenced by the limited information content of available atmospheric measurements, and therefore have correspondingly large uncertainties. The grid-scale flux distributions also reflect the assumption of a constant model of the trend used in GIM. As such, the grid-scale fluxes rely more heavily on the inferred autocorrelation of the flux distribution, yielding smooth spatial variability. As such, the purpose of estimating fluxes at a 3.75° × 5° resolution is to post aggregate to larger regions so that estimates are more accurate so they can be compared to other estimates of flux from both "top-down" and "bottom-up" methods;
- Contrary to the widely help assumption that additional information is needed with the limited network, the *a posteriori* fluxes aggregated to continental regions have uncertainties that are comparable to those reported by previous synthesis Bayesian inversions at monthly and inter-annual time scales;
- For poorly constrained continental regions such as Tropical America, South America, and Southern Africa, the large differences between the fluxes estimated by GIM and estimates from other Bayesian inversions studies illustrate the strong influence of explicit terrestrial priors used in synthesis Bayesian inversions; and,
- Estimates for the relatively well-constrained European region were also shown to vary between studies indicating that the partition of Northern Hemisphere sink is still not well understood.

<u>Contributions:</u>

- The study was the first real application of GIM to estimate surface CO_2 fluxes; and
- Unlike estimates from other Bayesian inversions, the flux estimates from GIM are relatively independent from process-based models and thus can be used in inter-comparison studies of both bottom-up and top-down estimates.

Overall, Objective 1 demonstrates that GIM can provide a valuable data-driven alternative to synthesis Bayesian inversion methods, by avoiding many *a priori* assumptions inherent to aggregation, uncertainty estimation, and the magnitude and

spatial patterns of flux distributions. However, more research is needed to develop a better understanding of the significant differences between the GIM estimates and those from other studies such as in the Northern mid-latitudes in order to ascertain which assumptions are having the largest impact. Such understanding is important to locate, protect, and possibly enhance natural sinks of atmospheric CO_2.

1.2 Objective 2: North American regional geostatistical inversion study

Objective 2 entailed assessing the ability of the expanding network of continuous CO_2 measurements to constrain monthly and annual fluxes at a 1° latitude × 1° longitude resolution for North America in 2008. The main conclusions and contributions from Objective 2 are listed below.

Conclusions:

- Although most regional inversions only use one measurement per day, including more temporal measurements when simulated transport can be trusted can significantly improves flux estimates once there is more spatial coverage. However, the estimation scale must be sub-daily to account for the variability of the underlying fluxes and transport;
- If the estimation scale is too coarse, as is the case with most inversion applications, the estimates are subject to significant temporal aggregation errors even at aggregated spatial and temporal scales;
- Although simulated transport may be more trustworthy during the mid-afternoon hours when well-mixed conditions prevail, an atmospheric CO2 observation from this time of the day appears to contain a diffuse signal in terms of surface exchange. Thus, mid-afternoon observations may only constrain carbon budgets for very large areas. The result may have implication for the use of aircraft, flask, and continuous measurements in regional inversions that are limited in both space and time; and,
- As with other studies, boundary conditions were found to play a large role only at budgeting monthly and particularly annual sources and sinks at the continental scale in regional inversions. The difference of the North American annual budgets due to the choice of boundary conditions was over 1PgC/yr.

Contributions:

- The study is the first to use measurements from the expanded measurement network (i.e. 35 tower locations in North America) to estimate fluxes for 2008;
- As part of the study and collaborative efforts (specifically of Vineet Yadav (University of Michigan), Sharon Gourdji (University of Michigan), and Charles Antonelli (University of Michigan)), published code, algorithms, and documentation of GIM has been made freely available to the scientific community (http://www.puorg.engin.umich.edu/); and,
- Also as part of the study and collaborate efforts (specifically of Sharon Gourdji (University of Michigan), Mike Trudeau (NOAA), Abhishek Chatterjee (University of Michigan) and Yoichi Shiga (University of Michigan)), the WRF-STILT particle trajectory and derived sensitivities for 2004 and 2008 North American domain, generated as part of the regional inversion, have also been made freely available via ftp (http://www.puorg.engin.umich.edu/) to the scientific community.

Objective 2 demonstrated that setup choices must be considered to best extract the information content on CO_2 flux exchange within the expanded regional continuous measurement network. The work showed that more research is needed to help determine what times of the day to include measurements from different tower sites as errors associated with simulated transport can bias flux results. In addition, more research is needed to reach a consensus on a set of boundary conditions to use in regional inversions as they have a large impact, particularly on continental annual carbon budgets.

1.3 Objective 3: Flux tower geostatistical regression study

Objective 3 involved assessing drivers of CO_2 variability at a landscape scale and the temporal dependency of the inferred statistical relationships between environmental variables and surface CO_2 exchange at the University of Michigan Biological Station (UMBS). The main conclusions and contributions from Objective 3 are listed below.

Conclusions:

- Overall, conclusions about carbon cycling from the GR study at UMBS are consistent with current understanding, including the strong correlation between respiration and temperature, with respect to the influence of solar radiation on carbon uptake during the growing season. The consensus partially validates the use of the method to infer carbon dynamics at flux tower sites;
- The study also highlights the influence of other variables such as precipitation, VPD, and fPAR on both carbon uptake and release across multiple temporal scales. These variables previously had not been noted as being important for carbon cycling at this site but identified by others (e.g. Anderson et al., 2000) as important controls of CO_2 exchange for Northern hardwood forests;
- Results confirm that many relationships between flux and auxiliary variables are scale-dependent. The result confirms conclusions from other studies (e.g. Stoy et al., 2009) that found that the statistical relationship between an auxiliary variable and flux can be scale-dependent, as well as seasonally-varying;
- The work showed that site-specific and remote-sensing leaf area index (LAI) and fraction of photosynthetically active radiation (fPAR) data are not interchangeable at finer temporal scales, indicating that the choice of the specific vegetative indices used in an analysis is as important as their spatial and temporal representation;
- The results show that a linear GR model is able to capture what initially appear to be nonlinear relationships due to the co-variability among individual auxiliary variables in the model. The results suggest that simple linear regression methods used in previous flux studies relying on relationships between carbon flux and individual auxiliary variables yield derived relationships that may be a result of the correlation in the seasonal cycles of flux and individual auxiliary variables, rather than a true explanatory relationship; and,
- Finally, GR is found to be able to identify variables that partially isolate GEE and R_{h+a} from the NEE signal at smaller time scales. Therefore, GR can be used to infer process-based information from observations of NEE using other available

datasets, without having to separate the signal into component fluxes, thereby avoiding a possible source of error.

Contributions:

- The study involved developing the Bayes Information Criteria (BIC) model selection to include correlated residuals. The study is the first to apply GR at a flux tower site to infer statistical relationships between flux and environmental variables; and,
- As part of the study and collaborative efforts (specifically of Vineet Yadav and Charles Antonelli (University of Michigan)), published code, algorithms, sample data and documentation of GR has been made freely available to the scientific community (http://www.puorg.engin.umich.edu/).

Objective 3 demonstrated that the GR algorithm can provide valuable insights into the controlling variables of flux at different temporal scales including the need to explicitly interpret statistical models only at the scales at which relationships were derived. The temporal scale dependency of a relationship between a variable and flux is only one example of the ways that GR inform process-based modeling of complex carbon dynamics at different spatiotemporal resolutions. The method could be expanded to GIM which uses atmospheric measurements along with auxiliary data (e.g. Michalak et al., 2004; Gourdji et al., 2008; Gourdji et al., in prep.) and an atmospheric transport model to infer CO_2 surface fluxes. In GIM, the method could be used elicit the spatial dependence of the relationship between flux and a variable as seen by the atmospheric network.

1.4 Overall contributions

The value in the statistical approaches developed and applied in this dissertation is that they provide strongly atmospheric data-driven estimates of surface fluxes and statistical relationships between carbon flux and environmental variables. Overall, the work demonstrates that geostatistical methods can provide a means of isolating the information content of the atmospheric measurements while highlighting potential problems associated with model assumptions that otherwise could go unnoticed. On the whole, the dissertation addresses the specific gaps in our knowledge in the carbon cycle

at different spatiotemporal scales as shown in Figure 7.1. Importantly, the work presented in this dissertation specifically fits into the community-wide effort to reduce the spread of flux estimates from different models (as shown in Figure 1.5) by:

- Providing independent estimates of CO_2 flux and associated uncertainties at continental scales;
- Showing promise in providing independent estimates of CO_2 flux and associated uncertainties at regional scales; and,
- Providing the means to test assumptions in process-based models (such as the scale dependency of a particular variable and flux) at the various spatiotemporal scales where the assumptions are applied.

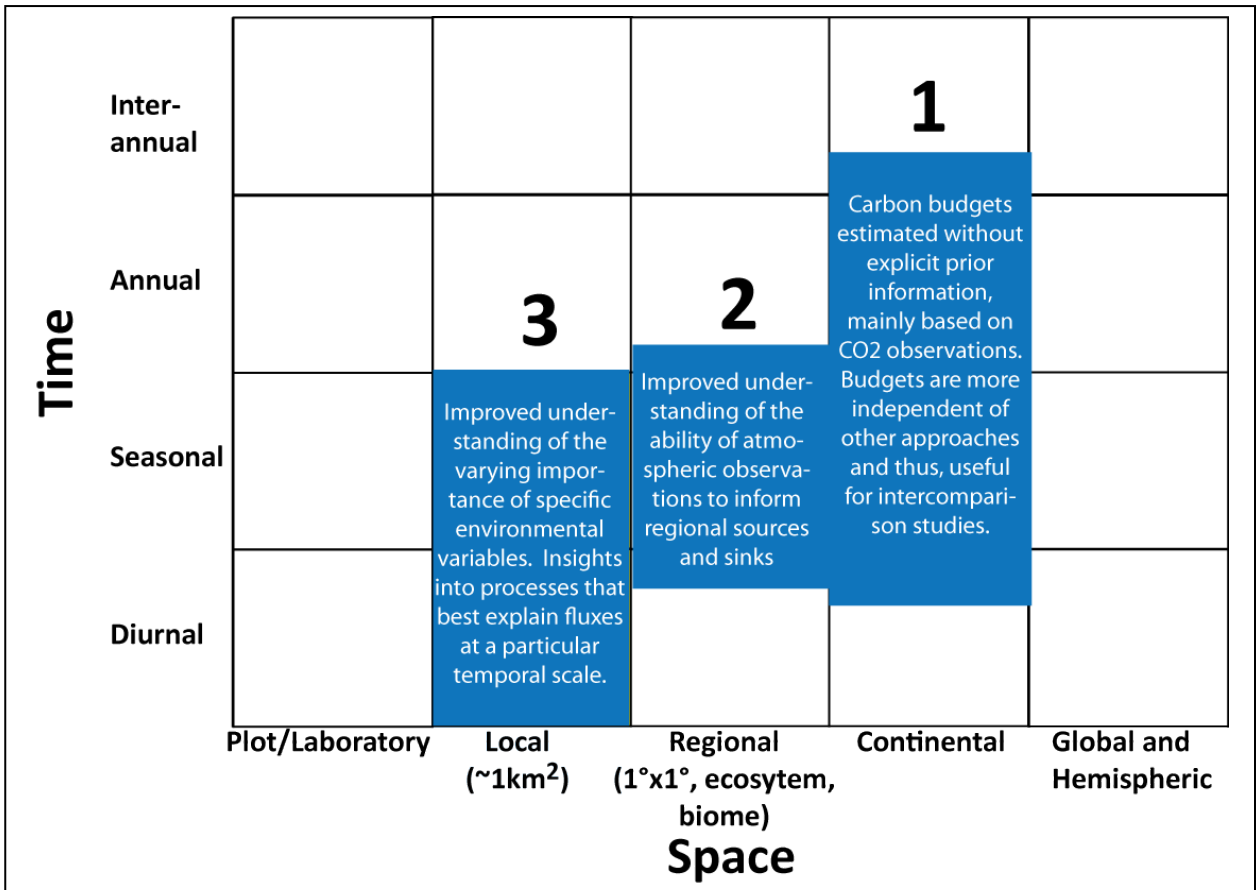

Figure 7.1: A schematic showing the specific contributions this dissertation addresses in terms of estimating flux and learning about processes influencing surface exchange at the different spatiotemporal resolutions.

2.0 Collaborative research

The research presented herein was a collaborative effort and part of a series of work that involved developing and applying geostatistical methods to infer carbon cycle dynamics. The following paragraphs summarize the other work, credit the collaborators, and explain how the collaborative research connects to the work of the dissertation.

In terms of GIM, a companion piece of work (Gourdji et al., 2008) to the global study presented in Chapter 4, explored the ability of auxiliary environmental variables (e.g. Air temperature, leaf area index, etc.) to further constrain flux distributions within the GIM framework, especially at fine spatial resolutions. Overall, the auxiliary variables allowed the inversion to recover more realistic CO_2 flux variability at the grid-scale with

lower *a posteriori* uncertainties relative to a setup relying exclusively on the limited atmospheric CO_2 measurement network. For regional inversions, addition work has been conducted with GIM to provide insight into the spread of mechanistic models estimating the biospheric component of land-atmosphere carbon exchange specifically over the North American continent for 2004 (Gourdji et al., in prep).

For GR model, the work presented in Chapter 5 was extended to account for the uncertainty of selecting a single "best" model of the trend when multiple sets of auxiliary variables provide comparable fits to the available observations (Yadav et al., 2010). The GR method was applied to six different flux towers sites in North America to assess the temporal scale dependencies between GPP and environmental variables representing plant function and climate. This work demonstrates and quantifies how the importance of environmental variables included in the model of the trend of GPP varies across temporal scales. In addition, the GR method was also used to assess differences in the environmental drivers that appear to have the greatest control over the spatial variability of process-based fluxes (Huntzinger et al., 2010). The approach highlighted those environmental variables that correlate to flux as predicted by each examined model, and provides a means for identifying the strength of the relationship between these variables and predicted flux.

3.0 Future directions

The following section provides future directions specifically for each objective of the dissertation. The section also provides some future directions for the carbon cycle community at large.

3.1 Global geostatistical inversion study

Objective 1 demonstrated that GIM can provide relatively independent estimates of CO_2 flux and associated uncertainties at continental scales compared to other synthesis Bayesian methods. Future work could include:

- Applying linear algebra techniques so that RML is computationally feasible to optimize for covariance parameters from solely atmospheric data. In this manner, the global GIM estimates would be completely independent of biospheric models;

- Using the RML method to optimize for individual model-data mismatch covariance parameters for each measurement location instead of a single scaling parameter. This would allow the inversion to improve assessments of errors associated with transport, aggregation, and representation instead of using the RMSD of the observations at the measurement sites as a proxy for these model-data mismatch errors;
- Using a global application of GIM to determine boundary conditions to be used for a GIM regional inversion for North America. The two inversions could be combined to solve for finer spatiotemporal fluxes for the North American continent while being consistent with one another; and,
- Extending the method to estimate fluxes for more than 5 years. In this manner, fluxes could be compared to estimates from other inversion studies, and biospheric models to investigate assumptions regarding inter-annual variability.

3.2 North American regional geostatistical inversion study

Objective 2 showed that GIM has the potential to provide independent estimates of CO_2 flux and associated uncertainties at regional scales for monthly and annual fluxes timescales using an expanded network for North America. Future work could include:

- Assessing that assumptions (as mentioned in Chapter 3, Section 7) of stationary residuals, Gaussian distribution of residuals, isotropic structure of the spatiotemporal covariance matrix, and independent transport errors do not have a large impact on GIM flux estimates. Note that most of these assumptions are also made in other inversion applications so a sensitivity analysis would help partially validate the use of inversion methods to infer carbon fluxes at resolutions associated with more complexity;
- Developing better methods for selecting observations to include in the inversion as well as diagnostic techniques to assess the validity of regional flux estimates. The latter may include a comparison of continental budgets from regional inversions to those from global inversions; and,
- Using other information associated with carbon exchange (Gourdji et al., 2008; Gourdji et al., in prep.) within the model of the trend to further refine carbon

budgets and to infer statistical relationships between a variable and flux at regional scales. Besides environmental data, there is an opportunity to learn more about fossil fuel emissions by analyzing the inferred coefficients on any flux variables included within the model of the trend, e.g. individual sectors from a fossil fuel inventory database, given the expansion of the measurement network. These flux variables can also be broken out spatially to identify how consistent is the atmospheric signal within the fossil fuel inventories by region of the continent. Such an analysis could provide policy makers an understanding of where inventory data are most consistent with the atmospheric data.

3.3 Flux tower geostatistical regression study

Objective 3 confirmed that GR could be used to test assumptions in process-based models (such as the scale dependency of a particular variable and flux) at the various spatiotemporal scales where the assumptions are applied. Future work could include:

- Modeling the heteroscedasticity in the residuals using a more complex temporal covariance matrix,**Q** instead of separating fluxes by seasons. In this manner, the onset of different growing seasons would not need to be assumed *a priori*;
- Conducting a sensitivity test to ensure that the linear assumption in GR does not eclipse a "true" nonlinear relationship between a variable and flux (such as the Q_{10} exponential relationship between temperature and heterotrophic respiration); and
- Nonlinear or lagged relationships could also be included to further improve the fit of the model to the data.

3.2 Community-wide future directions

As mentioned in Chapter 1 and 2, the carbon-cycling community is focused on better understanding the natural sinks of atmospheric CO_2 and their controls at regional scales. To do this, the spread of regional and continental flux estimates from both "top-down" and "bottom-up" methods must be reduced. Without reducing the spread, carbon budgets from any model (including GIM or GR) will always be questioned. In addition, future predictions carbon cycle feedbacks within climate models will always be limited

by large uncertainties. However, as mentioned throughout the dissertation, minimizing the spread is not easy because some of uncertainty associated with flux estimates currently is irreducible due to errors in transport models. In addition, there are no means to assess which of the estimates are more "correct" or "incorrect" as the community does not have ways to measure CO_2 flux estimates at large scales or diagnose model output. As such, the community is faced with a problem that will require a multi-pronged approach.

First, as discussed earlier, there needs to be a commitment to existing long-term measurements as well as improved measurement coverage. One of the most important conclusions from this dissertation is that measurements have the potential to inform carbon cycling dynamics at spatiotemporal scales where, in the past, researcher have relied more heavily on assumptions regarding the behavior of flux exchange. Although coordinated efforts (e.g. NEON) are already underway to synthesize a variety of data streams at local scales across spatial gradients, long term measurements (such as eddy-covariance measurements) are also essential for assessing decadal trends that currently cannot be determined with available datasets except at the global scale. Additional measurements will further reduce the reliance on assumptions but the observations, due to a variety of factors such as the impact of clouds and aerosols on satellite measurement coverage, will always have some limitations.

The limitations of both indirect and direct estimates of CO_2 flux, along with other complications such as atmospheric mixing, will always necessitate the use of assumptions within models. The goal of future research should not be to eliminate the use of assumptions, but instead understand where and when assumptions have the most influence on estimates. In this way, it can be better known what part of an estimate is based on observation and what portion rests on other assumptions of carbon cycling. In addition, obtaining estimates that are independent from process-based models is essential for assessing which assumptions of carbon dynamics are consistent with the atmospheric observations. Since direct estimates of CO_2 flux are not available at large spatial scales, such a comparison is crucial for building consensus on regional scale flux behavior. Ultimately, this will allow researchers to identify which parts of process-based models

are “correct” and which need to be modified to better predict future carbon cycling scenarios.

Regardless, the ability of the carbon science community to extract the information in the atmospheric observations of CO_2 will always be dependent on the capability to leverage the measurements through simulated model atmospheric transport. There is much work to be done in both improving models and making them more computationally efficient to be more useful and accessible to the scientific community. Nevertheless, in terms of this multi-pronged approach to further understanding natural carbon cycling at regional and continental scales, it has been demonstrated within this dissertation that geostatistical methods play an important role.

REFERENCES

Aber, J. D., J. M. Melillo, K. J. Nadelhoffer, J. Paster, and R. D. Boone (1991), Factors controlling nitrogen cycling and nitrogen saturation in northern temperate forest ecosystems, *Ecol. Appl.*, 1(3), 303–315, doi:10.2307/1941759.

Ahmadov, R., C. Gerbig, R. Kretschmer, S. Körner, C. Rödenbeck, P. Bousquet, and M. Ramonet (2009), Comparing high resolution WRF-VPRM simulations and two global CO_2 transport models with coastal tower measurements of CO2, *Biogeosciences*, 6, 807–817.

Albertson, J. D., G. G. Katul, and P. Wiberg (2001), Relative importance of local and regional controls on coupled water, carbon, and energy fluxes, *Adv. Water Resour.*, 24, 1103–1118, doi:10.1016/S0309 1708(01)00042-2.

Anderson, M. C., J. M. Norman, T. P. Meyers, and G. R. Diak (2000), An analytical model for estimating canopy transpiration and carbon assimilation fluxes based on canopy light-use efficiency, *Agric. For. Meteorol.*, 101, 265–289, doi:10.1016/S0168-1923(99)00170-7.

Andres, R. J., G. Marland, I. Fung, and E. Matthews (1996), A 1°x 1° distribution of carbon dioxide emissions from fossil fuel consumption and cement manufacture, 1950 – 1990, *Global Biogeochem. Cycles*, 10(3), 419–430, doi:10.1029/96GB01523.

Bacastow, R.B, C.D. Keeling, T.P. Whorf (1985) Seasonal amplitude increase in atmospheric CO_2 concentration at Mauna Loa, Hawaii, 1959-1982, *Journal of Geophysical Research-Atmospheres*, 90(ND6):10529-10540.

Baker, D. F., R.M. Law, K.R. Gurney, P. Rayner, P. Peylin, A.S. Denning, P. Bousquet, L. Bruhwiler, Y.H. Chen, P. Ciais, I.Y. Fung, M. Heimann, J. John, T. Maki, S. Maksyutov, K. Masarie, M. Prather, B. Pak, S. Taguchi, Z. Zhu (2006), TransCom 3 inversion intercomparison: Impact of transport model errors on the interannual variability of regional CO_2 fluxes, 1988 – 2003, *Global Biogeochem. Cycles*, 20, GB1002, doi:10.1029/2004GB002439.

Baker, I. T., L. Prihodko, A. S. Denning, M. Goulden, S. Miller, and H. R. da Rocha (2008), Seasonal drought stress in the Amazon: Reconciling models and observations, *Journal of Geophysical Research-Biogeosciences*, *113*.

Baldocchi, D., Falge, E., Gu, L. H., Olson, R., Hollinger, D., Running, S., Anthoni, P., Bernhofer, C., Davis, K., Evans, R., Fuentes, J., Goldstein, A., Katul, G., Law, B., Lee,

X. H., Malhi, Y., Meyers, T., Munger, W., Oechel, W., U, K. T. P., Pilegaard, K., Schmid, H. P., Valentini, R., Verma, S., Vesala, T., Wilson, K., and Wofsy, S. (2001), FLUXNET: A new tool to study the temporal and spatial variability of ecosystem-scale carbon dioxide, water vapor, and energy flux densities, *Bull. Am. Meteorol. Soc.*, 82(11), 2415–2434, doi:10.1175/1520-0477.

Baldocchi, D., J. Finnigan, K. Wilson, K. T. Paw U, and E. Falge (2000), On measuring net ecosystem carbon exchange over tall vegetation and complex terrain, *Boundary Layer Meteorol*., 96, 257–291, doi:10.1023/A:1002497616547.

Baldocchi, D. (2008). Breathing of the terrestrial biosphere: lessons learned from a global network of carbon dioxide flux measurement systems. *Austr. J. Botany* 56**,** 1–26.

Barr AG, T.A. Black, E.H. Hogg, T.J. Griffis, K. Morgenstern, N. Kljun, A. Theede, Z. Nesic (2007), Climatic controls on the carbon and water balances of a boreal aspen forest, 1994–2003. *Global Change Biology*, 13, 561–576. doi: 10.1111/j.1365-2486.2006.01220.x

Beerling, D. J., and W. P. Quick (1995), A new technique for estimating rates of carboxylation and electron transport in leaves of C3 plants for use in dynamic global vegetation models, *Global Change Biol.*, 1(4), 289–294, doi:10.1111/j.1365-2486.1995.tb00027.x.

Blackman, F. F. (1905), Optima and limiting factors, *Ann. Bot*., 19, 281–295.

Bousquet, P., P. Peylin, P. Ciais, C. Le Quere, P. Friedlingstein, and P. P. Tans (2000), Regional changes in carbon dioxide fluxes of land and oceans since 1980, *Science*, 290(5495), 1342 – 1346, doi:10.1126/ science.290.5495.1342.

Bradford, M. and Reynolds, J.: Scaling terrestrial biogeochemical processes contrasting intact and model experimental systems, in: Scaling and uncertainty analysis in ecology, edited by: Wu, J., Jones, K. B., Li, H., and Loucks, O. L., Springer, Dordrecht, The Netherlands, 109–130, 2006.

Brenkert, A. (1998), Carbon dioxide emission estimates from fossil-fuel burning, hydraulic cement production, and gas flaring for 1995 on a one degree grid cell basis, Tech. Rep. NDP-058A, Carbon Dioxide Inf. Anal. Cent., Oak Ridge Natl. Lab., Oak Ridge, Tenn. (Available at http:// cdiac.esd.ornl.gov/npds/npd058a.html).

Brilli, F., C. Barta, A. Fortunati, M. Lerdau, F. Loreto, M. Centritto (2007) The relationship between isoprene biosynthesis and photosynthesis in poplar (Populus alba) saplings in response to soil drying and rewatering. *New Phytologist*. 175: 244-254.

Brown, M. (1993), Deduction of emissions of source gases using an objective inversion algorithm and a chemical transport model, *J. Geophys. Res*., 98(D7), 12,639–12,660, doi:10.1029/93JD01003.

Burnham, K. P., and D. R. Anderson (1998), Model Selection and Inference: A Practical Information-Theoretic Approach, 353 pp., Springer, New York.

Butler, M. P., K. J. Davis, A. S. Denning, and S. R. Kawa (2010), Using continental observations in global atmospheric inversions of CO_2: North American carbon sources and sinks. *Tellus B*, doi: 10.1111/j.1600-0889.2010.00501.x.

Campbell, G. S., and J. M. Norman (1998), An Introduction to Environmental Biophysics, 286 pp., Springer-Verlag, New York.

Canadell J.G., H.A. Mooney, D.D. Baldocchi, J.A.Berry, J.R. Ehleringer, C.B. Field, S.T. Gower, D.Y. Hollinger, J.E. Hunt, R.B. Jackson, S.W. Running, G.R. Shaver, W. Steffen, S.E. Trumbore, R. Valentini, B.Y. Bond (2000), Carbon metabolism of the terrestrial biosphere: a multitechnique approach for improved understanding. *Ecosystems* **3**: 115–130.

Canadell, J.G., C. Le Quere, C., M.R. Raupach, C.B. Field, E.T. Buitenhuis,P. Ciais, T.J. Conway, N.P. Gillett, R.A. Houghton, G. Marland (2007) Contributions to accelerating atmospheric CO_2 growth from economic activity, carbon intensity, and efficiency of natural sinks, *Proceedings of the National Academy of Sciences of the United States of America*, 104(47): 18866-18870.

Canadell, J.G., P. Ciais, S. Dhakal, H. Dolman, P. Friedlingstein, K.R. Gurney, A. Held, R.B. Jackson, C. Le Quere, E.L. Malone, D.S. Ojima, A. Patwardhan, G.P. Peters, M.R. Raupach (2010), Interactions of the carbon cycle, human activity, and the climate system: a research portfolio, *Current Opinion in Environmental Sustainability*, 2(4): 201-311.

Carouge, C., P. Bousquet, P. Peylin, P. J. Rayner, and P. Ciais (2010a), What can we learn from European continuous atmospheric CO_2 measurements to quantify regional fluxes - Part 1: Potential of the 2001 network, *Atmospheric Chemistry and Physics*, *10*(6), 3107-3117.

Carouge, C., P. J. Rayner, P. Peylin, P. Bousquet, F. Chevallier, and P. Ciais (2010b), What can we learn from European continuous atmospheric CO_2 measurements to quantify regional fluxes - Part 2: Sensitivity of flux accuracy to inverse setup, *Atmospheric Chemistry and Physics*, *10*(6), 3119-3129.

Chen, J. M., J. Liu, J. Cihlar, and M. L. Goulden (1999), Daily canopy photosynthesis model through temporal and spatial scaling for remote sensing applications, *Ecological Modelling*, *124*(2-3), 99-119.

Chen, J.M., W. Ju, J. Cihlar, D. Price, J. Liu, W. Chen, J. Pan, A. Black, and A. Barr (2003), Spatial distribution of carbon sources and sinks in Canada's forests, *Tellus*, 55B, 622-641.

Chevallier, F., et al. (2010), CO_2 surface fluxes at grid point scale estimated from a global 21 year reanalysis of atmospheric measurements, *Journal of Geophysical Research-Atmospheres* 115, D21307, doi:10.1029/2010JD013887.

Chilés, J.P. and P. Delfiner (1999), Geostatistics: Modeling Spatial Uncertainty. Wiley, New York.

Ciais, P., J.G. Canadell, S. Luyssaert, F. Chevallier, A. Shvidenko, Z. Poussi, M. Jonas, P. Peylin, A.W. King, E.D. Schulze, S. Piao, C. Rödenbeck, W. Peters, F.M. Breon (2010), Can we reconcile atmospheric estimates of the Northern terrestrial carbon sink with land-based accounting? *Current Opinion in Environmental Sustainability*, 2 (4): 225-230.

Conway, T.J., P.P. Tans, L.S. Waterman, K.W., Thoning (1994) Evidence for interannual variability of the carbon-cycle from the national-oceanic-and-atmospheric-administration climate-monitoring-and-diagnostics laboratory global-air-sampling-network, *Journal of Geophysical Research-Atmospheres*, 99(d11):22831-22855.

Cramer, W., D. W. Kicklighter, A. Bondeau, B. Moore, C. Churkina, B. Nemry, A. Ruimy, and A. L. Schloss (1999), Comparing global models of terrestrial net primary productivity (NPP): overview and key results, *Global Change Biology*, 5, 1-15.

Cressie, N. A. C. (1993), Statistics for Spatial Data, 900 pp., John Wiley, New York.

Crevoisier, C., C. Sweeney, M. Gloor, J. L. Sarmiento, and P. P. Tans (2010), Regional US carbon sinks from three-dimensional atmospheric CO_2 sampling, *Proceedings of the National Academy of Sciences of the United States of America*, 107(43), 18348–18353.

Curtis, P. S., P. J. Hanson, P. Bolstad, C. Barford, J. C. Randolph, H. P. Schmid, and K. B. Wilson (2002), Biometric and eddy-covariance based estimates of annual carbon storage in five eastern North American deciduous forests, *Agric. For. Meteorol.*, 113, 3–19, doi:10.1016/S0168-1923 (02)00099-0.

Curtis, P.S., J.M. Jablonski, X.Z. Wang (2003), Assessing elevated CO_2 responses using meta-analysis. *New Phytologist*, 160: 6-7.

Curtis, P.S., C. S. Vogel, C. M. Gough, H. P. Schmid, H.-B. Su, and B. D. Bovard (2005), Respiratory carbon losses and the carbon-use efficiency of a northern hardwood forest, 1999–2003, *New Phytologist*, 167, 437–456, doi:10.1111/j.1469-8137.2005.01438.x.

Dargaville, R. J., M. Heimann, A. D. McGuire, I. C. Prentice, D. W. Kicklighter, F. Joos, J. S. Clein, G. Esser, J. Foley, J. Kaplan, R. A. Meier, J. M. Melillo, B. Moore, N. Ramankuty, T. Reichenau, A. Schloss, S. Sitch, H. Tian, L. J. Williams, and U. Wittenberg, (2002), Evaluation of terrestrial carbon cycle models with atmospheric

CO_2 measurements: Results from transient simulations considering increasing CO_2, climate, and land-use effects, *Global Biogeochemical Cycles*, *16*(4), doi: 10.1029/2001gb001426.

Davidson, E. A., K. Savage, L. V. Verchot, and R. Navarro (2002), Minimizing artifacts and biases in chamber-based measurements of soil respiration, Agric. *For. Meteorol.*, 113(1–4), 21–37, doi:10.1016/S0168-1923(02)00100-4.

Davidson, E. A., I. A. Janssens, and Y. Q. Luo (2006), On the variability of respiration in terrestrial ecosystems: Moving beyond Q(10), *Global Change Biology*, 12(2), 154–164, doi:10.1111/j.13652486.2005.01065.x.

Denman, K.L., G. Brasseur, A. Chidthaisong, P. Ciais, P.M. Cox, R.E. Dickinson, D. Hauglustaine, C. Heinze, E. Holland, D. Jacob, U. Lohmann, S Ramachandran, P.L. da Silva Dias, S.C. Wofsy and X. Zhang, 2007: Couplings Between Changes in the Climate System and Biogeochemistry. In: Climate Change 2007: The Physical Science Basis. Contribution of Working Group I to the Fourth Assessment Report of the Intergovernmental Panel on Climate Change (eds. Solomon, S., D. Qin, M. Manning, Z. Chen, M. Marquis, K.B. Averyt, M.Tignor and H.L. Miller). Cambridge University Press, Cambridge, United Kingdom and New York, NY, USA.

Denning, A. S., M. Nicholls, L. Prihodko, I. Baker, P. L. Vidale, K. Davis, and P. Bakwin (2003), Simulated variations in atmospheric CO_2 over a Wisconsin forest using a coupled ecosystem-atmosphere model, *Global Change Biology*, *9*(9), 1241-1250.

Denning, A. S., and et al. (2005), Science Implementation Strategy for the North American Carbon Program*Rep.*, 68 pp, NACP Implementation Strategy Group of the U.S. Carbon Cycle Interagency Working Group, Washington, DC.

Desai, A. R., B. R. Helliker, P. R. Moorcroft, A. E. Andrews, and J. A. Berry (2010), Climatic controls of interannual variability in regional carbon fluxes from top-down and bottom-up perspectives, *Journal of Geophysical Research-Atmospheres*, 115, G02011, doi:10.1029/2009JG001122.

Dolman, A.J., J. Noilhan, P. Durand, C. Sarrat, A. Brut, B. Piguet, A. Butet, N. Jarosz, Y. Brunet, Y D. Loustau, E. Lamaud, L. Tolk, R. Ronda, F. Miglietta, B. Gioli, V. Magliulo, M. Esposito, C. Gerbig, S. Korner, R. Glademard, M. Ramonet, P. Ciais, B. Neininger, R.W.A. Hutjes, J.A. Elbers, R. Macatangay, R O. Schrems, G. Perez-Landa, M.J. Sanz, Y. Scholz, G, Facon, E. Ceschia, P. Beziat (2006), The CarboEurope regional experiment strategy, *Bull. Am. Meteorol. Soc*., 87(10):1367-1379.

Dorrepaal, E. (2007), Are plant growth-form-based classifications useful in predicting northern ecosystem carbon cycling feedbacks to climate change?, *J. Ecol*., 95(6), 1167–1180, doi:10.1111/j.1365-2745.2007.01294.x.

Engelen, R. J., A. S. Denning, and K. R. Gurney (2002), On error estimation in atmospheric CO_2 inversions, *J. Geophys. Res.*, 107(D22), 4635, doi:10.1029/2002JD002195.

Engelen, R. J. (2006), Publisher's correction to "On error estimation in atmospheric CO_2 inversions," *J. Geophys. Res*., 111, D14199, doi:10.1029/2006JD007428.

Enting, I. G. and G. N. Newsam (1990), Atmospheric constituent inversion problems: Implications for baseline monitoring, J. *Atmos. Chem.*, 11, 69-87.

Enting, I. G. (2002), Inverse Problems in Atmospheric Constituent Transport, Cambridge Univ. Press, Cambridge, U. K. Enting, I. G., and G. N. Newsam (1990), Atmospheric constituent inversion problems—Implications for base-line monitoring, J. Atmos. Chem., 11(1–2), 69– 87.

Erickson, T. A., Williams, M. W., and Winstral, A.: Persistence of topographic controls on the spatial distribution of snow in rugged mountain terrain, Colorado, united states, *Water Resources Research*, 41, W04014, doi:10.1029/2003wr002973.

Fan, S., T. L. Blaine, and J. L. Sarmiento, Terrestrial carbon sink in the northern hemisphere estimated from atmospheric CO_2 difference between Mauna Loa and South Pole since 1959, *Tellus*, 51, 863–870.

Faraway, J. (2005) Linear Models with R, CRC Press, Boca Raton, Fla., ISBN:1384884258,9781584884255.

Farquhar, G. D., S. V. Caemmerer, and J. A. Berry (1980), A biochemical-model of photosynthetic CO_2 assimilation in leaves of C-3 species , *Planta*, *149*(1), 78-90.

Farquhar, G. D., and S. von Caemmerer (1982), Modeling of photosynthetic response to environmental conditions, in *Physiological Plant Ecology. II. Water Relations and Carbon Assimilation*, edited by O. L. Lange, P. S. Nobel, C. B. Osmond and H. Zeigler, Springer-Verlag, New York.

Field, C.B., M.J. Behrenfeld, J.T. Randerson, P. Falkowski (1998), Primary production of the biosphere: integrating terrestrial and oceanic components. *Science*, 281:237–240.

Field, C.B. (2001) Plant physiology of the "missing sink" carbon sink. *Plant Physiology*, 125**,** 25–28.

Forster, Malcolm R. (2000) Key Concepts in Model Selection Performance and Generalizability, *Journal of Mathematical Psychology*, 44, 205-231.

Friedlingstein, P and I.C. Prentice (2010), Carbon-climate feedbacks: a review of model and observation based estimates, *Current Opinion in Environmental Sustainability*, 2(4), 251-257, doi: 10.1016/ /j.cosust.2010.06.002

Geels, C., M. Gloor, P. Ciais, P. Bousquet, P. Peylin, A. T. Vermeulen, R. Dargaville, T. Aalto, J. Brandt, J. H. Christensen, L. M. Frohn, L. Haszpra, U. Karstens, C. Rodenbeck, M. Ramonet, G. Carboni, and R. Santaguida,(2007), Comparing atmospheric transport models for future regional inversions over Europe - Part 1: mapping the atmospheric CO_2 signals, *Atmospheric Chemistry and Physics*, *7*(13), 3461-3479.

Gerbig, C., J. C. Lin, S. C. Wofsy, B. C. Daube, A. E. Andrews, B. B. Stephens, P. S. Bakwin, and C. A. Grainger (2003a), Toward constraining regional-scale fluxes of CO_2 with atmospheric observations over a continent: 1. Observed spatial variability from airborne platforms, *Journal of Geophysical Research-Atmospheres*, *108*(D24), doi:10.1029/2002jd003018.

Gerbig, C., J. C. Lin, S. C. Wofsy, B. C. Daube, A. E. Andrews, B. B. Stephens, P. S. Bakwin, and C. A. Grainger (2003b), Toward constraining regional-scale fluxes of CO_2 with atmospheric observations over a continent: 2. Analysis of COBRA data using a receptor-oriented framework, *Journal of Geophysical Research-Atmospheres*, *108*(D24). doi: 10.1029/2003jd003770.

Gerbig, C., Lin, J. C., Munger, J. W. and Wofsy, S. C. 2006. What tracer observations in the continental boundary layer tell us about surface-atmosphere fluxes? *Atmos. Chem. Phys.* 6, 539–554.

Gerbig, C., A. J. Dolman, and M. Heimann (2009), On observational and modelling strategies targeted at regional carbon exchange over continents, *Biogeosciences*, 6(10), 1949-1959.

Giglio, L., I. Csiszar, and C. O. Justice (2006), Global distribution and seasonality of active fires as observed with the Terra and Aqua Moderate Resolution Imaging Spectroradiometer (MODIS) sensors *Journal of Geophysical Research-Atmospheres*, 111, G02016, doi:10.1029/2005JG000142.

Gilmanov T.G., T.J. Svejcar, D.A. Johnson, R.E. Angell, N.Z. Saliendra, B.K. Wylie (2006), Long-term dynamics of production, respiration, and net CO_2 exchange in two sagebrush-steppe ecosystems. *Rangeland Ecology & Management* 59, 585–599. doi: 10.2111/05-198R1.1

GLOBALVIEW-CO2 (2008), Cooperative Atmospheric Data Integration Project—Carbon dioxide [CD-ROM], Clim. Monit. and Diag. Lab., NOAA, Boulder, Colo. (also available via anonymous ftp to ftp.cmdl.noaa.gov, Path: ccg/co2/GLOBALVIEW).

Gloor, M., N. Gruber, J. Sarmiento, C. L. Sabine, R. A. Feely, and C. Rödenbeck (2003), A first estimate of present and preindustrial air-sea CO_2 flux patterns based on ocean interior carbon measurements and models, *Geophysical Research Letters*, 30(1), 1010, doi:10.1029/2002GL015594.

Göckede, M., A. M. Michalak, D. Vickers, D. P. Turner, and B. E. Law (2010), Atmospheric inverse modeling to constrain regional-scale CO_2 budgets at high spatial and temporal resolution, *Journal of Geophysical Research-Atmospheres*, 115, D15113, doi:10.1029/2009JD012257.

Gough, C. M., C. S. Vogel, K.H. Harrold, K. George, and P.S. Curtis (2007a), The legacy of harvest and fire on ecosystem carbon storage in a north temperate forest. *Global Change Biology*, 13: 1935–1949. doi: 10.1111/j.1365-2486.2007.01406.x.

Gough, C. M., C. S. Vogel, C. Kazanski, L. Nagel, C. E. Flower, and P. S. Curtis (2007), Coarse woody debris and the carbon balance of a north temperate forest, *For. Ecol. Manage*., 244, 60–67, doi:10.1016/j.foreco.2007.03.039.

Gough, C. M., C. S. Vogel, H. P. Schmid, and P. S. Curtis (2008), Controls on annual forest carbon storage: Lessons from the past and predictions for the future, *BioScience*, 58(7), 609–619, doi:10.1641/B580708.

Gourdji, S. M., K. L. Mueller, K. Schaefer, and A. M. Michalak (2008), Global monthly averaged CO_2 fluxes recovered using a geostatistical inverse modeling approach: 2. Results including auxiliary environmental data, *Journal of Geophysical Research-Atmospheres,* 113, D21115, doi:10.1029/2007JD009733.

Gourdji, S. M., A. I. Hirsch, K. L. Mueller, A. E. Andrews, and A. M. Michalak (2010), Regional-scale geostatistical inverse modeling of North American CO_2 fluxes: a synthetic data study, *Atmospheric Chemistry and Physics, 10(13)*, 6151-6167, doi: 10.5194/acp-10-6151-2010.

Gourdji, S.M., K.L. Mueller, V. Yadav, D.N. Huntzinger, A.E. Andrews, M. Trudeau, G. Petron, D. Worthy, W. Munger, M. Fischer, A.M. Michalak (in prep), Results from a regional grid-scale North American atmospheric CO_2 inversion for 2004 with a comparison to independent bottom-up flux estimates.

Gurney, K. R., et al. (2003), TransCom 3 CO_2 inversion intercomparison: 1. Annual mean control results and sensitivity to transport and prior flux information, *Tellus*, Ser. B, 55, 555– 579.

Gurney, K. R., et al. (2004), Transcom 3 inversion intercomparison: Model mean results for the estimation of seasonal carbon sources and sinks, *Global Biogeochemical Cycles*, *18*(1), 21.

Gurney, K. R., Y. H. Chen, T. Maki, S. R. Kawa, A. Andrews, and Z. X. Zhu (2005), Sensitivity of atmospheric CO_2 inversions to seasonal and interannual variations in fossil fuel emissions, *Journal of Geophysical Research-Atmospheres*, 110, D10308, doi:10.1029/2004JD005373.

Gurney, K. R., Mendoza, D. L., Zhou, Y., Fischer, M. L., Miller (2009), High resolution fossil fuel combustion CO_2 emission fluxes for the United States. *Environ. Sci. Technol.* 43, doi:10.1021/es900806c.

Hanson, P. J., N. T. Edwards, C. T. Garten, and J. A. Andrews (2000), Separating root and soil microbial contributions to soil respiration: A review of methods and observations, *Biogeochemistry*, 48(1), 115–146, doi:10.1023/A:1006244819642.

Hargrove, W. H., F. Hoffman, and B. E. Law (2003), New analysis reveals representativeness of the AmeriFlux network, *Eos Trans*. AGU, 84(48), 529–544, doi:10.1029/2003EO480001.

Heimann, M., G. Esser, A. Haxeltine, J. Kaduk, D. W. Kicklighter, W. Knorr, G. H. Kohlmaier, A. D. McGuire, J. Melillo, B. Moore, R. D. Otto, I. C. Prentice, W. Sauf, A. Schloss, S. Sitch, U. Wittenberg, and G. Wurth,(1998), Evaluation of terrestrial Carbon Cycle models through simulations of the seasonal cycle of atmospheric CO_2: First results of a model intercomparison study, *Global Biogeochemical Cycles*, 12(1), 1-24.

Heimann, M. and S. Körner (2003), The Global Atmospheric Tracer Model TM3: Model description and user's manual, release 3.8a, Tech. Rep. 5, Max Planck Inst. for Biogeochem., Jena, Germany.

Heimann, M. and M. Reichstein (2008), Terrestrial ecosystem carbon dynamics and climate feedbacks. *Nature***,** 451, 289–292.

Hein, R., P. Crutzen, and M. Heimann (1997), An inverse modeling approach to investigate the global atmospheric methane cycle, *Global Biogeochemical Cycles*, 11(1), 43– 76.

Hibbard, K. A., B. E. Law, M. Reichstein, and J. Sulzman (2005), An analysis of soil respiration across northern hemisphere temperate ecosystems, *Biogeochemistry*, 73(1), 29–70, doi:10.1007/s10533-004-2946-0.

Hoeting, J. A., R. A. Davis, A. A. Merton, and S. E. Thompson (2006), Model selection for geostatistical models, *Ecol. Appl.,* 16(1), 87–98, doi:10.1890/04-0576.

Houghton RA (2000) Interannual variability in the global carbon cycle. *Journal of Geophysical Research*, 105 (D15), 20,121–20,130.

Huang, H.-C., and C.-S. Chen (2007), Optimal geostatistical model selection, *J. Am. Stat. Assoc.,* 102(479), 1009–1024, doi:10.1198/016214507000000491.

Hui, D., Y. Luo, and G. Katul (2003), Partitioning interannual variability in net ecosystem exchange between climatic variability and functional change, *Tree Physiol.,* 23(7), 433–442.

Huntzinger, D.N., W.M. Post, A.M. Michalak, Y.Wei, A. Jacobson, R. Cook, et al., (in prep), North American Carbon Project (NACP) Regional Interim Synthesis: Terrestrial Biospheric Model Intercomparison, in preparation, to be submit to *Global Biogeochemical Cycles* in January of 2011.

Huntzinger, D.N., S.M. Gourdji, K.L. Mueller, and A.M. Michalak (in press), The Influence of North American Carbon Flux Spatial Distribution on the Temporal Variability of Atmospheric Carbon Dioxide, *Journal of Geophysical Research – Atmospheres*, 2010.

Huntzinger, D.N., A.M. Michalak, S.M. Gourdji, and K.L. Mueller (2010), An Approach for Intercomparison of Modeled Biospheric Carbon Flux Estimates, *Biogeosciences Discussions*, 7, 7903-7943.

Janssens, I. A., et al. (2001), Productivity overshadows temperature in determining soil and ecosystem respiration across European forests, *Global Change Biol.*, 7(3), 269–278, doi:10.1046/j.1365-2486.2001. 00412.x.

Judd, C. M., and G. H. McClelland (1989), Data Analysis: A Model-Comparison Approach, 635 pp., Harcourt Brace Jovanovich, San Diego, Calif.

Kalnay, E., et al. (1996), The NCEP/NCAR 40-Year Reanalysis Project, *Bull. Am. Meteorol. Soc*., 77(3), 437– 471.

Kaminski, T., M. Heimann, and R. Giering (1999), A coarse grid three dimensional global inverse model of the atmospheric transport: 2. Inversion of the transport of CO_2 in the 1980s, *J. Geophys. Res*., 104(D15), 18,555–18,582, doi:10.1029/1999JD900146.

Kaminski, T., P. J. Rayner, M. Heimann, and I. G. Enting (2001), On aggregation errors in atmospheric transport inversions, *J. Geophys. Res.*, 106(D5), 4703–4716, doi:10.1029/2000JD900581.

Keeling, C.D., T.P. Whorf, C.S. Wong, R.D. Bellagay, (1985) The Concentration of Atmospheric Carbon-Dioxide at ocean weather station-P from 1969-1981. *Journal of Geosphysical Research-Atmospheres,* 90(ND6):10511-10528.

Keeling, C.D., R.B. Bacastow, A.F. Carter, S.C. Piper, T.P Whorf, M. Heimann, W.G. Mook, H.A. Roeloffzen: A three-dimensional model of atmospheric CO_2 transport based on observed winds. 1. Analysis of observational data. In Aspects of Climate Variability in the Pacific and Western Americas, Geophysical Monogr. Ser., vol 55. Edited by Peterson DH. AGU; 1989:165-236.

Kicklighter, D. W., A. Bondeau, A. L. Schloss, J. Kaduk, A. D. McGuire, and N. P. P. M. I. Participants Potsdam (1999), Comparing global models of terrestrial net primary productivity (NPP): global pattern and differentiation by major biomes, *Global Change Biology, 5*, 16-24.

King, A. W., L. Dilling, G. P. Zimmerman, D. M. Fairman, R. A. Houghton, G. Marland, A. Z. Rose, and T. J. Wilbanks (2007), What is the Carbon Cycle and Why Care?*Rep.*, U.S. Climate Change Science Program and the Subcommittee on Global Change Research.

Kitanidis, P. K. (1986), Parameter uncertainty in estimation of spatial functions: Bayesian analysis, *Water Resour. Res.*, 22(4), 499– 507.

Kitanidis, P. K. (1995), Quasi-linear geostatistical theory for inversing, *Water Resour. Res*., 31(10), 2411 – 2419.

Kitanidis, P. K., and K.-F. Shen (1996), Geostatistical interpolation of chemical concentration, *Adv. Water Resour.*, 19(6), 369–378, doi:10.1016/0309-1708(96)00016-4.

Kitanidis, P. K. (1997), A variance-ratio test for supporting a variable mean in kriging, *Math. Geol*., 29(3), 335–348, doi:10.1007/BF02769639.

Knorr, W. (2000), Annual and interannual CO_2 exchanges of the terrestrial biosphere: Process-based simulations and uncertainties, *Global Ecology and Biogeography*, 9, 225-252.

Krakauer, N. Y., T. Schneider, J. T. Randerson, and S. C. Olsen (2004), Using generalized cross validation to select parameters in inversions for regional carbon fluxes, *Geophys. Res. Lett*., 31, L19108, doi:10.1029/2004GL020323.

Lauvaux, T., M. Uliasz, C. Sarrat, F. Chevallier, P. Bousquet, C. Lac, K. J. Davis, P. Ciais, A. S. Denning, and P. J. Rayner (2008), Mesoscale inversion: first results from the CERES campaign with synthetic data, *Atmospheric Chemistry and Physics*, *8*(13), 3459-3471.

Law, B. E., M. G. Ryan, and P. M. Anthoni (1999a), Seasonal and annual respiration of a ponderosa pine ecosystem, *Global Change Biology*, 5(2), 169–182, doi:10.1046/j.1365-2486.1999.00214.x.

Law, B. E., E. Falge, L. Gu, D.D. Baldocchi, P. Bakwin, P. Berbigier, K. Davis, A.J. Dolman, M. Falk, J.D. Fuentes, A. Goldstein, A. Granier, A. Grelle, D. Hollinger, I.A. Janssens, P. Jarvis, N.O. Jensen, G. Katul, Y. Mahli, G. Matteucci, T. Meyers, R. Monson, W. Munger, W. Oechel, R. Olson, K. Pilegaard, K.T. Paw, H. Thorgeirsson, R. Valentini, S. Verma, T. Vesala, K. Wilson, S. Wofsy (2002), Environmental controls over carbon dioxide and water vapor exchange of terrestrial vegetation, *Agric. For. Meteorol.*, 113(1–4), 97–120, doi:10.1016/S0168-1923(02)00104-1.

Law, R. M., P. J. Rayner, L. P. Steele, and I. G. Enting (2002), Using high temporal frequency data for CO_2 inversions, *Global Biogeochemical Cycles*, *16*(4), doi: 10.1029/2001gb001593.

Law, R. M., Y. H. Chen, and K. R. Gurney (2003), TransCom 3 CO_2 inversion intercomparison: 2. Sensitivity of annual mean results to data choices, *Tellus*, Ser. B, 55, 580– 595.

Le Quere, C., M.R. Raupach, J.G. Canadell, G. Marland, L. Bopp, P. Ciais, T.J. Conway, S.C. Doney, R.A. Feely, P. Foster, P. Friedlingstein, K. Gurney, R.A. Houghton, J.I. House, C. Huntingford, P.E. Levy, M.R. Lomas, J. Majkut, N. Metzl, J.P. Ometto, G.P. Peters, I.C. Prentice, J.T. Randerson,S.W. Running, J.L. Sarmiento, U. Schuster, S. Sitch, T. Takahashi, N. Viovy, G.R. van der Werf, F.I. Woodward, (2009), Trends in the sources and sinks of carbon dioxide, *Nature Geoscience*, 2 (12): 831-836.

Le Quere, C. (2010), Trends in the land and ocean carbon uptake. *Current Opinion in Environmental Sustainability*, 2(2): 219-224.

Lin, J. C., C. Gerbig, S. C. Wofsy, A. E. Andrews, B. C. Daube, K. J. Davis, and C. A. Grainger (2003), A near-field tool for simulating the upstream influence of atmospheric observations: The Stochastic Time-Inverted Lagrangian Transport (STILT) model, *Journal of Geophysical Research-Atmospheres*, *108*(D16), doi: 10.1029/2002JD003161.

Lindroth, A., L. Klemedtsson, A. Grelle, P. Weslien, and O. Langvall (2008), Measurement of net ecosystem exchange, productivity and respiration in three spruce forests in Sweden shows unexpectedly large soil carbon losses, *Biogeochemistry*, 89(1), 43–60, doi:10.1007/s10533-007-9137-8.

Lloyd, J., and J. A. Taylor (1994), On the temperature-dependence of soil respiration, *Functional Ecology*, *8*(3), 315-323.

Mahadevan, P., S. C. Wofsy, D. M. Matross, X. M. Xiao, A. L. Dunn, J. C. Lin, C. Gerbig, J. W. Munger, V. Y. Chow, and E. W. Gottlieb (2008), A satellite-based biosphere parameterization for net ecosystem CO_2 exchange: Vegetation Photosynthesis and Respiration Model (VPRM), *Global Biogeochem. Cycles*, 22, GB2005, doi:10.1029/2006GB002735.

Maki, T., M. Ikegami, T. Fujita, T. Hirahara, K. Yamada, K. Mori, A. Takeuchi, Y. Tsutsumi, K. Suda, and T.J. Conway (2010) New technique to analyse global distributions of CO_2 concentrations and fluxes from non-processed observational data, *Tellus*, *62B, 797–80*, DOI: 10.1111/j.1600-0889.2010.00488.x.

Matross, D.M., A. Andrews, M. Pathmathevan, C. Gerbig, J.C. Lin, S.C. Wofsy, B.C. Daube, E.W. Gottlieb, V.Y. Chow, J.T. Lee, C. Zhao, P.S. Bakwin, J.W. Munger, and D.Y. Hollinger (2006), Estimating regional carbon exchange in New England and

Quebec by combining atmospheric, ground-based and satellite data. *Tellus* B, 58: 344–358. doi: 10.1111/j.1600-0889.2006.00206.x

Michalak, A. M., L. Bruhwiler, and P. P. Tans (2004), A geostatistical approach to surface flux estimation of atmospheric trace gases, *Journal of Geophysical Research-Atmospheres*, 109, D14109, doi:10.1029/2003JD004422.

Michalak, A. M., A. Hirsch, L. Bruhwiler, K. R. Gurney, W. Peters, and P. P. Tans (2005), Maximum likelihood estimation of covariance parameters for Bayesian atmospheric trace gas surface flux inversions, *Journal of Geophysical Research-Atmospheres*, 110, D24107, doi:10.1029/2005JD005970.

Monteith, J. L. (1966), Photosynthesis and transpiration of crops, *Exp. Agric.*, 2(1), 1–14, doi:10.1017/S0014479700003938.

Mueller, K. L., S. M. Gourdji, and A. M. Michalak (2008), Global monthly averaged CO_2 fluxes recovered using a geostatistical inverse modeling approach: 1. Results using atmospheric measurements, *Journal of Geophysical Research-Atmospheres*, 113, D21114, doi:10.1029/2007JD009734.

Mueller, K. L., V. Yadav, P. S. Curtis, C. Vogel, and A. M. Michalak (2010), Attributing the variability of eddy-covariance CO_2 flux measurements across temporal scales using geostatistical regression for a mixed northern hardwood forest, *Global Biogeochem. Cycles*, 24, GB3023, doi:10.1029/2009GB003642.

Myneni, R. B., S. Hoffman, Y. Knyazikhin, J. L. Privette, J. Glassy, Y. Tian, Y. Wang, X. Song, Y. Zhang, and G. R. Smith (2002), Global products of vegetation leaf area and fraction absorbed PAR from year one of MODIS data, *Remote Sens. Environ.*, 83(1–2), 214–231, doi:10.1016/S0034-4257(02)00074-3.

Nehrkorn, T., J. Eluszkiewicz, S.C. Wofsy, J.C. Lin, C. Gerbig, M. Longo, S. Freitas (2010), Coupled weather research and forecasting–stochastic time-inverted lagrangian transport (WRF–STILT) model, *Meteorol Atmos Phys*, 107:51–64.doi:10.1007/s00703-010-0068-x.

Nevison, C. D., N. M. Mahowald, S. C. Doney, I. D. Lima, G. R. Van der Werf, J. T. Randerson, D. F. Baker, P. Kasibhatla, and G. A. McKinley (2008), Contribution of ocean, fossil fuel, land biosphere, and biomass burning carbon fluxes to seasonal and interannual variability in atmospheric CO_2, *Journal of Geophysical Research-Biogeosciences*, *113*(G1), doi: 10.1029/2007JG000408.

Nicholls, M. E., Denning, A. S., Prihodko, L., Vidale, P. L., Baker, I., Davis, K., and Bakwin, P.: A multiple-scale simulation of variations in atmospheric carbon dioxide using a coupled biosphere-atmospheric model, *Journal of Geophysical Research-Atmospheres*, 109, D18117, doi:10.1029/2003jd004482.

Olea, R.A. (1994), Fundamentals of Semivariogram Estimation, Modeling, and Usage, In: Stochastic Modeling and Geostatistics: Principles, Methods, and Case Studies (eds. Yarus, J.M and Chambers, R.L.). *The American Association of Petroleum Geologist*, Tulsa Oklahoma. ISBN: 0-89181-702-6.

Oliphant, A., C. Susan, B. Grimmond, H. P. Schmid, and C. A. Wayson (2006), Local-scale heterogeneity of photosynthetically active radiation (PAR), absorbed PAR and net radiation as a function of topography, sky conditions and leaf area index, *Remote Sens. Environ.*, 103(3), 324–337, doi:10.1016/j.rse.2005.09.021.

Olivier, J.G.J. and J.J.M. Berdowski (2001a) Global emissions sources and sinks. In: Berdowski, J., Guicherit, R. and B.J. Heij (eds.) "The Climate System", pp. 33-78. A.A. Balkema Publishers/Swets & Zeitlinger Publishers, Lisse, The Netherlands. ISBN 90 5809 255 0.

Pacala, S. W., et al. (2001), Consistent land- and atmosphere-based US carbon sink estimates, *Science*, *292*(5525), 2316-2320.

Patra, P. K., S. Maksyutov, M. Ishizawa, T. Nakazawa, T. Takahashi, and J. Ukita (2005), Interannual and decadal changes in the sea-air CO_2 flux from atmospheric CO_2 inverse modeling, *Global Biogeochem. Cycles*, 19, GB4013, doi:10.1029/2004GB002257.

Peters, W., et al. (2007), An atmospheric perspective on North American carbon dioxide exchange: CarbonTracker, *Proceedings of the National Academy of Sciences of the United States of America*, 104(48), 18,925–18,930.

Peylin, P., P. J. Rayner, P. Bousquet, C. Carouge, F. Hourdin, P. Heinrich, P. Ciais, and A. contributors (2005), Daily CO_2 flux estimates over Europe from continuous atmospheric measurements: 1, inverse methodology, *Atmospheric Chemistry and Physics*, *5*, 3173-3186.

Potter, C. S., J. T. Randerson, C. B. Field, P. A. Matson, P. M. Vitousek, H. A. Mooney, and S. A. Klooster (1993), Terrestrial ecosystem production – A process model based on global satellite and surfact data, *Global Biogeochemical Cycles*, *7*(4), 811-841

Randerson, J. T., M. V. Thompson, T. J. Conway, I. Y. Fung, and C. B. Field (1997), The contribution of terrestrial sources and sinks to trends in the seasonal cycle of atmospheric carbon dioxide, *Global Biogeochem. Cycles*, 11(4), 535–560, doi:10.1029/97GB02268.

Ravishanker , N. and Dey, D.K. (2002), "A First Course in Linear Model Theory: Texts in Statistical *Science*." Chapman and Hall/CRC, 473 pp., ISBN 1-58488-247-6.

Raupach, M., and J.G. Canadell (2010), Carbon and the Anthropocene. *Current Opinion in Environmental Sustainability*, 2(2): 210-218.

Rayner, P. J., I. G. Enting, R. J. Francey, and R. Langenfelds (1999), Reconstructing the recent carbon cycle from atmospheric CO2, delta C-13 and O-2/N-2 observations, *Tellus*, Ser. B, 51, 213–232.

Reichstein, M., et al. (2003), Modeling temporal and large-scale spatial variability of soil respiration from soil water availability, temperature and vegetation productivity indices, *Global Biogeochem. Cycles*, 17(4), 1104,doi:10.1029/2003GB002035.

Reichstein, M., T. Katterer, O. Andren, P. Ciais, E. D. Schulze, W. Cramer, D. Papel, and R. Valentini (2005), Temperature sensitivity of decomposition in relation to soil organic matter pools: Critique and outlook, *Biogeosciences*, 2(4), 317–321, doi:10.5194/bg-2-317-2005.

Richardson, A., et al. (2006), A multi-site analysis of random error in tower-based measurements of carbon and energy fluxes, *Agric. For. Meteorol*., 136(1–2), 1–18, doi:10.1016/j.agrformet.2006.01.007.

Riley, W. J., S. C. Biraud, M. S. Torn, M. L. Fischer, D. P. Billesbach, and J. A. Berry (2009), Regional CO_2 and latent heat surface fluxes in the Southern Great Plains: Measurements, modeling, and scaling, *Journal of Geophysical Research-Atmospheres*, 114, G04009, doi:10.1029/2009JG001003.

Roden, J. (2003), Modeling the light interception and carbon gain of individual fluttering aspen (Populus tremuloides Michx) leaves, *Trees*, 17(2), 117–126, doi:10.1007/s00468-002-0213-3.

Rödenbeck, C., S. Houweling, M. Gloor, and M. Heimann (2003), CO_2 flux history 1982– 2001 inferred from atmospheric data using a global inversion of atmospheric transport, *Atmos. Chem. Phys*., 3, 1919–1964.

Rödenbeck, C. (2005), Estimating CO_2 sources and sinks from atmospheric mixing ratio measurements using a global inversion of atmospheric transport, Tech. Rep. 6, 61 pp., Max Planck Inst. for Biogeochem., Jena, Germany.

Running, S.W., D.D. Baldocchi, D.P. Turner, S.T. Gower, P.S. Bakwin, K.A. Hibbard (1999), A Global Terrestrial Monitoring Network Integrating Tower Fluxes, Flask Sampling, Ecosystem Modeling and EOS Satellite Data. *Remote Sens. Environment*, 70:108-127.

Running, S. W., R. R. Nemani, F. A. Heinsch, M. Zhao, M. Reeves, and H. Hashimoto (2004), A continuous satellite-derived measure of global terrestrial primary production, *BioScience*, 54, 547–560, doi:10.1641/0006-3568

Schlesinger, W.H., E.S. Bernhardt, E. H. DeLucia, D.S. Ellsworth, A.C. Finzi, G. R. Hendrey, K.S. Hofmockel, J Lichter, R.Matamala, D.Moore, R. Oren, J.S. Pippen, and

R.B. Thomas (2006), The Duke Forest FACE Experiment: CO2 enrichment of a Loblolly Pine Forest, *Ecological Studies*,Vol. 187.

Schmid, H. P., H.-B. Su, C. S. Vogel, and P. S. Curtis (2003), Ecosystem atmosphere exchange of carbon dioxide over a mixed hardwood forest in northern lower Michigan, *Journal of Geophysical Research-Atmospheres* 108(D14), 4417,doi:10.1029/2002JD003011.

Schuh, A. E., A. S. Denning, M. Uliasz, and K. D. Corbin (2009), Seeing the forest through the trees: Recovering large scale carbon flux biases in the midst of small-scale variability, *Journal of Geophysical Research-Atmospheres,114*(G03007),doi: 10.1029/2008JG000842.

Schuh, A. E., A. S. Denning, K. D. Corbin, I. T. Baker, M. Uliasz, N. Parazoo, A. E. Andrews, and D. E. J. Worthy (2010), A regional high-resolution carbon flux inversion of North America for 2004, *Biogeosciences*, *7*(5), 1625-1644, doi: 10.5194/bg-7-1625-2010.

Schwarz, G. (1978), Estimating the dimension of a model, *Ann. Stat.*, 6(2), 461–464, doi:10.1214/aos/1176344136.

Schwartz, M.D., and J.M Hanes (2010), Intercomparing multiple measures of the onset of spring in eastern North America, *International Journal of Climatology*, 30(11):1614-1626, doi: 10.1002/joc.2008.

Sims, D. A., et al. (2006), On the use of MODIS EVI to assess gross primary productivity of North American ecosystems, *Journal of Geophysical Research-Atmospheres*, 111, G04015, doi:10.1029/2006JG000162.

Sitch, S., I. Prentice, B. Smith, W. Cramer, J. Kaplan, W. Lucht, M. Sykes, K. Thonicke, and S. Venevsky (2000), LPJ—A coupled model of vegetation dynamics and the terrestrial carbon cycle, in The role of vegetation dynamics in the control of atmospheric CO_2 content, edited by S. Sitch, Ph.D. thesis, chap. 8, Lund Univ., Lund, Sweden.

Sitch, S., et al. (2003), Evaluation of ecosystem dynamics, plant geography and terrestrial carbon cycling in the LPJ dynamic global vegetation model, *Global Change Biology*, *9*(2), 161-185.

Stoy, P. C., et al. (2009), Biosphere-atmosphere exchange of CO_2 in relation to climate: A cross-biome analysis across multiple time scales, *Biogeosciences*, 6(10), 2297–2312, doi:10.5194/bg-6-2297-2009.

Swallow, W.H. and J.F. Monahan (1984), Monte Carlo Comparison of Anova, MIVQUE, REML, and ML Estimators and Variance Components, *Technometrics*, Vol. 26, No. 1, pp. 47-57.

Takahashi, T., R. H. Wanninkhof, R. A. Feely, R. F. Weiss, D. W. Chipman, N. Bates, J. Olafsson, C. Sabine, and S. C. Sutherland (1999), Net sea-air CO_2 flux over the global oceans: An improved estimate based on the seaair CO_2 difference, in Proceedings of the 2nd International Symposium: CO_2 in the Oceans, edited by Y. Nojiri, Natl. Inst. for Environ. Stud., Environ. Agency of Jpn., Tokyo.

Takahashi, T., C. Stewart, C. Sweeney, A. Poisson, N. Metzl, B. Tilbrook, N. Bates, R. Wanninkhof, R. Feely, C. Sabine, J. Olafsson, Y. Nojiri (2002), Global sea-air CO_2 flux based on climatological surface ocean pCO (2), and seasonal biological and temperature effects, *Deep Sea Res.*, Part II, 49(9– 10), 1601– 1622.

Tans, P.P., I.Y. Fung, T. Takahashi (1990), Observational constraints on the global atmospheric CO_2 budget. *Science*, 247(4949):1431-1438.

Tans, P.P. and T. J. Conway (2005), Monthly atmospheric CO_2 mixing ratios from the NOAA CMDL Carbon Cycle Cooperative Global Air Sampling Network, 1968 – 2002, in Trends: A Compendium of Data on Global Change, Carbon Dioxide Inf. Anal. Cent., Oak Ridge Natl. Lab., Oak Ridge, Tenn.

Tarantola, A. (2005), "Inverse Problem Theory and Methods for Model Parameter Estimation." Society for Industrial and Applied Mathematics, Philadelphia, 342 pp., 1995, ISBN 0-89871-572-5.

Urbanski, S., C. Barford, S. Wofsy, C. Kucharik, E. Pyle, J. Budney, K. McKain, D. Fitzjarrald, M. Czikowsky, and J. W. Munger (2007), Factors controlling CO_2 exchange on timescales from hourly to decadal at Harvard Forest, *Journal of Geophysical Research-Atmospheres*, 112, G02020, doi:10.1029/2006JG000293.

Wackernagel, Hans (2003), "Multivariate Geostatistics. An Introduction with Applications." Springer-Verlag, Berlin, Heidelberg, New York, 235 pp., 1995, DM 68. ISBN 3-540-601279.

Ward, E. J. (2008), A review and comparison of four commonly used Bayesian and maximum likelihood model selection tools, *Ecol. Modell.*, 211(1–2), 1–10, doi:10.1016/j.ecolmodel.2007.10.030.

Wasserman, Larry (2000), Bayesian Model Selection and Model Averaging, *Journal of Mathematical Psychology*, 44, 92-107.

West, T., G. Marland, N. Singh, B.L. Bhaduri, A. Roddy (2009), The human carbon budget: an estimate of the spatial distribution of metabolic carbon consumption and release in the United States, *Biogeochemistry*,94(29-41),doi:10.1007/s10533-009-9306-z.

Yadav, V., K. L. Mueller, D. Dragoni, A. M. Michalak (2010), A geostatistical synthesis study of factors affecting gross primary productivity in various ecosystems of North America, *Biogeosciences*, 7, 1445–1487, doi:10.5194/bgd-7-1445-2010.

Zhou, T., Shi, P. J., Hui, D. F., and Luo, Y. Q., (2010) Global pattern of temperature sensitivity of soil heterotrophic respiration (Q(10)) and its implications for carbon-climate feedback, *Journal of Geophysical Research-Biogeosciences*, 114, doi:10.1029/2008jg000850.

Zhou, Y., and A.M. Michalak, (2009), "Characterizing attribute distributions in water sediments by geostatistical downscaling," *Environmental Science and Technology*, 43 (24), 9267-9273, doi:10.1021/es901431y.